THESIS

EFFECTS OF NANOSTRUCTURED POLYMERIC SURFACES ON BACTERIAL ADHESION AND ERYTHROCYTE (RBCs) INTEGRITY

Submitted by

Vignesh Sathyanarayanan

Department of Mechanical Engineering

In partial fulfilment of the requirements

For the Degree of Master of Science

Colorado State University

Fort Collins, Colorado

Fall 2024

Master's Committee:

Advisor: Ketul C. Popat

Soham Ghosh
Yan Vivian Li

ABSTRACT

EFFECTS OF NANOSTRUCTURED POLYMERIC SURFACES ON BACTERIAL ADHESION AND ERYTHROCYTE (RBCs) INTEGRITY

Blood-contacting devices, such as stents, artificial heart valves, vascular grafts and catheters, placed within a host body, are subjected to complications such as thrombosis, restenosis, hemolysis etc. These complications result in the frequent need for revision surgeries or long-term drug therapies post implantations. Natural and synthetic biocompatible polymers are used as potential solutions for these issues due to their superior characteristic of biodegradability. Recent advancements in nanoscale fabrication and modification of these surfaces has shown improved results with platelets, leukocytes and other whole blood components. However, disruptions in erythrocyte’s cell structure, caused by the foreign body materials, can compromise their oxygen-carrying capacity. This can further affect the overall tissue oxygenation and potentially lead to myocardial ischemic conditions. Therefore, it is also vital to understand the effect of bio-implant surfaces on erythrocyte integrity and viability, to enhance their biocompatibility. In this study, PCL nanostructured surfaces, nanofibers and nanowires, were fabricated and modified with organic compounds, Tanfloc and CMKC, to investigate their antibacterial properties and their effect on erythrocyte’s cell integrity. Results indicate that the modified PCL nanostructured surfaces exhibit enhanced antibacterial properties and retain erythrocyte integrity.

ACKNOWLEDGEMENTS

I would like to express my sincere gratitude to several people without whose contribution and support, the completion of this thesis could not have been possible.

First and foremost, I am profoundly grateful to my advisor, Dr. Ketul C. Popat, for his belief in me and for granting me this remarkable opportunity. The one and only factor that motivated me to pursue this path was his unwavering trust and esteem for me. I'm forever grateful for his unconditional help and guidance. It feels like a blessing in disguise, to be chosen to do my research, under such a patient, intelligent and supportive mentor, who has never failed to encourage and motive me throughout this journey. His proficiency in this discipline is impeccable. He consistently allocates time to address my queries and remains highly responsive despite his busy schedules. Above all, he not only cares about my professional development but also respects and prioritizes my personal well-being. Ketul, thank you for being this wonderful human being that you are and for constantly inspiring me.

I would also like to extend my sincerest gratitude to my committee members, Dr. Soham Ghosh and Dr. Yan Vivian Li for their encouragement, support and helpful insights. A special thanks to Dr. Matt Kipper for his valuable input towards my research and his generosity in permitting me to utilize his laboratory equipment. I would like to thank all the staff of the analytical Resources Core (ARC), particularly Dr. Rebecca Miller, for her guidance in the utilization of different instruments.

I whole-heartedly thank Dr. Paulo Soares of Pontifical Catholic University of Paraná in Curitiba, Brazil for his timely help with XRD and Nano indentation of material samples.

Special thanks and immense gratitude to one of the coolest professors I've ever met, Dr. Laurel Bond, for her invaluable guidance towards my professional writing and communication.

I would like to acknowledge my department of Mechanical Engineering for their financial support and assistantship. Special thanks to Amanda, my graduate coordinator, for always standing by my side and for her assistance in resolving issues.

I would also like to thank my lab mates, Abhishek Bhattacharjee, Somayeh Baghersad, Aniruddha Savargaonkar, Fernanda Veregue for their friendship, assistance and all the wonderful moments we had together. I would also like express my gratitude to my lab seniors, Vignesh Manivasagam, Roberta Sabino and Harvindar Singh for their earlier works, which has been a great inspiration and help for my research. Most importantly, I cannot thank Dr. Liszt Madruga enough for his contribution and support for my research. He has taught me most of the research works that I did and has drawn blood innumerable times for my study. He has always been a person that I look up to and admire for his professionalism and lab etiquette. Liszt, thank you for all the time and efforts you dedicated for me, from my initial day in the lab to the end of this thesis.

I would also like to thank Dr. V Chandrasekar, Dr. N Saravanakumar, Dr. P. Manoj Kumar, Dr. T. Prem Kumar and Mr. R Avinash Kumar for their guidance.

I personally thank Akshay Kumar, Sushma Kanth, Oto, Shashank, Kumaran, Soundarya, Karthick, Sudharsan, Vishnu Charan, Pradeep, Swamy uncle, Bharathi aunty, Andy, Lauren, Balaji, Lavanya, Baheeradhan, Bhuvana and Kumar uncle who made me feel at home.

I also thank my friends Aswitha, Mons, UV, Yash, Sharath, Anitha, Steph, Shakthi and others, for their love which kept me going without giving up.

I wish to express my love and gratitude to Ilayaraja, A R Rahman, and a few other Tamil film music directors whose musical contributions provided solace during my difficult times and instilled a sense of appreciation for life during my moments of happiness.

Above all, I thank my family, especially my parents Chitra Krishnamoorthy and Sathyanarayanan Natarajan for their endless support and love. Without them I couldn’t have made this possible.

DEDICATION

To my parents, Chitra and Sathyanarayanan,

And to my advisor, Dr. Ketul C. Popat

For their pure love, support and sacrifice.

TABLE OF CONTENTS

LIST OF TABLES

LIST OF FIGURES

HYPOTHESIS AND SPECIFIC AIMS

Fundamental Hypothesis: Polycaprolactone nanostructured surfaces, modified with Tanfloc and Carboxymethyl Kappa-Carrageenan, reduce bacterial adhesion and maintain erythrocyte cell integrity.

Specific aim 1: The main aim of this study is fabrication and characterization of PCL nanostructured surfaces. This research is discussed in chapter 2 and will cover:

(a) Fabrication of PCL nanofiber surfaces.
(b) Fabrication of PCL nanowire surfaces.
(c) Modification of PCL nanostructured surfaces with TN and CMKC.
(d) Characterization of PCL nanostructured surfaces (before and after chemical surface modification) – surface morphology, wettability, chemistry, crystallinity and mechanical properties.

Specific aim 2: The main aim of this study is to investigate the antibacterial properties of PCL nanostructured surfaces. This research is discussed in chapter 3 and will cover:

(a) Evaluation of bacterial adhesion and proliferation on different surfaces after 6 hours and 24 hours of bacterial incubation using fluorescence microscopy.
(b) Evaluation of bacterial morphology and biofilm formation on different surfaces after 6 hours and 24 hours of bacterial incubation using scanning electron microscopy.

Specific aim 3: The main aim of this study is to investigate the effects of PCL nanostructured surfaces on erythrocyte integrity. This research is discussed in chapter 4 and will cover:

(a) Evaluation of cytotoxicity of different surfaces using LDH assay kit.

(b) Evaluation of erythrocytes adhesion on different surfaces after 1.5 hours and 6 hours of erythrocyte incubation using fluorescence microscopy.

(c) Evaluation of erythrocytes morphology on different surfaces after 1.5 hours and 6 hours of erythrocyte incubation using scanning electron microscopy.

CHAPTER 1

LITERATURE REVIEW

1.1 Introduction

Recent statistics regarding cardiovascular diseases (CVD) has revealed alarming trends that concerns the ongoing public health crisis posed by these conditions. World Health Organization (WHO) has reported that cardiovascular diseases remain the major cause of death on a global scale, accounting for 32% of all the deaths in 2019, which is equivalent to about 17.9 million fatalities annually [1]. This statistic has remained consistent over the previous years, emphasizing the persistent burden of CVD on global health systems [1,2]. During COVID-19 pandemic, the impact on cardiovascular health has been severe. Recent studies highlighted that individuals with pre-existing cardiovascular conditions faced a significantly higher risk of severe outcomes from COVID-19, including hospitalization and mortality [3–6]. Individuals with such conditions, including hypertension, coronary artery disease, and heart failure, face a high-risk rate of CVD. In the context of hypertension, reports indicate that nearly 1.3 billion people worldwide suffer from hypertension, with only about 1 in 5 individuals having their condition under control [7,8]. According to American Heart Association, over 48.6% of US adult population (127.9 million in 2020) were affected by CVD and has been reported to increase with the age in both males and females [9]. This underscores the substantial burden these diseases impose on society and healthcare systems.

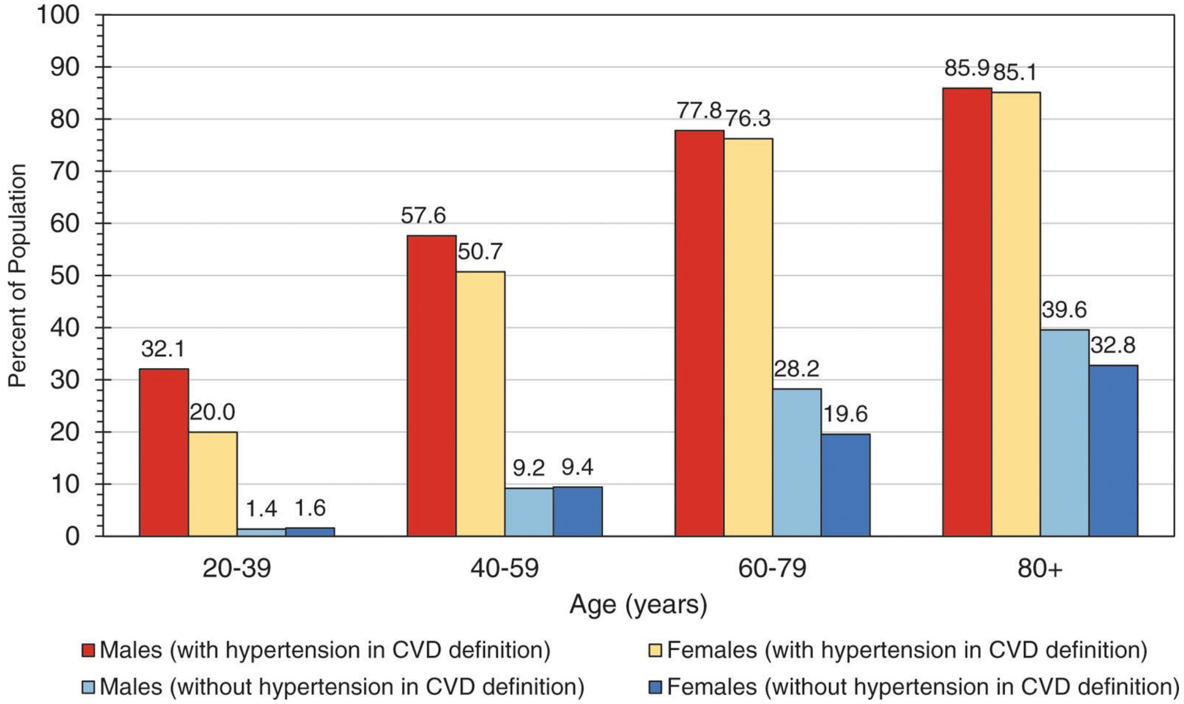

Figure 1.1.1: Prevalence of CVD in US adults ≥20 years of age, by age and sex**.** These data include coronary heart disease, heart failure, stroke, and with and without hypertension [9].

1.2 Blood contacting devices

There are several major causes for CVD as discussed above, with coronary heart disease being an important factor in causing it [9–11]. It is a very common type of cardiovascular disease characterized by the narrowing of coronary arteries due to atherosclerosis, leading to myocardial ischemia and potential myocardial infarction. The leading cause of coronary heart disease is the gradual deposition of plaque, cholesterol and fat on the inner wall of coronary arteries. This deposition can build up to partially or completely block the blood flow.

Contemporary treatment techniques for coronary heart disease include revascularization of the occluded vessel via percutaneous coronary intervention (PCI). Initially, preferred treatment procedure was balloon angioplasty where a stent is inserted into the artery at the blockage site to restore normalized blood flow through the afflicted vasculature. This technique failed due to the prevalence of postoperative arterial recoil and coronary dissection. The need for better treatment techniques has driven researchers and scientists to develop modern coronary stents [12,13]. Bare-metal stents (BMS) were the first generation of stents used, which were constructed with metal alloys. Different metals such as stainless steel, cobalt, nickel and titanium were employed in the construction of BMS [12,14]. Even though BMS had high mechanical strength, which can maintain the arterial diameter, it led to further complications like scar tissue formation and thrombosis. This resulted in restenosis, which is the reoccurrence of the blockage inside the blood vessel due to proliferation of endothelial cells followed by dedifferentiation of smooth muscle cells [15–17]. To resolve this problem, drug eluting stents (DES) were developed, which released pharmacological agents to inhibit neointimal hyperplasia and reduced risk of in-stent restenosis (ISR) [18,19]. DES have shown superior results in preventing ISR compared to BMS, making them a preferred choice in clinical practice [20]. The introduction of second-generation DES and drug-coated balloon (DCB) further improved safety and reduced restenosis rate up to <10% [21]. Hence, the main cause of failure of the stents that encounter tissue and blood flow remains the material surface interaction with the biological environment (22.9% failure rate after 13 months). Studies have also showed that exposure of red blood cells to thrombogenic metallic surfaces such as these stent placements also results in hemolysis and compromises integrity of red blood cells [22].

Increased oxidative stress and inflammation on red blood cells can further exaggerate vascular injury and lead to complications [23]. Hence, the choice of stent material and coating are crucial as they can impact the cell integrity and viability of red blood cells [24].

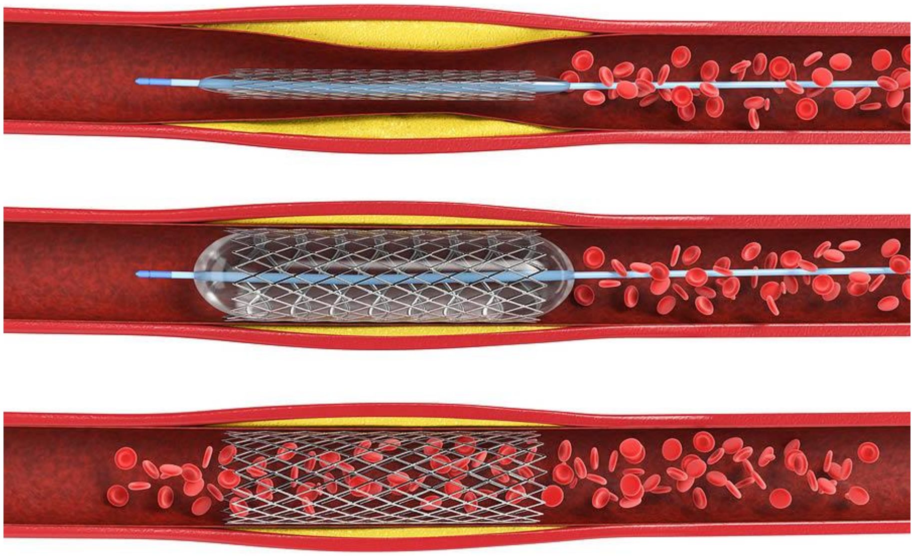

Figure 1.2.1: Coronary stent with balloon angioplasty [25].

The other widely used blood-contacting medical device is an artificial heart valve. Artificial heart valves are used to replace the heart valve that is dysfunctional. Heart valves synchronously operate with every heartbeat to maintain blood flow inside the human body. During improper health conditions, heart valves can leak and fail to work, resulting in heart malfunction. In cases where the heart valve cannot be repaired, an open-heart surgery procedure is done to replace it with an artificial heart valve. Heart valves can be placed surgically or through a transcatheter procedure [26]. There are mainly two types of artificial heart valves: mechanical valves and biological valves. Mechanical heart valves (MHVs) are more susceptible to thrombus formation than bioprosthetic heart valves (BHVs), which are developed from bovine or porcine tissue mounted on a metal frame [27]. However, the lifespan of BHVs is about 10 to 20 years whereas MHVs can last a patient's lifetime [28]. The thrombosis on the heart valve is not only increased through intrinsic pathways but also through hemostatic and hemodynamic factors. The incidence of hemolysis in patients with MHVs has been reported to be a major concern, with some studies indicating that it can occur in up to 30% of patients, depending on the valve design and patient-specific factors [29,30]. The turbulent flow is one of the hemodynamic factors that can damage tissue around the prosthesis, initiate platelet activation and prevent re-endothelialization [27]. In addition to these complications, both mechanical and bioprosthetic valves are not immune to infection, particularly from aggressive pathogens such as Staphylococcus aureus, which has a high affinity for adhering to prosthetic materials [31]. Therefore, the blood contacting devices used within a patient's body must have enhanced antibacterial properties and be compatible with components of blood for better functionality and improved patient's health.

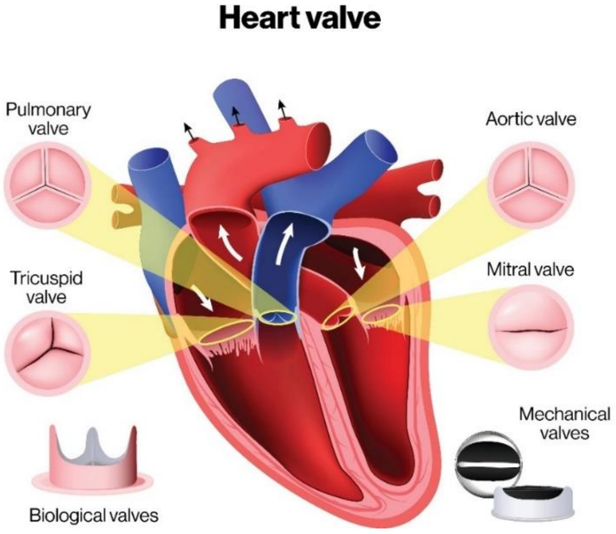

Figure 1.2.2: Illustration of native heart valves, biological valves and mechanical valves [32].

1.3 Effects on integrity of red blood cells

Red blood cells, also known as erythrocytes, are primarily composed of a lipid bilayer interspersed with proteins, which together facilitate the cell’s flexibility and deformability. Cell integrity of erythrocytes refers to the structural and functional stability of the erythrocyte membrane, which is crucial for maintaining the physiological roles of the cells, particularly in oxygen transport and overall hemodynamics. This integrity of erythrocytes can be influenced by various factors including membrane composition, mechanical properties, surface characteristics of materials in contact and external stressors. High shear stress, often encountered in devices like ventricular assist devices (VADs) and prosthetic heart valves, can lead to mechanical hemolysis. This occurs when erythrocytes are subjected to forces that exceed their structural integrity, resulting in the rupture of the cell membrane and the release of hemoglobin into the plasma [33,34]. In addition to mechanical stress, the biochemical environment created by blood-contacting devices can also compromise erythrocyte integrity. The oxidative stress on the cells can alter the membrane lipid composition and protein structure, further impairing the deformability and the functionality of erythrocytes [35,36]. When the cells lose its integrity, its shape changes abnormally, resulting in a type of cells called poikilocytes. The term poikilocytes refers to the presence of these irregularly shaped cells in the blood, which can arise due to variety of causes. When blood-contacting devices, such as stents or valves, are introduced into the host body, they influence the morphology of the erythrocytes, potentially leading to the formation of poikilocytes. There are different types of morphological changes observed as shown in **Figure 1.3.1**, with each of it having its own unique causes [37]. For instance, the presence of stents can create regions of turbulence and shear stress that causes the erythrocytes to deform, leading to the formation of schistocytes (fragmented cells) and other poikilocytes [38,39]. The aggregation of cells in these turbulent flow regions can also contribute to their abnormal shapes [38]. Erythrocyte's exposure to foreign materials can also trigger inflammatory responses, which affects the lipid composition of the erythrocytes, resulting in formation of echinocytes (burr cells) or acanthocytes (spur or spiky cells) [40]. These abnormal morphological changes in erythrocytes can lead to hemolysis, myocardial ischemia and eventually result in myocardial infarction. Thus, improving the surface properties of blood-contacting devices by making it more biocompatible for erythrocytes is essential to maintain their health, integrity and functionality.

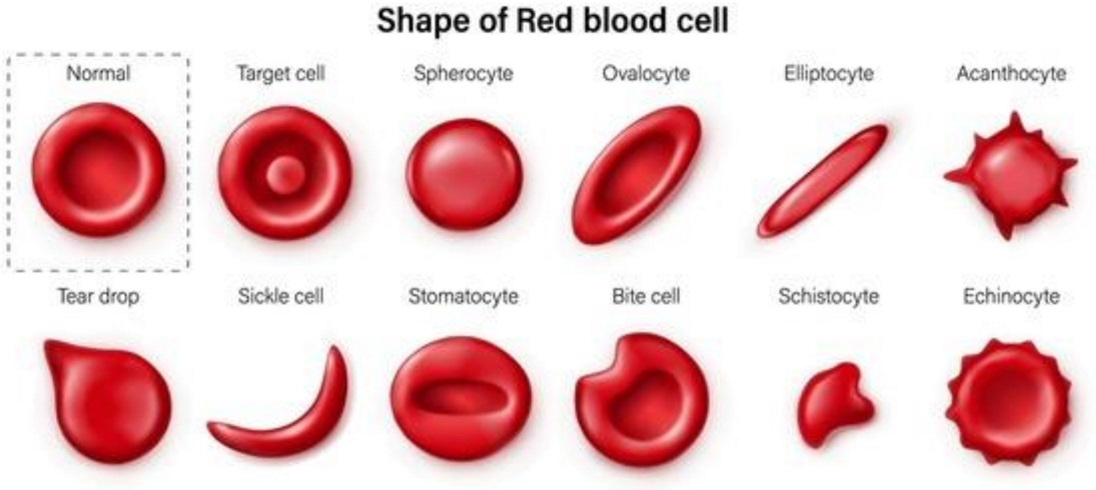

Figure 1.3.1: Different types of morphological changes in red blood cells [41].

1.4 Current applications of biodegradable polymers

There are several research done in the field of polymeric biomaterials aimed at improving hemocompatibility, reducing thrombus formation and inhibiting bacterial adhesion.

They have been employed for potential applications in medical devices such as vascular grafts, stents and catheters. The most advantageous property of biopolymers is their biodegradability, which is a significant improvement over the permanent nature of metal stents. Conventional metallic stents often led to revision surgeries and complications such as stent migration and clogging from microbial biofilms [42,43]. In contrast, biopolymer stents can be designed to degrade over time and leave a healed vessel behind without requiring any additional surgical interventions [43]. This not only reduces the risk of complications associated with long-term foreign body presence but also promotes natural vascular remodeling as the stent material is absorbable by the body [44]. They have also shown exceptional flexibility without any compromise in the mechanical strength, which is advantageous for stent functionality [45]. Additionally, biopolymer coatings can be engineered to enhance endothelialization, which is vital for the integration of the stent with the vascular tissue and for reducing the risk of thrombosis [46]. Incorporation of antibacterial and antimicrobial agents into the biopolymer matrices further addresses the complications of biofilm formation which is prevalent in metallic stents [42].

Polyurethanes (PUs) have gained attention for their tunable properties and ability to form biocompatible surfaces. Recent studies highlight the importance of the phase separation structure in PUs, which influences their mechanical properties and hemocompatibility, thereby affecting blood coagulation responses [47,48]. Chitooligosaccharide grafted onto segmented poly(ester-urethane) films have shown to improve the surface biocompatibility. The natural polysaccharides like chitooligosaccharide help in reducing platelet adhesion and activation, which are critical factors in thrombus formation upon contact with blood [49].

Another widely used polymer in hemodialysis devices is Polysulfone. Research has shown that Polysulfone membranes can be modified to enhance their hydrophilicity, which helps in reduction of protein adsorption and platelet activation [50,51]. Polyvinyl alcohol (PVA) is characterized by its high hydrophilicity due to the presence of hydroxyl (-OH) groups. This hydrophilic nature leads to a water-rich environment on the surface of the device [52]. Such surfaces are less prone to protein adsorption, which is a critical factor in the initiation of thrombus formation. Studies have shown that PVA-based hydrogels create smooth surfaces that minimize blood coagulation, making them suitable for applications like vascular grafts [53]. Polyhydroxyalkanoates (PHAs) are another class of biodegradable polyesters produced by microbial fermentation. Recent studies highlighted the potential of low molecular weight PHAs for applications like bio-adhesives and drug coating systems [54]. Polylactic acid (PLA) is another widely used biopolymer in the fabrication of DES, sutures and drug delivery systems. The ability of PLA to be engineered into various forms allows the incorporation of therapeutic agents that can be released over time to prevent restenosis. The gradual release of drugs like sirolimus from PLA-based stents has shown to significantly reduce platelet aggregation and smooth muscle cell proliferation [55]. Recent advancements have focused on enhancing PLA composites with materials like lignin to improve their mechanical properties and antioxidant capabilities [56]. Chitosan, a natural biopolymer, derived from chitin exhibits excellent biocompatibility, biodegradability and antimicrobial properties. It has been widely used in wound dressings, drug delivery systems and tissue engineering scaffolds.

Chitosan-based hydrogel's ability to form gel-like structure, which can encapsulate drugs, helps in promoting cell adhesion [57,58].

Silk fibroin, derived from silkworms, has been utilized in the fabrication of vascular grafts and has exhibited promising results in small-diameter applications, where traditional synthetic grafts often fail due to thrombosis or initial hyperplasia. For instance, research demonstrated that silk fibroin grafts could replace small-caliber blood vessels, promoting tissue regeneration and reducing the risk of complications associated with synthetic materials [59,60]. Polyethylene Glycol (PEG) has been evaluated for its use in arteriovenous connections for hemodialysis [61]. Also, incorporation of PEG into valve materials can enhance their resistance to calcification, a common issue in long-term implants [62,63]. Collagen and Elastin are few other natural biopolymers used in development of Tissue-Engineered Vascular Grafts. These grafts are designed to mimic the mechanical and biological properties of native blood vessels [64]. These are few contemporary solutions with the incorporation of biopolymers in place of conventional metallic implants and blood contacting devices.

1.5 Benefits of PCL as a biomaterial

Polycaprolactone (PCL) has been shown as a potential biomaterial for blood contacting devices such as stents, vascular grafts and heart valves due to its unique properties that enhance biocompatibility and functionality. Its advantages in these applications attributes to its favorable mechanical properties, biodegradability and ability to be modified for improved blood compatibility. Mechanical strength and flexibility are few of its significant properties which are crucial for the dynamic environment of blood vessels [65]. PCL exhibits a high ultimate elongation at point of failure, which is essential for vascular grafts that need to accommodate the pulsatile nature of blood flow without rupturing [66].

PCL’s biodegradability is a critical factor in its use for temporary implants. PCL’s slow biodegradation, which can last up to 24 months, provides sufficient time for tissue regeneration while minimizing the risk of chronic inflammation associated with permanent implants [67]. This property is very useful in vascular applications, where the scaffold must support tissue growth until the host tissue can take over the function [68]. Even the degradation products of PCL are non-toxic and can be metabolized by the body, which emphasizes the biocompatible nature of PCL [69]. Also, the surface characteristics of PCL, which can be engineered to improve blood compatibility, makes it stand out from other materials used for bio-implants. The hydrophobic nature of PCL can lead to protein adsorption and platelet activation, which eventually ends in thrombosis [70]. However, surface modifications, such as the incorporation of heparin or other anticoagulants, can significantly enhance its compatibility by reducing the platelet adhesion and activation [71]. Also, the ability of PCL to be fabricated into different complex geometries, using techniques like electrospinning and 3D printing, enables a vast range of applications for it. This property allows it to be customized into implants that fit specific patient anatomies, which is beneficial in vascular applications where precise dimensions are critical for functionality [72]. The FDA’s approval of various PCL-based devices establishes its potential for clinical use, facilitating faster transition from laboratory to clinical settings [73]. Research has shown that PCL’s versatility can further be enhanced due to its ability to modify its physical and chemical properties through copolymerization and blending with other materials, such as polylactic acid (PLA), chitosan, hydroxyapatite etc [74–76].

Similarly, PCL composites with natural polymers like gelatin or cellulose have exhibited improved hydrophilicity and promoted cellular interactions [77,78]. These advantageous properties promote PCL as a key biomaterial in the development of innovative solutions for tissue engineering, drug delivery and cardiovascular bioimplants.

1.6 PCL nanostructured surfaces

1.6.1 Benefits of nanomodification

One of the primary advantages of nanostructured PCL is the enhancement of its mechanical properties. Nanostructures can increase the elastic modulus and tensile strength of PCL scaffolds, which is crucial for load-bearing applications in bone tissue engineering. For instance, incorporation of nanoclay into PCL matrices has shown to reinforce the mechanical strength of the resulting scaffolds, leading to a 140-200% increase in elastic modulus [79]. This characteristic is essential for scaffolds to withstand physiological loads while promoting cell attachment and proliferation. In addition to mechanical improvements, nanostructures significantly enhance the biocompatibility of PCL. The hydrophobic nature of PCL often limits cell adhesion and proliferation; however, the introduction of nanostructures modifies the surface properties to improve wettability and promote cellular interactions [80]. Nanostructured surfaces can provide topographical cues that influence cell behavior, such as differentiation and migration. For instance, retinal progenitor cells cultured on nanostructured PCL surfaces has shown regulation of specific markers associated with differentiation, suggesting that surface topography plays a vital role in guiding cell fate [81]. Conversely, nanostructured PCL surfaces can also be engineered to be superhydrophobic, which significantly decreases the contact area between bacteria and the surface.

For instance, Hizal et al. demonstrated that a hydrophobic nanopillared surface resulted in a 98% reduction in Staphylococcus aureus and a 99% reduction in Escherichia coli adhesion compared to hydrophilic surfaces, primarily due to reduced van der Waals interactions [82]. The sharp edges and high aspect ratios of nanostructures can induce physical damage to bacterial cells on contact, leading to cell lysis or impaired function [83,84]. Leszczak et. al investigated the impact of surface topography on cell adhesion, proliferation and differentiation for various cell types, including mesenchymal stem cells (MSCs) and fibroblasts. Their studies demonstrated that the introduction of nanoscale features, such as nanowires, increased the surface area available for cell attachment, thereby promoting stronger cell-substrate interactions [85,86]. They have also studied whole blood clotting kinetics, platelet adhesion and activation on nanostructured surfaces such as nanofibers and nanowires **(Figure 1.6.1.1)** [87,88]. However, there are insufficient studies done specifically about erythrocytes interaction with nanostructured PCL surfaces. Works indicating the effects of nanostructured PCL surfaces on the cell viability and integrity of erythrocytes were less, providing more scope for further research in that area.

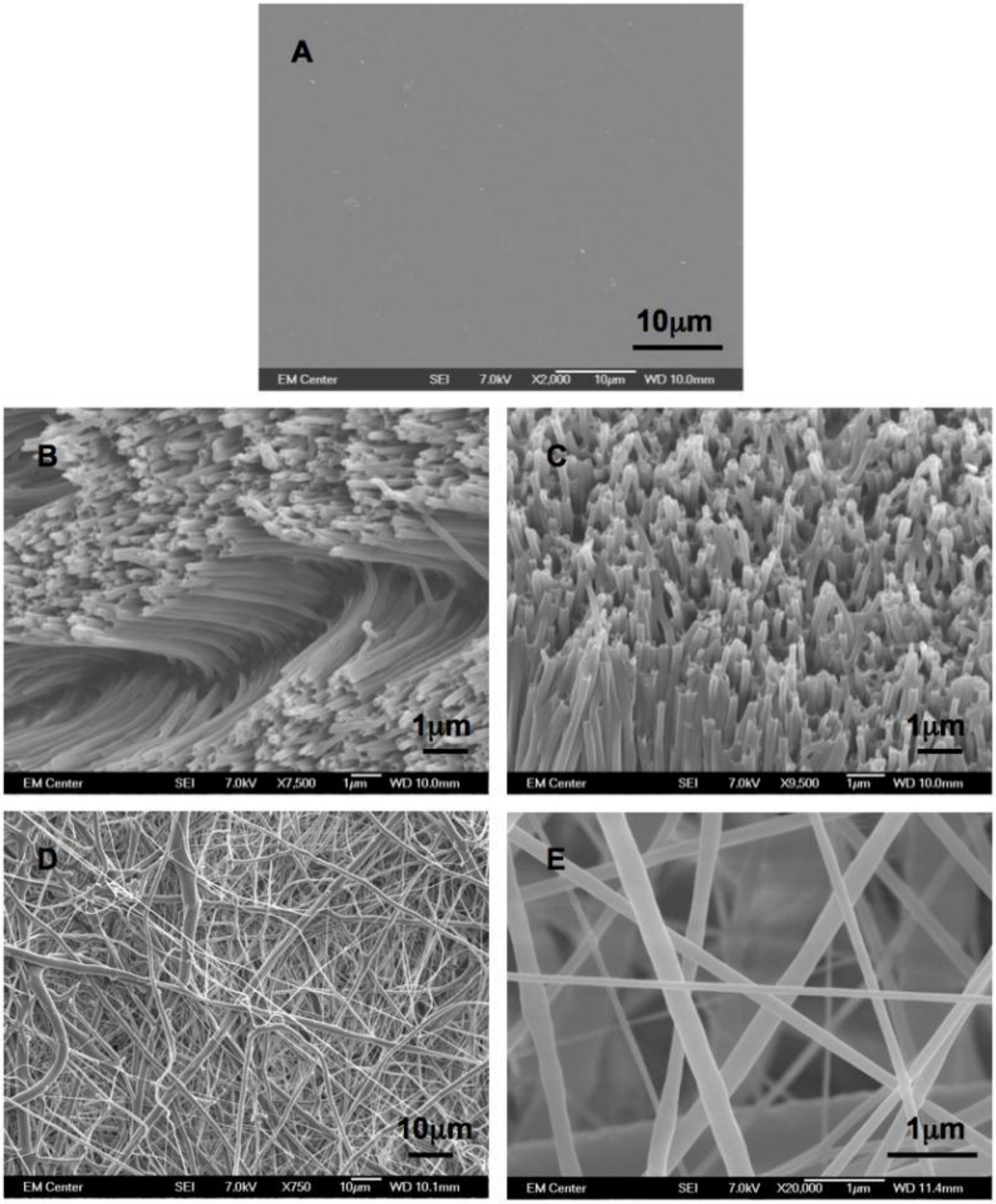

Figure 1.6.1.1: Representative SEM images of PCL (A), NW (B and C) and NF (D and E) surfaces [88]. Reproduced with permission from ref. 88. Copyright 2013, Taylor & Francis.

1.6.2 Fabrication methods

Various fabrication techniques have been developed to produce PCL nanostructured surfaces, each with distinct advantages and applications. Few of the fabrication methods for nanostructured PCL surfaces have been discussed below.

Electrospinning is one of the most predominant techniques for fabricating PCL nanofibers **(Figure 1.6.2.1)**. This method is used to fabricate nanofibers with diameters typically ranging from 200-900 nm, which closely mimic the extracellular matrix (ECM) [89,90]. The process involves applying a high voltage to a polymer solution, which causes the solution to form a jet that stretches and solidifies into fibers as it travels towards a collector [91,92].

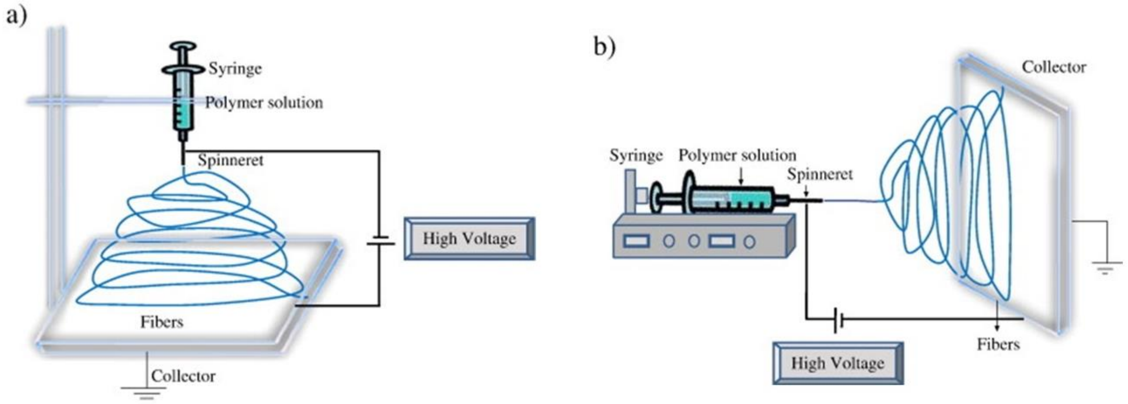

Figure 1.6.2.1: Schematic diagram of set up of an electrospinning apparatus (a) vertical setup (b) horizontal setup [92]. Reproduced with permission from ref. 92. Copyright 2010, Elsevier.

Electrospray technique is commonly used for producing PCL nanospheres. This technique involves the application of a high voltage to polymer solution, which creates a fine mist of charged droplets that evaporate to form nanospheres.

Electrospray allows for precise control over the size and morphology of the nanospheres, making it suitable for drug delivery applications where uniformity is crucial. The encapsulation efficiency of bioactive compounds can exceed 70%, enabling sustained release profiles that are beneficial for therapeutic applications [93,94].

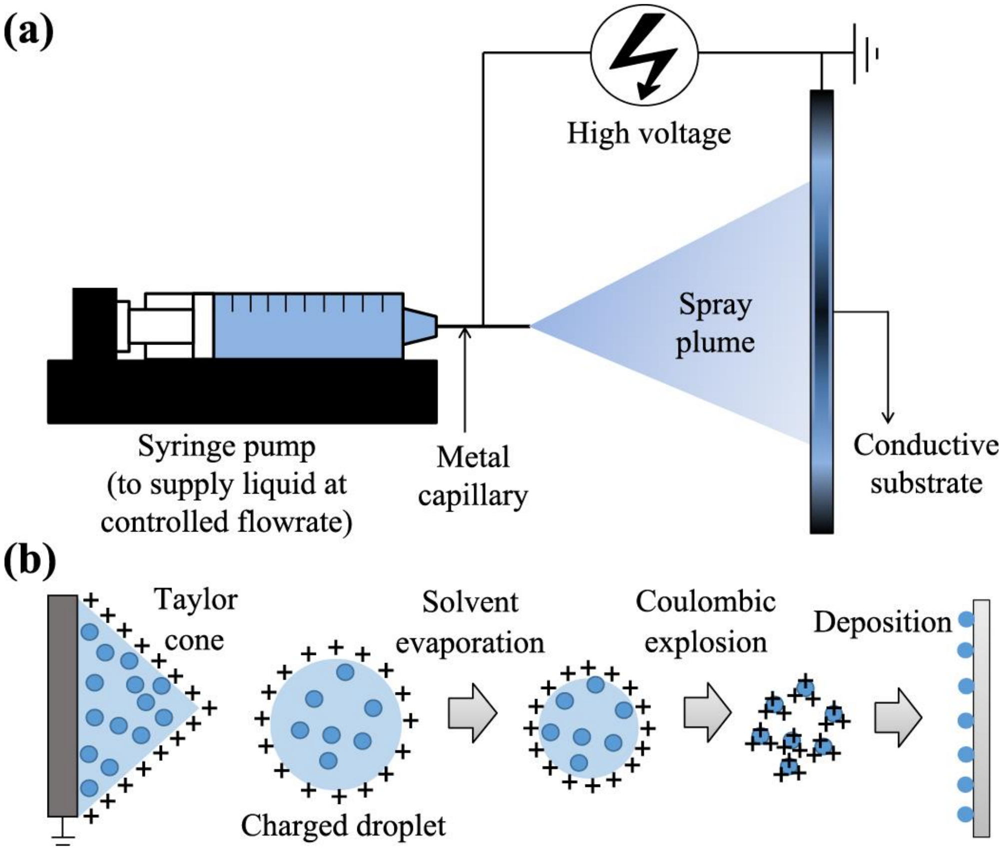

Figure 1.6.2.2: (a) Basic electrospraying setup and (b) Electrospraying mechanism [94]. Reproduced from ref. 94. Copyright 2018, Hosokawa Powder Technology Foundation.

Template assisted methods, particularly using anodic aluminum oxide (AAO) templates, have been utilized to create PCL nanowires with controlled dimensions and high aspect ratios. In this approach, PCL is deposited into the nanopores of the AAO template, and after solidification, the template is removed, leaving behind PCL nanowires.

This method allows precise control over the diameter and length of the nanowires, which can be tailored for specific applications. The use of templates also enables the fabrication of nanowires with complex geometries and arrangements [95,96].

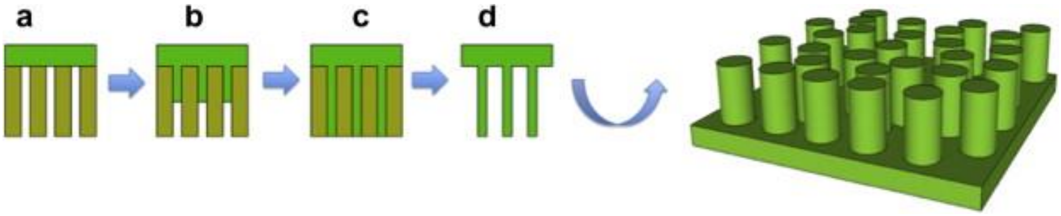

Figure 1.6.2.3: Schematic of PCL nanowire fabrication – (a) PCL is placed on top of the alumina nanoporous membrane; (b, c) PCL is extruded through the nanoporous membrane in a vacuum oven; (d) Alumina nanoporous membrane is dissolved in NaOH to release the nanowires [95]. Reproduced from ref. 95. Copyright 2010, Elsevier.

PCL nanoparticles can be synthesized using miniemulsion polymerization, where a PCL solution is emulsified in an aqueous phase, followed by polymerization under specific conditions. This method allows for the production of nanoparticles with controlled sizes and surface properties, which can be beneficial for drug delivery applications [97].

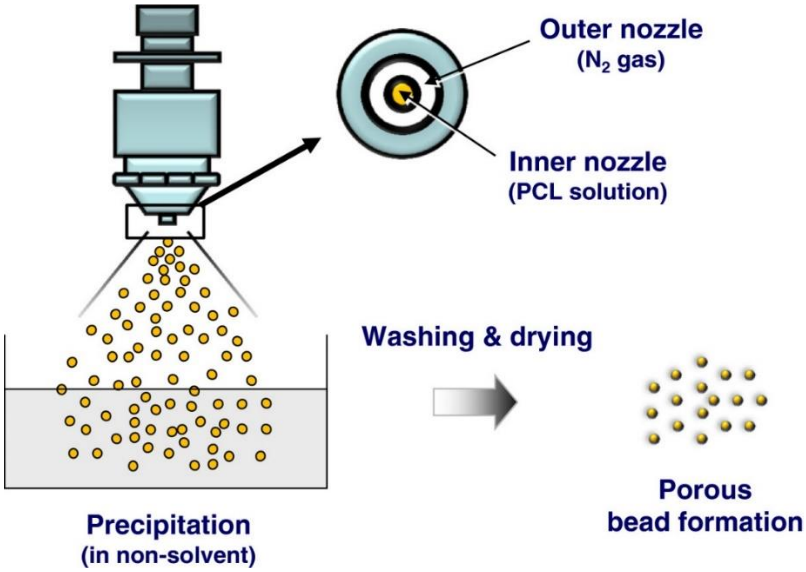

Figure 1.6.2.4: Schematic diagram showing the porous PCL beads fabrication procedure [97]. Reproduced with permission from ref. 97. Copyright 2014, Springer Nature.

1.7 Benefits of Organic Coatings

Organic coatings on bio-implants play a crucial role in enriching hemocompatibility, which is necessary for successful integration of the implants within the human body. Various organic coatings, including polymeric and biomolecular modifications, have been extensively studied for their capacity to improve the hemocompatibility of bio-implants. Organic coatings such as hydroxyapatite [98], chitosan [99–101], collagen [102–104], gelatin [105,106], keratin [107–110], cellulose [111–113], and silk fibroin [114,115] have been extensively researched and proven effective in enhancing the performance of bio-implants. For instance, fibrin-based coatings have been reported for showing significant reduction in platelet adhesion on nitinol implants [116]. Moreover, the use of zwitterionic polymers in coatings has been shown to further enhance hemocompatibility. PCL films modified with zwitterionic polymer brushes have been reported to exhibit reduced platelet adhesion and improved resistance to blood coagulation [117]. In this work, two such organic compounds, Tanfloc (TN) and Carboxymethyl Kappa-Carrageenan (CMKC), were chosen to examine their effects on the biocompatibility of PCL nanostructured surfaces.

TN coatings, derived from condensed tannins **(Figure 1.7.1)**, have gained attention in the field of biomaterials for its multifaceted benefits, particularly in enhancing biocompatibility, antibacterial properties and promoting osteogenesis. The unique chemical structure of TN, which includes catechol and pyrogallol groups, contributes to its superior antimicrobial activity compared to other natural polycations like chitosan [118,119]. Studies have demonstrated that TN/heparin polyelectrolyte multilayers significantly enhance blood compatibility by reducing fibrinogen adsorption and platelet adhesion, which are critical factors in preventing thrombosis on implant surfaces

[119,120]. This becomes an important characteristic for blood contacting devices, where maintaining blood flow and minimizing clot formation are essential for the longevity of the device and patient’s health. Additionally, TN’s inherent antibacterial properties contribute to its effectiveness in preventing biomaterial associated infections. The mechanism of action includes enzyme inactivation and chelation of trace metal ions, which disrupts bacterial growth and biofilm formation [118,121]. These advantageous properties of TN have compelled it to be incorporated in this study of hemocompatibility and antibacterial properties of surfaces.

Similarly, CMKC derived from kappa-carrageenan, a natural polysaccharide extracted from red algae **(Figure 1.7.1)**, has shown to be advantageous due to its biocompatibility, biodegradability and non-toxicity [122]. Studies have shown that CMKC exhibits favorable interactions with human cells, enhancing cell adhesion and proliferation [123]. Furthermore, CMKC has shown to significantly reduce bacterial colonization, which is an important factor in biomaterial implants. Thus, CMKC was chosen for this study due to its above-mentioned beneficial properties.

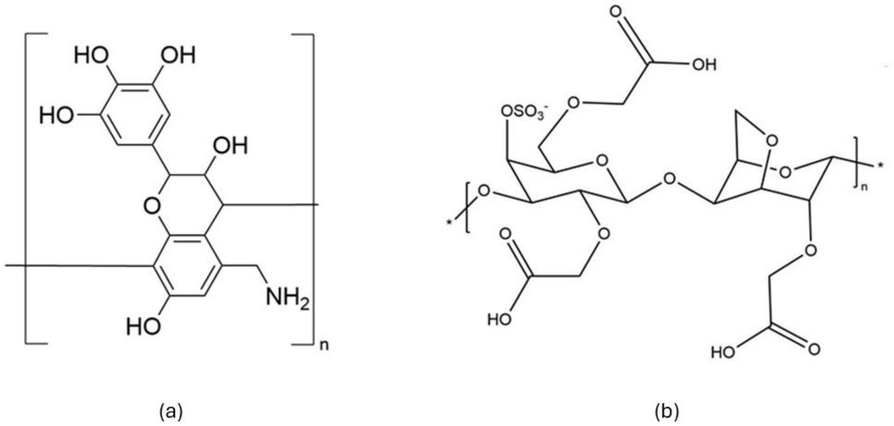

(a) (b)

Figure 1.7.1: (a) Chemical Structure of **TN** [124]. Adapted with permission from ref. 124. Copyright 2023, MDPI. (b) Chemical Structure of **CMKC** [122]. Adapted with permission from ref. 122. Copyright 2020, Elsevier.

REFERENCES

[1] M. Chaudhary, V. Balu, P. Sapkota, S. Kamei, Y.S. Devi, Effectiveness of SMART heart package on knowledge and practice regarding prevention of coronary artery disease among high-risk adults in selected urban community at Bangalore, J Educ Health Promot 12 (2023). https://doi.org/10.4103/JEHP.JEHP_260_23.

[2] S. Davalagi, R. Amuje, S. H, Cardiovascular Risk Assessment Among People With Type 2 Diabetes Mellitus in Urban Slums of Central Karnataka, India, Cureus 15 (2023). https://doi.org/10.7759/CUREUS.46687.

[3] D. Rath, Á. Petersen-Uribe, A. Avdiu, K. Witzel, P. Jaeger, M. Zdanyte, D. Heinzmann, E. Tavlaki, K. Müller, M.P. Gawaz, Impaired cardiac function is associated with mortality in patients with acute COVID-19 infection, Clinical Research in Cardiology 109 (2020) 1491–1499. https://doi.org/10.1007/S00392-020-01683-0/TABLES/3.

[4] F. Alzoughool, S. Abumweis, L. Alanagreh, M. Atoum, Associations of pre-existing cardiovascular morbidity with severity and the fatality rate in COVID-19 patients: a systematic review and meta-analysis, Osong Public Health Res Perspect 13 (2022) 37–50. https://doi.org/10.24171/J.PHRP.2021.0186.

[5] A.M.A. Shafi, S.A. Shaikh, M.M. Shirke, S. Iddawela, A. Harky, Cardiac manifestations in COVID-19 patients—A systematic review, J Card Surg 35 (2020) 1988–2008. https://doi.org/10.1111/JOCS.14808.

[6] T. Dalia, S. Lahan, S. Ranka, P. Acharya, A. Gautam, A. Goyal, I. Mastoris, A. Sauer, Z. Shah, Impact of congestive heart failure and role of cardiac biomarkers in

COVID-19 patients: A systematic review and meta-analysis, Indian Heart J 73 (2021) 91–98. https://doi.org/10.1016/J.IHJ.2020.12.002.

[7] K.O. Ndede, Z. Khan, F.K. Akumiah, M. Wanyoike, K.O. Ndede, Z. Khan, F.K. Akumiah, M. Wanyoike, A Retrospective Five-Year Study of Cardiovascular Risk Assessment and Risk-Based Interventions Among Hypertensive Patients in Nairobi Hospital, Kenya, Cureus 15 (2023). https://doi.org/10.7759/CUREUS.46097.

[8] N.G. Galiano, N. Eiro, A. Martín, O. Fernández-Guinea, C. del B. Martínez, F.J. Vizoso, Relationship between Arterial Calcifications on Mammograms and Cardiovascular Events: A Twenty-Three Year Follow-Up Retrospective Cohort Study, Biomedicines 2022, Vol. 10, Page 3227 10 (2022) 3227. https://doi.org/10.3390/BIOMEDICINES10123227.

[9] S.S. Martin, A.W. Aday, Z.I. Almarzooq, C.A.M. Anderson, P. Arora, C.L. Avery, C.M. Baker-Smith, B. Barone Gibbs, A.Z. Beaton, A.K. Boehme, Y. Commodore-Mensah, M.E. Currie, M.S.V. Elkind, K.R. Evenson, G. Generoso, D.G. Heard, S. Hiremath, M.C. Johansen, R. Kalani, D.S. Kazi, D. Ko, J. Liu, J.W. Magnani, E.D. Michos, M.E. Mussolino, S.D. Navaneethan, N.I. Parikh, S.M. Perman, R. Poudel, M. Rezk-Hanna, G.A. Roth, N.S. Shah, M.P. St-Onge, E.L. Thacker, C.W. Tsao, S.M. Urbut, H.G.C. Van Spall, J.H. Voeks, N.Y. Wang, N.D. Wong, S.S. Wong, K. Yaffe, L.P. Palaniappan, 2024 Heart Disease and Stroke Statistics: A Report of US and Global Data from the American Heart Association, Circulation 149 (2024) E347–E913. https://doi.org/10.1161/CIR.0000000000001209/SUPPL_FILE/SUB-SAHARAN.

[10] C. V. Ananth, C. Rutherford, E.B. Rosenfeld, J.S. Brandt, H. Graham, W.J. Kostis, K.M. Keyes, Epidemiologic trends and risk factors associated with the decline in mortality from coronary heart disease in the United States, 1990-2019, Am Heart J 263 (2023) 46–55. https://doi.org/10.1016/J.AHJ.2023.05.006.

[11] J. Stewart, G. Manmathan, P. Wilkinson, Primary prevention of cardiovascular disease: A review of contemporary guidance and literature, Http://Dx.Doi.Org/10.1177/2048004016687211 6 (2017) 204800401668721. https://doi.org/10.1177/2048004016687211.

[12] J. Iqbal, J. Gunn, P.W. Serruys, Coronary stents: historical development, current status and future directions, Br Med Bull 106 (2013) 193–211. https://doi.org/10.1093/BMB/LDT009.

[13] S. Borhani, S. Hassanajili, S.H. Ahmadi Tafti, S. Rabbani, Cardiovascular stents: overview, evolution, and next generation, Progress in Biomaterials 2018 7:3 7 (2018) 175–205. https://doi.org/10.1007/S40204-018-0097-Y.

[14] D. He, W. Liu, T. Zhang, The Development of Carotid Stent Material, Interv Neurol 3 (2015) 67–77. https://doi.org/10.1159/000369480.

[15] T. Simard, B. Hibbert, F.D. Ramirez, M. Froeschl, Y.X. Chen, E.R. O'Brien, The Evolution of Coronary Stents: A Brief Review, Canadian Journal of Cardiology 30 (2014) 35–45. https://doi.org/10.1016/J.CJCA.2013.09.012.

[16] K.R. Bainey, C.M. Norris, M.M. Graham, W.A. Ghali, M.L. Knudtson, R.C. Welsh, Clinical in-stent restenosis with bare metal stents: Is it truly a benign phenomenon?, Int J Cardiol 128 (2008) 378–382. https://doi.org/10.1016/J.IJCARD.2007.06.024.

[17] T. Suzuki, G. Kopia, S.I. Hayashi, L.R. Bailey, G. Llanos, R. Wilensky, B.D. Klugherz, G. Papandreou, P. Narayan, M.B. Leon, A.C. Yeung, F. Tio, P.S. Tsao, R. Falotico, A.J. Carter, Stent-based delivery of sirolimus reduces neointimal formation in a porcine coronary model, Circulation 104 (2001) 1188–1193. https://doi.org/10.1161/HC3601.093987/ASSET/3A99FDD6-B2E7-4360-90AB-846DB770ECC7/ASSETS/GRAPHIC/G5781F5.JPEG.

[18] A.M. Cherian, J. Joseph, M.B. Nair, S. V. Nair, V. Maniyal, D. Menon, Successful Reduction of Neointimal Hyperplasia on Stainless Steel Coronary Stents by Titania Nanotexturing, ACS Omega 5 (2020) 17582–17591. https://doi.org/10.1021/ACSOMEGA.0C02045/SUPPL_FILE/AO0C02045_SI_007.AVI.

[19] J. Wang, C. Song, Y. Xiao, B. Liu, In vivo and in vitro analyses of the effects of a novel high-nitrogen low-nickel coronary stent on reducing in-stent restenosis, Https://Doi.Org/10.1177/0885328218773306 33 (2018) 64–71. https://doi.org/10.1177/0885328218773306.

[20] M. Chiarito, R. Mehran, Panta rhei, also drug eluting stent technology, Catheterization and Cardiovascular Interventions 95 (2020) 1074–1075. https://doi.org/10.1002/CCD.28918.

[21] P. Rola, S. Włodarczak, A. Doroszko, M. Lesiak, A. Włodarczak, The bioresorbable magnesium scaffold (Magmaris)—State of the art: From basic concept to clinical application, Catheterization and Cardiovascular Interventions 100 (2022) 1051–1058. https://doi.org/10.1002/CCD.30435.

[22] T. Gori, Vascular Wall Reactions to Coronary Stents—Clinical Implications for Stent Failure, Life 2021, Vol. 11, Page 63 11 (2021) 63. https://doi.org/10.3390/LIFE11010063.

[23] T.T.H. Phan, J.E. Jones, M. Chen, T.L. Strawn, H.B. Khoukaz, Y. Ji, A. Kumar, D.K. Bowles, W.P. Fay, Q. Yu, In vitro biological responses of plasma nanocoatings for coronary stent applications, J Biomed Mater Res A 111 (2023) 1768–1780. https://doi.org/10.1002/JBM.A.37587.

[24] I. Marei, B. Ahmetaj-Shala, C.R. Triggle, Biofunctionalization of cardiovascular stents to induce endothelialization: Implications for in- stent thrombosis in diabetes, Front Pharmacol 13 (2022) 982185. https://doi.org/10.3389/FPHAR.2022.982185/BIBTEX.

[25] Coronary Stents | Capitol Cardiology Associates, (n.d.). https://www.capitolcardiology.com/coronary-stents (accessed October 13, 2024).

[26] L.J. Davidson, C.J. Davidson, Transcatheter Treatment of Valvular Heart Disease: A Review, JAMA 325 (2021) 2480–2494. https://doi.org/10.1001/JAMA.2021.2133.

[27] G.D. Dangas, J.I. Weitz, G. Giustino, R. Makkar, R. Mehran, Prosthetic Heart Valve Thrombosis, J Am Coll Cardiol 68 (2016) 2670–2689. https://doi.org/10.1016/J.JACC.2016.09.958.

[28] C.M. Otto, C.-C.A. Rick Nishimura, C.-C.O. Robert Bonow, F.A. Blase Carabello, F.P. John Erwin III, F. Federico Gentile, F. Hani Jneid, F. V Eric Krieger, F. Michael Mack, M. Christopher McLeod, F.T. Patrick O, Faha.H. Vera Rigolin, F.M. Thoralf Sundt III, F. Annemarie Thompson, C. Toly, C.M. Sana Al-Khatib, Faha. Anastasia Armbruster, A.K. Kim Birtcher, A. Joaquin Ciggaroa, Facc. Anita Deswal, F.L. Dave Dixon, F.A. Lee Fleisher, Faha. Lisa de las Fuentes, F. Federico Gentile, Facc.D. Zachary Goldberger, F.

Bulent Gorenek, F. Norrisa Haynes, M.F. Adrian Hernandez, M.A. Mark Hlatky, Faha.A. José Joglar, F.W. Schuyler Jones, F.E. Joseph Marine, Facc. Daniel Mark, F. Latha Palaniappan, F.R. Mariann Piano, F.S. Erica Spatz, F. Jacqueline Tamis-Holland, F.N. Duminda Wijeysundera, P.Y. Joseph Woo, 2020 ACC/AHA Guideline for the Management of Patients With Valvular Heart Disease: A Report of the American College of Cardiology/American Heart Association Joint Committee on Clinical Practice Guidelines, J Am Coll Cardiol 77 (2021) e25–e197. https://doi.org/10.1016/J.JACC.2020.11.018.

[29] F. Zhou, L.L. Wu, Y.Y. Cui, Y. Chen, J. Yang, N. Huang, A Method to Measure the Station of Artificial Mechanical Heart Valves, Adv Mat Res 683 (2013) 712–715. https://doi.org/10.4028/WWW.SCIENTIFIC.NET/AMR.683.712.

[30] J. Ghanbari, A. Dehparvar, A. Zakeri, Design and Analysis of Prosthetic Heart Valves and Assessing the Effects of Leaflet Design on the Mechanical Attributes of the Valves, Front Mech Eng 8 (2022) 764034. https://doi.org/10.3389/FMECH.2022.764034/BIBTEX.

[31] L. Liesenborghs, S. Meyers, M. Lox, M. Criel, J. Claes, M. Peetermans, S. Trenson, G. Vande Velde, P. Vanden Berghe, P. Baatsen, D. Missiakas, O. Schneewind, W.E. Peetermans, M.F. Hoylaerts, T. Vanassche, P. Verhamme, Staphylococcus aureus endocarditis: distinct mechanisms of bacterial adhesion to damaged and inflamed heart valves, Eur Heart J 40 (2019) 3248–3259. https://doi.org/10.1093/EURHEARTJ/EHZ175.

[32] Valvular heart disease | Heart and Stroke Foundation, (n.d.). https://www.heartandstroke.ca/heart-disease/conditions/valvular-heart-disease (accessed October 13, 2024).

[33] N. Roberts, U. Chandrasekaran, S. Das, Z. Qi, S. Corbett, Hemolysis associated with Impella heart pump positioning: In vitro hemolysis testing and computational fluid dynamics modeling, Https://Doi.Org/10.1177/0391398820909843 43 (2020) 710–718. https://doi.org/10.1177/0391398820909843.

[34] H.M. Ezzeldin, M.D. de Tullio, M. Vanella, S.D. Solares, E. Balaras, A Strain-Based Model for Mechanical Hemolysis Based on a Coarse-Grained Red Blood Cell Model, Ann Biomed Eng 43 (2015) 1398–1409. https://doi.org/10.1007/S10439-015-1273-Z/FIGURES/8.

[35] L. Li, L. Wei, H. Wang, Z. Zeng, J. Tan, S. Liu, G. Hao, Y. Weng, J. Chen, Proactive Hemocompatibility Platform Initiated by PAMAM Dendrimer Adapting to Key Components in Coagulation System, Mol Pharm 19 (2022) 4685–4695. https://doi.org/10.1021/ACS.MOLPHARMACEUT.2C00736/ASSET/IMAGES/MEDIUM/MP2C00736_0009.GIF.

[36] Q. Shi, Q. Fan, W. Ye, J. Hou, S.C. Wong, X. Xu, J. Yin, Controlled lecithin release from a hierarchical architecture on blood-contacting surface to reduce hemolysis of stored red blood cells, ACS Appl Mater Interfaces 6 (2014) 9808–9814. https://doi.org/10.1021/AM502241V/SUPPL_FILE/AM502241V_SI_001.PDF.

[37] J. Ford, J. Ford, Red blood cell morphology, Int J Lab Hematol 35 (2013) 351–357. https://doi.org/10.1111/IJLH.12082.

[38] C.W. Ong, P. Ho, H.L. Leo, Effects of Microporous Stent Graft on the Descending Aortic Aneurysm: A Patient-Specific Computational Fluid Dynamics Study, Artif Organs 40 (2016) E230–E240. https://doi.org/10.1111/AOR.12802.

[39] X. Wang, J. Miao, H. Zhao, C. Mao, X. Chen, J. Shen, Fabrication of nonbiofouling metal stent and in vitro studies on its hemocompatibility, Http://Dx.Doi.Org/10.1177/0885328213512703 29 (2013) 14–25. https://doi.org/10.1177/0885328213512703.

[40] M.S. Karbiner, L. Sierra, C. Minahk, M.C. Fonio, M.P. De Bruno, S. Jerez, The role of oxidative stress in alterations of hematological parameters and inflammatory markers induced by early hypercholesterolemia, Life Sci 93 (2013) 503–508. https://doi.org/10.1016/J.LFS.2013.08.003.

[41] Shape Variation Red Blood Cell Morphology Stock Vector (Royalty Free) 2454458759 | Shutterstock, (n.d.). https://www.shutterstock.com/image-vector/shape-variation-red-blood-cell-morphology-2454458759?irclickid=wu7SLxUqcxyKRKkyYAVkLSLUUkCRW-w1IxZLWY0&irgwc=1&pl=77643-108110&utm_campaign=TinEye&utm_content=108110&utm_medium=Affiliate&utm_source=77643&utm_term= (accessed October 13, 2024).

[42] K. Škrlová, K. Malachová, A. Muñoz-Bonilla, D. Měřinská, Z. Rybková, M. Fernández-García, D. Plachá, Biocompatible Polymer Materials with Antimicrobial Properties for Preparation of Stents, Nanomaterials 2019, Vol. 9, Page 1548 9 (2019) 1548. https://doi.org/10.3390/NANO9111548.

[43] F. Jummaat, E.B. Yahya, H.P.S. Abdul Khalil, A.S. Adnan, A.M. Alqadhi, C.K. Abdullah, A.K. Atty Sofea, N.G. Olaiya, M. Abdat, The Role of Biopolymer-Based

Materials in Obstetrics and Gynecology Applications: A Review, Polymers 2021, Vol. 13, Page 633 13 (2021) 633. https://doi.org/10.3390/POLYM13040633.

[44] T. Narancic, F. Cerrone, N. Beagan, K.E. O'Connor, Recent Advances in Bioplastics: Application and Biodegradation, Polymers 2020, Vol. 12, Page 920 12 (2020) 920. https://doi.org/10.3390/POLYM12040920.

[45] J. Cheng, J. Li, D. Deng, G. Wu, M. Zhou, G. Zhao, Z. Ni, Improved mechanical properties of poly(l-lactic acid) stent coated by poly(d, l-lactic acid) and poly(l-lactic-co-glycolic acid) biopolymer blend, Polym Adv Technol 33 (2022) 1109–1115. https://doi.org/10.1002/PAT.5584.

[46] S. Uthamaraj, B.J. Tefft, O. Hlinomaz, G.S. Sandhu, D. Dragomir-Daescu, Ferromagnetic Bare Metal Stent for Endothelial Cell Capture and Retention, J Vis Exp 2015 (2015) e53100. https://doi.org/10.3791/53100.

[47] L. Nguyen, L.C. Xu, E. Yeager, W.J. Weiss, C.A. Siedlecki, In vitro evaluation of blood plasma coagulation responses to four medical-grade polyurethane polymers, J Biomater Appl 38 (2023) 302–310. https://doi.org/10.1177/08853282231191410/ASSET/IMAGES/LARGE/10.1177_08853282231191410-FIG6.JPEG.

[48] H. Wang, Y. Hu, D. Lynch, M. Young, S. Li, H. Cong, F.J. Xu, G. Cheng, Zwitterionic Polyurethanes with Tunable Surface and Bulk Properties, ACS Appl Mater Interfaces 10 (2018) 37609–37617. https://doi.org/10.1021/ACSAMI.8B10450/SUPPL_FILE/AM8B10450_SI_001.PDF.

[49] Y. Liu, Z. Liu, Y. Gao, W. Gao, Z. Hou, Y. Zhu, Facile Method for Surface-Grafted Chitooligosaccharide on Medical Segmented Poly(ester-urethane) Film to Improve Surface Biocompatibility, Membranes 2021, Vol. 11, Page 37 11 (2021) 37. https://doi.org/10.3390/MEMBRANES11010037.

[50] Y. Koga, H. Fujieda, H. Meguro, Y. Ueno, T. Aoki, K. Miwa, M. Kainoh, Biocompatibility of Polysulfone Hemodialysis Membranes and Its Mechanisms: Involvement of Fibrinogen and Its Integrin Receptors in Activation of Platelets and Neutrophils, Artif Organs 42 (2018) E246–E258. https://doi.org/10.1111/AOR.13268.

[51] Y. Koga, H. Meguro, H. Fujieda, Y. Ueno, K. Miwa, M. Kainoh, A new hydrophilic polysulfone hemodialysis membrane can prevent platelet–neutrophil interactions and successive neutrophil activation, International Journal of Artificial Organs 42 (2019) 175–181. https://doi.org/10.1177/0391398818823767/ASSET/IMAGES/LARGE/10.1177_0391398818823767-FIG4.JPEG.

[52] T.T. Li, M. Yan, Q. Jiang, H.K. Peng, J.H. Lin, C.W. Lou, Characterization and Microstructure of Linear Electrode-Electrospun Graphene-Filled Polyvinyl Alcohol Nanofiber Films, Materials 2018, Vol. 11, Page 1033 11 (2018) 1033. https://doi.org/10.3390/MA11061033.

[53] N. Alexandre, J. Ribeiro, A. Gärtner, T. Pereira, I. Amorim, J. Fragoso, A. Lopes, J. Fernandes, E. Costa, A. Santos-Silva, M. Rodrigues, J.D. Santos, A.C. Maurício, A.L. Luís, Biocompatibility and hemocompatibility of polyvinyl alcohol hydrogel used for

vascular grafting—In vitro and in vivo studies, J Biomed Mater Res A 102 (2014) 4262–4275. https://doi.org/10.1002/JBM.A.35098.

[54] L. Meneses, A. Esmail, M. Matos, C. Sevrin, C. Grandfils, S. Barreiros, M.A.M. Reis, F. Freitas, A. Paiva, Subcritical Water as a Pre-Treatment of Mixed Microbial Biomass for the Extraction of Polyhydroxyalkanoates, Bioengineering 9 (2022) 302. https://doi.org/10.3390/bioengineering9070302.

[55] L.Y. Huang, M.C. Yang, H.M. Tsou, T.Y. Liu, Hemocompatibility and anti-fouling behavior of multilayer biopolymers immobilized on gold-thiolized drug-eluting cardiovascular stents, Colloids Surf B Biointerfaces 173 (2019) 470–477. https://doi.org/10.1016/J.COLSURFB.2018.10.014.

[56] J. Domínguez-Robles, N.K. Martin, M.L. Fong, S.A. Stewart, N.J. Irwin, M.I. Rial-Hermida, R.F. Donnelly, E. Larrañeta, Antioxidant PLA Composites Containing Lignin for 3D Printing Applications: A Potential Material for Healthcare Applications, Pharmaceutics 2019, Vol. 11, Page 165 11 (2019) 165. https://doi.org/10.3390/PHARMACEUTICS11040165.

[57] A. Rasool, M. Rizwan, A. Islam, H. Abdullah, S.S. Shafqat, M.K. Azeem, T. Rasheed, M. Bilal, Chitosan-Based Smart Polymeric Hydrogels and Their Prospective Applications in Biomedicine, Starch - Stärke 76 (2024) 2100150. https://doi.org/10.1002/STAR.202100150.

[58] G.A. Martau, M. Mihai, D.C. Vodnar, The Use of Chitosan, Alginate, and Pectin in the Biomedical and Food Sector—Biocompatibility, Bioadhesiveness, and

Biodegradability, Polymers 2019, Vol. 11, Page 1837 11 (2019) 1837. https://doi.org/10.3390/POLYM11111837.

[59] E. Valsecchi, M. Biagiotti, A. Alessandrino, D. Gastaldi, P. Vena, G. Freddi, Silk Vascular Grafts with Optimized Mechanical Properties for the Repair and Regeneration of Small Caliber Blood Vessels, Materials 15 (2022) 3735. https://doi.org/10.3390/MA15103735/S1.

[60] T. Tanaka, R. Tanaka, Y. Ogawa, Y. Takagi, M. Sata, T. Asakura, Evaluation of small-diameter silk vascular grafts implanted in dogs, JTCVS Open 6 (2021) 148–156. https://doi.org/10.1016/j.xjon.2021.02.008.

[61] K.T. Valencia-Rivero, J.C. Cruz, N. Wagner-Gutierrez, A. D’Amore, M.C. Miranda, R. López, A. Guerrero, W. Wagner, N. Sandoval, J.C. Bricenõ, Evaluation of Microscopic Structure-Function Relationships of PEGylated Small Intestinal Submucosa Vascular Grafts for Arteriovenous Connection, ACS Appl Bio Mater 2 (2019) 3706–3721. https://doi.org/10.1021/ACSABM.9B00158/ASSET/IMAGES/MEDIUM/MT-2019-00158C_0014.GIF.

[62] R. Guo, Y. Zhou, S. Liu, C. Li, C. Lu, G. Yang, J. Nie, F. Wang, N.G. Dong, J. Shi, Anticalcification Potential of POSS-PEG Hybrid Hydrogel as a Scaffold Material for the Development of Synthetic Heart Valve Leaflets, ACS Appl Bio Mater 4 (2021) 2534–2543. https://doi.org/10.1021/ACSABM.0C01544/ASSET/IMAGES/MEDIUM/MT0C01544_0008.GIF.

[63] C. Li, Y. Zhou, S. Liu, R. Guo, C. Lu, D. Yin, Y. Zhang, X. Xu, N. Dong, J. Shi, Surface Modification of Decellularized Heart Valve by the POSS-PEG Hybrid Hydrogel to

Prepare a Composite Scaffold Material with Anticalcification Potential, ACS Appl Bio Mater 5 (2022) 3923–3935. https://doi.org/10.1021/ACSABM.2C00449/ASSET/IMAGES/MEDIUM/MT2C00449_0013.GIF.

[64] D. Radke, W. Jia, D. Sharma, K. Fena, G. Wang, J. Goldman, F. Zhao, Tissue Engineering at the Blood-Contacting Surface: A Review of Challenges and Strategies in Vascular Graft Development, Adv Healthc Mater 7 (2018) 1701461. https://doi.org/10.1002/ADHM.201701461.

[65] E. Malikmammadov, T.E. Tanir, A. Kiziltay, V. Hasirci, N. Hasirci, PCL and PCL-based materials in biomedical applications, J Biomater Sci Polym Ed 29 (2018) 863–893. https://doi.org/10.1080/09205063.2017.1394711.

[66] Y. Pan, X. Zhou, Y. Wei, Q. Zhang, T. Wang, M. Zhu, W. Li, R. Huang, R. Liu, J. Chen, G. Fan, K. Wang, D. Kong, Q. Zhao, Small-diameter hybrid vascular grafts composed of polycaprolactone and polydioxanone fibers, Scientific Reports 2017 7:1 7 (2017) 1–11. https://doi.org/10.1038/s41598-017-03851-1.

[67] N. Diban, S. Haimi, L. Bolhuis-Versteeg, S. Teixeira, S. Miettinen, A. Poot, D. Grijpma, D. Stamatialis, Hollow fibers of poly(lactide-co-glycolide) and poly(ε-caprolactone) blends for vascular tissue engineering applications, Acta Biomater 9 (2013) 6450–6458. https://doi.org/10.1016/J.ACTBIO.2013.01.005.

[68] L. Zhao, X. Li, L. Yang, L. Sun, S. Mu, H. Zong, Q. Li, F. Wang, S. Song, C. Yang, C. Zhao, H. Chen, R. Zhang, S. Wang, Y. Dong, Q. Zhang, Evaluation of remodeling and

regeneration of electrospun PCL/fibrin vascular grafts in vivo, Materials Science and Engineering: C 118 (2021) 111441. https://doi.org/10.1016/J.MSEC.2020.111441.

[69] A.P. Khandwekar, D.P. Patil, Y. Shouche, M. Doble, Surface engineering of polycaprolactone by biomacromolecules and their blood compatibility, J Biomater Appl 26 (2011) 227–252. https://doi.org/10.1177/0885328210367442/SUPPL_FILE/SUPPLEMENTARY_MATERIAL.DOC.

[70] I.H. Jaffer, J.C. Fredenburgh, J. Hirsh, J.I. Weitz, Medical device-induced thrombosis: What causes it and how can we prevent it?, Journal of Thrombosis and Haemostasis 13 (2015) S72–S81. https://doi.org/10.1111/JTH.12961/ASSET/4B8B3685-B0CD-41BE-B249-0BDDE8A7A501/MAIN.ASSETS/JTH12961-FIG-0001-M.JPG.

[71] R.A. Hoshi, R. Van Lith, M.C. Jen, J.B. Allen, K.A. Lapidos, G. Ameer, The blood and vascular cell compatibility of heparin-modified ePTFE vascular grafts, Biomaterials 34 (2013) 30–41. https://doi.org/10.1016/J.BIOMATERIALS.2012.09.046.

[72] F.J. Calero Castro, Y. Yuste, S. Pereira, M.D. Garvín, M.Á. López García, F.J. Padillo, F. de la Portilla, Proof of concept, design, and manufacture via 3-D printing of a mesh with bactericidal capacity: Behaviour in vitro and in vivo, J Tissue Eng Regen Med 13 (2019) 1955–1964. https://doi.org/10.1002/TERM.2944.

[73] S.A. Stewart, J. Domínguez-Robles, V.J. McIlorum, Z. Gonzalez, E. Utomo, E. Mancuso, D.A. Lamprou, R.F. Donnelly, E. Larrañeta, Poly(caprolactone)-Based Coatings on 3D-Printed Biodegradable Implants: A Novel Strategy to Prolong Delivery of Hydrophilic Drugs, Mol Pharm 17 (2020) 3487–3500.

https://doi.org/10.1021/ACS.MOLPHARMACEUT.0C00515/SUPPL_FILE/MP0C00515_LIVESLIDES.MP4.

[74] M. Delgado-Aguilar, R. Puig, I. Sazdovski, P. Fullana-i-Palmer, Polylactic Acid/Polycaprolactone Blends: On the Path to Circular Economy, Substituting Single-Use Commodity Plastic Products, Materials 2020, Vol. 13, Page 2655 13 (2020) 2655. https://doi.org/10.3390/MA13112655.

[75] R. Pawar, A. Pathan, S. Nagaraj, H. Kapare, P. Giram, R. Wavhale, Polycaprolactone and its derivatives for drug delivery, Polym Adv Technol 34 (2023) 3296–3316. https://doi.org/10.1002/PAT.6140.

[76] J. Schmid, S. Schwarz, M. Fischer, S. Sudhop, H. Clausen-Schaumann, M. Schieker, R. Huber, A laser-cutting-based manufacturing process for the generation of three-dimensional scaffolds for tissue engineering using Polycaprolactone/Hydroxyapatite composite polymer, J Tissue Eng 10 (2019). https://doi.org/10.1177/2041731419859157/ASSET/IMAGES/LARGE/10.1177_2041731419859157-FIG8.JPEG.

[77] H. Lönnberg, K. Larsson, T. Lindström, A. Hult, E. Malmström, Synthesis of polycaprolactone-grafted microfibrillated cellulose for use in novel bionanocomposites-influence of the graft length on the mechanical properties, ACS Appl Mater Interfaces 3 (2011) 1426–1433. https://doi.org/10.1021/AM2001828/ASSET/IMAGES/MEDIUM/AM-2011-001828_0012.GIF.

[78] N. Sriputtha, F. Wiwatwongwana, N. Promma, Investigation of Polycaprolactone/Carboxymethyl Cellulose Scaffolds by Mechanical and Thermal

Analysis, Engineering, Technology & Applied Science Research 12 (2022) 8175–8179. https://doi.org/10.48084/ETASR.4711.

[79] N.K. Singh, S.K. Singh, D. Dash, B.P. Das Purkayastha, J.K. Roy, P. Maiti, Nanostructure controlled anti-cancer drug delivery using poly(ε-caprolactone) based nanohybrids, J Mater Chem 22 (2012) 17853–17863. https://doi.org/10.1039/C2JM32340K.

[80] F.C. Menezes, N.M. Siqueira, S. Fung, J.M. Scheibel, D.J. Moura, M. Guvendiren, J. Kohn, R.M.D. Soares, Effect of crosslinking, hydroxyapatite addition, and fiber alignment to stimulate human mesenchymal stem cells osteoinduction in polycaprolactone-based electrospun scaffolds, Polym Adv Technol 33 (2022) 2682–2695. https://doi.org/10.1002/PAT.5723.

[81] M.R. Steedman, S.L. Tao, H. Klassen, T.A. Desai, Enhanced differentiation of retinal progenitor cells using microfabricated topographical cues, Biomed Microdevices 12 (2010) 363–369. https://doi.org/10.1007/S10544-009-9392-7/FIGURES/4.

[82] F. Hizal, N. Rungraeng, J. Lee, S. Jun, H.J. Busscher, H.C. Van Der Mei, C.H. Choi, Nanoengineered Superhydrophobic Surfaces of Aluminum with Extremely Low Bacterial Adhesivity, ACS Appl Mater Interfaces 9 (2017) 12118–12129. https://doi.org/10.1021/ACSAMI.7B01322/SUPPL_FILE/AM7B01322_SI_001.PDF.

[83] J. Jenkins, J. Mantell, C. Neal, A. Gholinia, P. Verkade, A.H. Nobbs, B. Su, Antibacterial effects of nanopillar surfaces are mediated by cell impedance, penetration and induction of oxidative stress, Nature Communications 2020 11:1 11 (2020) 1–14. https://doi.org/10.1038/s41467-020-15471-x.

[84] E.P. Ivanova, D.P. Linklater, M. Werner, V.A. Baulin, X.M. Xu, N. Vrancken, S. Rubanov, E. Hanssen, J. Wandiyanto, V.K. Truong, A. Elbourne, S. Maclaughlin, S. Juodkazis, R.J. Crawford, The multi-faceted mechano-bactericidal mechanism of nanostructured surfaces, Proc Natl Acad Sci U S A 117 (2020) 12598–12605. https://doi.org/10.1073/PNAS.1916680117/SUPPL_FILE/PNAS.1916680117.SAPP.PDF.

[85] V. Leszczak, D.A. Baskett, K.C. Popat, Endothelial Cell Growth and Differentiation on Collagen-Immobilized Polycaprolactone Nanowire Surfaces, J Biomed Nanotechnol 11 (2015) 1080–1092. https://doi.org/10.1166/JBN.2015.2021.

[86] V. Leszczak, D.A. Baskett, K.C. Popat, Smooth Muscle Cell Functionality on Collagen Immobilized Polycaprolactone Nanowire Surfaces, Journal of Functional Biomaterials 2014, Vol. 5, Pages 58-77 5 (2014) 58–77. https://doi.org/10.3390/JFB5020058.

[87] V. Leszczak, K.C. Popat, Improved in vitro blood compatibility of polycaprolactone nanowire surfaces, ACS Appl Mater Interfaces 6 (2014) 15913–15924. https://doi.org/10.1021/AM503508R/ASSET/IMAGES/LARGE/AM-2014-03508R_0015.JPEG.

[88] V. Leszczak, B.S. Smith, K.C. Popat, Hemocompatibility of polymeric nanostructured surfaces, J Biomater Sci Polym Ed 24 (2013) 1529–1548. https://doi.org/10.1080/09205063.2013.777228.

[89] B. Ekram, B.M. Abdel-Hady, A.M. El-Kady, S.M. Amr, A.I. Waley, O.W. Guirguis, Optimum parameters for the production of nano-scale electrospun polycaprolactone to

be used as a biomedical material, Advances in Natural Sciences: Nanoscience and Nanotechnology 8 (2017) 045018. https://doi.org/10.1088/2043-6254/AA92B4.

[90] C.J. Luo, E. Stride, M. Edirisinghe, Mapping the influence of solubility and dielectric constant on electrospinning polycaprolactone solutions, Macromolecules 45 (2012) 4669–4680. https://doi.org/10.1021/MA300656U/SUPPL_FILE/MA300656U_SI_001.PDF.

[91] Z. Fang, S. Zhang, H. Wang, X. Geng, L. Ye, A.Y. Zhang, Z.G. Feng, Preparation and Evaluation of Core-Shell Nanofibers Electrospun from PEU and PCL Blends via a Single-Nozzle Spinneret, ACS Appl Polym Mater 5 (2023) 2382–2393. https://doi.org/10.1021/ACSAPM.2C02076/SUPPL_FILE/AP2C02076_SI_001.PDF.

[92] N. Bhardwaj, S.C. Kundu, Electrospinning: A fascinating fiber fabrication technique, Biotechnol Adv 28 (2010) 325–347. https://doi.org/10.1016/J.BIOTECHADV.2010.01.004.

[93] N.J. Castro, C.M. O'Brien, L.G. Zhang, Biomimetic biphasic 3-D nanocomposite scaffold for osteochondral regeneration, AIChE Journal 60 (2014) 432–442. https://doi.org/10.1002/AIC.14296.

[94] S. Saallah, I.W. Lenggoro, Nanoparticles Carrying Biological Molecules: Recent Advances and Applications, KONA Powder and Particle Journal 35 (2018) 89–111. https://doi.org/10.14356/KONA.2018015.

[95] S.L. Bechara, A. Judson, K.C. Popat, Template synthesized poly(ε-caprolactone) nanowire surfaces for neural tissue engineering, Biomaterials 31 (2010) 3492–3501. https://doi.org/10.1016/J.BIOMATERIALS.2010.01.084.

[96] M.R. Koblischka, A. Koblischka-Veneva, Fabrication of Superconducting Nanowires Using the Template Method, Nanomaterials 2021, Vol. 11, Page 1970 11 (2021) 1970. https://doi.org/10.3390/NANO11081970.

[97] J.H. Byun, H.A.R. Lee, T.H. Kim, J.H. Lee, S.H. Oh, Effect of porous polycaprolactone beads on boneregeneration: Preliminary in vitro and in vivo studies, Biomater Res 18 (2014). https://doi.org/10.1186/2055-7124-18-18/SUPPL_FILE/2055-7124-18-18.F7.PDF.

[98] S.M. Kim, J.H. Jo, S.M. Lee, M.H. Kang, H.E. Kim, Y. Estrin, J.H. Lee, J.W. Lee, Y.H. Koh, Hydroxyapatite-coated magnesium implants with improved in vitro and in vivo biocorrosion, biocompatibility, and bone response, J Biomed Mater Res A 102 (2014) 429–441. https://doi.org/10.1002/JBM.A.34718.

[99] H. Ruan, A. Aulova, V. Ghai, S. Pandit, M. Lovmar, I. Mijakovic, R. Kádár, Polysaccharide-based antibacterial coating technologies, Acta Biomater 168 (2023) 42–77. https://doi.org/10.1016/J.ACTBIO.2023.07.023.

[100] S. Kumari, H.R. Tiyyagura, Y.B. Pottathara, K.K. Sadasivuni, D. Ponnamma, T.E.L. Douglas, A.G. Skirtach, M.K. Mohan, Surface functionalization of chitosan as a coating material for orthopaedic applications: A comprehensive review, Carbohydr Polym 255 (2021) 117487. https://doi.org/10.1016/J.CARBPOL.2020.117487.

[101] J. Ballarre, T. Aydemir, L. Liverani, J.A. Roether, W.H. Goldmann, A.R. Boccaccini, Versatile bioactive and antibacterial coating system based on silica, gentamicin, and chitosan: Improving early stage performance of titanium implants, Surf Coat Technol 381 (2020) 125138. https://doi.org/10.1016/J.SURFCOAT.2019.125138.

[102] C. Ersanli, A. Tzora, I. Skoufos, C. Voidarou, D.I. Zeugolis, Recent Advances in Collagen Antimicrobial Biomaterials for Tissue Engineering Applications: A Review, International Journal of Molecular Sciences 2023, Vol. 24, Page 7808 24 (2023) 7808. https://doi.org/10.3390/IJMS24097808.

[103] B. Kaczmarek-Szczepańska, I. Polkowska, M. Małek, J. Kluczyński, K. Paździor-Czapula, M. Wekwejt, A. Michno, A. Ronowska, A. Pałubicka, B. Nowicka, I. Otrocka-Domagała, The characterization of collagen-based scaffolds modified with phenolic acids for tissue engineering application, Scientific Reports 2023 13:1 13 (2023) 1–12. https://doi.org/10.1038/s41598-023-37161-6.

[104] E. Rezvani Ghomi, N. Nourbakhsh, M. Akbari Kenari, M. Zare, S. Ramakrishna, Collagen-based biomaterials for biomedical applications, J Biomed Mater Res B Appl Biomater 109 (2021) 1986–1999. https://doi.org/10.1002/JBM.B.34881.

[105] A. Bin Rashid, N.N. Showva, M.E. Hoque, Gelatin-based scaffolds: An intuitive support structure for regenerative therapy, Curr Opin Biomed Eng 26 (2023) 100452. https://doi.org/10.1016/J.COBME.2023.100452.

[106] I. Lukin, I. Erezuma, L. Maeso, J. Zarate, M.F. Desimone, T.H. Al-Tel, A. Dolatshahi-Pirouz, G. Orive, Progress in Gelatin as Biomaterial for Tissue Engineering, Pharmaceutics 14 (2022) 1177. https://doi.org/10.3390/PHARMACEUTICS14061177.

[107] H. Diwan, M.K. Sah, Exploring the potential of keratin-based biomaterials in orthopedic tissue engineering: a comprehensive review, Emergent Materials 2023 6:5 6 (2023) 1441–1460. https://doi.org/10.1007/S42247-023-00545-5.

[108] S. Feroz, N. Muhammad, J. Ranayake, G. Dias, Keratin - Based materials for biomedical applications, Bioact Mater 5 (2020) 496–509. https://doi.org/10.1016/J.BIOACTMAT.2020.04.007.

[109] G.M. Fortunato, F. Da Ros, S. Bisconti, A. De Acutis, F. Biagini, A. Lapomarda, C. Magliaro, C. De Maria, F. Montemurro, D. Bizzotto, P. Braghetta, G. Vozzi, Electrospun structures made of a hydrolyzed keratin-based biomaterial for development of in vitro tissue models, Front Bioeng Biotechnol 7 (2019) 470697. https://doi.org/10.3389/FBIOE.2019.00174/BIBTEX.

[110] F. Costa, R. Silva, A.R. Boccaccini, Fibrous protein-based biomaterials (silk, keratin, elastin, and resilin proteins) for tissue regeneration and repair, Peptides and Proteins as Biomaterials for Tissue Regeneration and Repair (2018) 175–204. https://doi.org/10.1016/B978-0-08-100803-4.00007-3.

[111] J. Jeevanandam, J. Rodrigues, S. Pan, M.K. Danquah, Cellulose-based bionanocomposites: Synthesis, properties, and applications, Advances in Bionanocomposites: Materials, Applications, and Life Cycle (2024) 191–210. https://doi.org/10.1016/B978-0-323-91764-3.00011-5.

[112] E. Rezvani Ghomi, N. Nourbakhsh, M. Akbari Kenari, M. Zare, S. Ramakrishna, Collagen-based biomaterials for biomedical applications, J Biomed Mater Res B Appl Biomater 109 (2021) 1986–1999. https://doi.org/10.1002/JBM.B.34881.

[113] K. Lin, D. Zhang, M.H. Macedo, W. Cui, B. Sarmento, G. Shen, Advanced Collagen-Based Biomaterials for Regenerative Biomedicine, Adv Funct Mater 29 (2019) 1804943. https://doi.org/10.1002/ADFM.201804943.

[114] A.G. Păun, C. Dumitriu, C. Ungureanu, S. Popescu, Silk Fibroin/ZnO Coated TiO2 Nanotubes for Improved Antimicrobial Effect of Ti Dental Implants, Materials 2023, Vol. 16, Page 5855 16 (2023) 5855. https://doi.org/10.3390/MA16175855.

[115] Y. Kambe, Functionalization of silk fibroin-based biomaterials for tissue engineering, Polymer Journal 2021 53:12 53 (2021) 1345–1351. https://doi.org/10.1038/s41428-021-00536-5.

[116] A. Link, T. Michel, M. Schaller, T. Tronser, S. Krajewski, G. Cattaneo, In vitro investigation of an intracranial flow diverter with a fibrin-based, hemostasis mimicking, nanocoating, Biomedical Materials 16 (2020) 015026. https://doi.org/10.1088/1748-605X/ABC8D3.

[117] H. Jiang, X.B. Wang, C.Y. Li, J.S. Li, F.J. Xu, C. Mao, W.T. Yang, J. Shen, Improvement of hemocompatibility of polycaprolactone film surfaces with zwitterionic polymer brushes, Langmuir 27 (2011) 11575–11581. https://doi.org/10.1021/LA202101Q/ASSET/IMAGES/LARGE/LA-2011-02101Q_0009.JPEG.

[118] S. Baghersad, L.Y.C. Madruga, A.F. Martins, K.C. Popat, M.J. Kipper, Expanding the Scope of an Amphoteric Condensed Tannin, Tanfloc, for Antibacterial Coatings, J Funct Biomater 14 (2023) 554. https://doi.org/10.3390/JFB14110554/S1.

[119] V.K. Manivasagam, R.M. Sabino, P. Kantam, K.C. Popat, Surface modification strategies to improve titanium hemocompatibility: a comprehensive review, Mater Adv 2 (2021) 5824–5842. https://doi.org/10.1039/D1MA00367D.

[120] R.M. Sabino, K. Kauk, L.Y.C. Madruga, M.J. Kipper, A.F. Martins, K.C. Popat, Enhanced hemocompatibility and antibacterial activity on titania nanotubes with tanfloc/heparin polyelectrolyte multilayers, J Biomed Mater Res A 108 (2020) 992–1005. https://doi.org/10.1002/JBM.A.36876.

[121] P. Li, R. Yin, J. Cheng, J. Lin, Bacterial Biofilm Formation on Biomaterials and Approaches to Its Treatment and Prevention, International Journal of Molecular Sciences 2023, Vol. 24, Page 11680 24 (2023) 11680. https://doi.org/10.3390/IJMS241411680.

[122] L.Y.C. Madruga, R.M. Sabino, E.C.G. Santos, K.C. Popat, R. de C. Balaban, M.J. Kipper, Carboxymethyl-kappa-carrageenan: A study of biocompatibility, antioxidant and antibacterial activities, Int J Biol Macromol 152 (2020) 483–491. https://doi.org/10.1016/J.IJBIOMAC.2020.02.274.

[123] S. Abbasi-Ravasjani, H. Seddiqi, A. Moghaddaszadeh, M.E. Ghiasvand, J. Jin, E. Oliaei, R.G. Bacabac, J. Klein-Nulend, Sulfated carboxymethyl cellulose and carboxymethyl κ-carrageenan immobilization on 3D-printed poly-ε-caprolactone scaffolds differentially promote pre-osteoblast proliferation and osteogenic activity, Front Bioeng Biotechnol 10 (2022) 957263. https://doi.org/10.3389/FBIOE.2022.957263/BIBTEX.

[124] S. Baghersad, L.Y.C. Madruga, A.F. Martins, K.C. Popat, M.J. Kipper, Expanding the Scope of an Amphoteric Condensed Tannin, Tanfloc, for Antibacterial Coatings, J Funct Biomater 14 (2023) 554. https://doi.org/10.3390/jfb14110554.

CHAPTER 2

FABRICATION AND CHARACTERIZATION OF PCL NANOSTRUCTURED SURFACES

2.1 Introduction

Surface properties of materials used for biomedical implants and blood contacting devices have a major influence on the biocompatibility of the materials. Modifying surface properties such as surface topography, surface chemistry, surface wettability has shown a large impact on the compatibility of the materials. In synthetic polymers, PCL has been widely used in the production of many bio-implants because of its advantageous properties such as biocompatibility, biodegradability and favorable mechanical properties. Previous studies have shown that PCL-based scaffolds have been favorable for their compatibility with many cell types, including osteoblasts and mesenchymal stem cells, essential for bone regeneration [1,2]. The potential of PCL for copolymerization with other biomaterials, including collagen and chitosan, adds to its mechanical properties and biocompatibility, making it suitable for scaffolds requiring specific mechanical attributes in tissue engineering [3]. The adaptability of PCL is further enhanced by its potential to be fabricated into various forms, including nanospheres [4,5], nanowires [6,7], nanofibers [8], ultra-thin membranes [9], and scaffolds, utilizing methods such as electrospinning, 3D printing and so on. These techniques facilitate the fabrication of scaffolds that replicate the extracellular matrix, enhancing cell adhesion and proliferation [10,11].

Several recent studies have revealed that nanostructured surfaces of PCL, such as nanofibers and nanowires, can play a vital role in improving the blood compatibility and endothelial cell growth and differentiation [12–14]. In this work, these two nano topographies have been explored to understand their responses to erythrocytes interactions. NFs and NWs were chosen because they have features of similar size range but aligned in a very contrasting orientation; NFs are aligned parallel to the surface, while NWs are aligned perpendicular to the surface. Furthermore, these nanostructured surfaces were modified with organic compounds, TN and CMKC, to study their effects on the surfaces. It is hypothesized that this difference in alignment of nanostructures on the surface and the additional layer of organic coatings will cause a highly distinctive response to blood components, thus altering the erythrocyte compatibility.

In this study, fabricated PCL nanostructured surfaces were characterized for their surface wettability, surface chemistry, surface morphology, surface crystallinity and mechanical properties. Surface wettability was evaluated by measuring contact angles via goniometry. Surface chemistry was determined using X-ray photoelectron spectroscopy (XPS) analysis. Surface morphology was examined using scanning electron microscopy (SEM) imaging and surface crystallinity was analyzed using X-ray diffraction analysis (XRD). To understand the mechanical properties of all the surfaces, indentation hardness and elastic modulus were analyzed using the nanoindentation technique.

2.2 Methods and Materials

2.2.1 Fabrication of PCL Nanofiber (NF) surfaces

PCL Nanofibers surfaces (NF) were fabricated using the electrospinning method. The electrospinning device comprised a glass syringe, a 19-gauge blunt tip catheter, a syringe pump, and a male luer lock adapter. The catheter tip was attached to the positive terminal of a high-voltage power source with an alligator clip. The collector consisted of an aluminium foil fastened onto a 0.5” thick copper plate with electrical tape and positioned horizontally in line with the catheter tip. The negative terminal of the high-voltage power source was clipped to the aluminium foil using another alligator clip. The polymer solution was prepared by dissolving PCL pellets (MW = 80,000) in chloroform and then the solution was mixed with sodium salt of oleic acid (OLA) in methanol. A magnetic stir plate was used to produce a homogenous mixture of the solution with a 4:1 chloroform: methanol volume ratio. The final solution was 12% solid w/w and the PCL:OLA ratio of the solid weight was 97:3. The tip-to-collector distance was 10 cm, the applied voltage was 21 kV, and the volumetric flow rate was 2.8 ml hr^{-1} [6]. The resulting collector aluminium foil was removed from the copper plate and stored overnight in a desiccator to remove moisture from the surfaces.

2.2.2 Fabrication of PCL Nanowire (NW) surfaces

PCL control surfaces (PCL) were fabricated using a Prusa i3 3D printer with a nozzle diameter of 1.75 mm. Facilan™ PCL 100 Filament, with a diameter of 1.75 mm and molecular mass of 50 kDa, was used to 3D print PCL discs of 10 mm diameter and 2 mm thickness on a flatbed. The PCL disc was originally modelled in SOLIDWORKS and was sliced in Prusa slicer by importing it in STL.file format.

The nozzle and bed temperature of the printer were set to 180 °C and 45 °C, respectively. The printed control discs were collected in a well plate and stored in a desiccator overnight to remove moisture from the control surfaces.

Commercially available 200 nm diameter nanoporous aluminium oxide membranes (ANOPORE^{TM}, Whatman) were used to fabricate PCL Nanowire surfaces (notation: NW) using the solvent-free nano-templating process. The PCL control surfaces (as previously produced) were placed on the nanoporous membrane surface inside a custom-made 3D printed template and were covered with glass slides on the top and bottom. The template was modelled using SOLIDWORKS and 3D printed with PETG material to withstand high temperatures **(Figure 2.2.2.1)**. The polymer control surfaces, placed on the nanoporous alumina membrane, were allowed to gravimetrically extrude through the membrane for 15 minutes at 74 °C in an oven. The extruded NWs were then released by dissolving the aluminium oxide membranes in 1 M NaOH for 75 minutes [15]. Once dried, the NW surfaces were washed thrice with DI water and then stored in a desiccator to remove moisture from the surfaces.

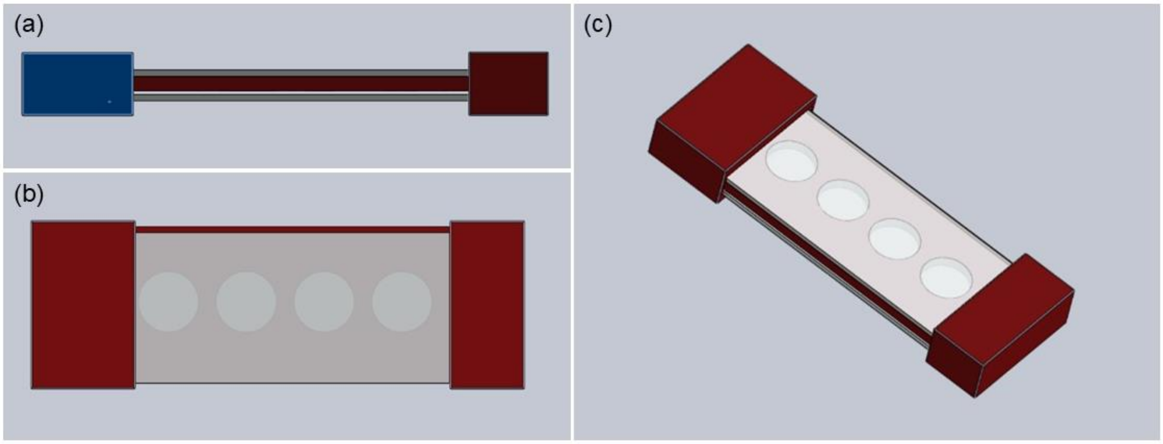

Figure 2.2.2.1: The (a) side, (b) top and (c) isometric views of SOLIDWORKS model of NW fabrication template.

2.2.3 Modification of PCL Nanostructured surfaces

2.2.3.1 Tanfloc purification

Tanac SA (Montenegro-RS, Brazil) has generously donated Tanfloc (TN), an amino-functionalized polyphenolic tannin derivative with a molecular weight of approximately 600 kDa [16] for this study. The Commercial TN product is produced by polymerizing tannin with the addition of formaldehyde, ammonium chloride, and hydrochloric acid [17]. Dialysis can remove the excess chloride ions in the TN structure transferred from the ammonium chloride used in TN synthesis. The hydrolyzable tannins and other low molecular weight substances in the commercial TN can also be removed through dialysis. A solution of TN in sodium acetate buffer (pH 5.0 and 0.2 mol L^{-1}) was produced at a concentration of 10 g L^{-1} and stirred overnight on a magnetic stir plate to ensure complete dissolution. The TN solution was then dialyzed using a Snakeskin Dialysis Tubing (10 kDa MWCO) in DI water for three consecutive days. The dialysate (DI water) was replaced bi-daily to maintain its purity during dialysis. After the 72-hour dialysis, the solution was filtered using a Whatman filter paper (110 mm) to eliminate residual contaminants. The filtered TN solution was frozen at -80 °C and lyophilized for five days to yield a dry, purified TN [16].

2.2.3.2 CMKC synthesis

Kappa-carrageenan containing small amounts of iota-carrageenan (KC) and monochloroacetic acid (MCA) were purchased from Sigma-Aldrich (USA). The Carboxymethyl-kappa-carrageenan (CMKC) was synthesized in-house by Dr. Kipper's group, who were generous enough to donate it for this study. The carboxymethylation of kappa-carrageenan (KC) was done following Williamson's ether synthesis method.

The system used for the carboxymethylation process consists of a 250 mL three-necked glass flask combined with a reflux condenser, thermometer, and a mechanical stirrer placed in a water bath. For the reactions, 2 g of KC was suspended in 40 mL of an aqueous solution containing 80% (w/v) of 2-propanol in the 3-necked glass flask coupled with a reflux condenser. 4 mL of a 20% NaOH aqueous solution was added dropwise over 15 minutes. The mixture was stirred rapidly at 40 °C for 1 hour. Monochloroacetic acid solution (MCA) was dissolved in 4 mL of 20% NaOH aqueous solution and stirred at ambient temperature for 30 minutes to achieve alkaline activation. The activated MCA solution was then added dropwise using a syringe to the KC solution for a duration of 20 minutes while maintaining a temperature of 55 °C for 4 hours of stirring. The reaction was carried out with the degree of substitution (DS) being 1.1 for the molar ratios of MCA to KC monomer of 3.5:1. Following the reaction, the product was isolated using vacuum filtration and washed thrice with 80% 2-propanol aqueous solution and pure 2-propanol. Later, the product was dried in an oven at 50 °C for an entire night. The resultant powder was dissolved in 300 mL of DI water overnight and underwent dialysis against water using a membrane with a maximum molecular weight cut-off (MWCO) 7000 Da (pore 22 x 35mm) until the conductivity went below 20 $\mu S.cm^{-1}$. Ultimately, the product was lyophilized in a ModulyoD lyophilizer (ThermoSavant), resulting in CMKC ($M_w = 4.3 \times 10^5$ $gmol^{-1}$) with a DS of 1.1, as mentioned above. The reaction conditions were uniform for both products [18,19]

2.2.3.3 Layer-by-layer deposition

The experimental procedure, used to prepare the Layer-by-Layer (LbL) deposition, was adapted from the methods reported before by our research group [16,20]. In this procedure, NF and NW surfaces were modified by treating them with TN and CMKC solutions to obtain NF_{TN}, $NF_{TN+CMKC}$, NW_{TN} and $NW_{TN+CMKC}$ groups. TN (polycation) and CMKC (polyanion) solutions were prepared in an acetic acid-acetate buffer (0.2 M sodium acetate and acetic acid at pH 5.0) at a concentration of 5 mg mL^{-1} and 1 mg mL^{-1} respectively. The solutions were stirred overnight. After that, the solutions were filtered using 0.22 µm polyvinylidene fluoride (PVDF) syringe filters from Fisher Scientific (Waltham, MA, USA). An aqueous acetic acid solution (pH 4.0) was used as a rinse solution. Prior to surface modification with polyelectrolytes, the NF and NW surfaces were treated with oxygen plasma at 200 V in 10 cm^3 min^{-1} of oxygen gas for 5 minutes. The surfaces were placed in 24-well plates and were modified via oxidation using oxygen plasma to facilitate the deposition of the polyelectrolytes. The rinse and deposition steps were all conducted on an orbital shaker (100 rpm). The oxidized surfaces were rinsed with the rinse solution for 4 minutes before the LbL deposition. The rinse solution was aspirated, and LbL deposition was carried out on the oxidized surfaces by adding the TN solution (polycation). After 5 minutes, the TN solution was aspirated, and the surface was rinsed again for 4 minutes. Subsequently, the rinse solution was aspirated, and the surfaces were washed with DI water for 30 seconds to obtain NF_{TN} and NW_{TN} groups. For $NF_{TN+CMKC}$ and $NW_{TN+CMKC}$, an additional layer of CMKC solution was deposited on the surfaces. The CMKC (polyanion) solution was added to the oxidized surfaces containing one layer of polycation (TN) for 5 minutes.

Then, the CMKC solution was aspirated, and the surfaces were rinsed for 4 minutes. Finally, the rinse solution was aspirated, and the surfaces were washed with DI water for 30 seconds. Following this LbL deposition, all the modified surfaces were stored in a desiccator until further use.

2.2.4 Statistical analysis

Surface characterizations with SEM and contact angles were done using at least 3 different surfaces for each group at 3 different locations on the surface (n_{min}=9). Statistical one-way analysis of variance test (ANOVA) was conducted, followed by a post-hoc analysis (t-test). The results were considered statistically significant when the p-value was ≤ 0.05. Analysis was done OriginPro 2024 software.

2.3 Results and Discussion

2.3.1 Characterization of different surfaces

The morphological features on the surfaces play a crucial role in affecting the cell and bacteria adhesion on surfaces [21,22]. The surface topography and architecture of the nanostructured surfaces were examined using scanning electron microscopy (SEM, JEOL JSM-6500F) **(Figure 2.3.1.1 and 2.3.1.2)**. Prior to imaging, a 10 nm coating of gold was applied to the surfaces, and the imaging was performed at 5 kV. SEM images of PCL do not show any unique topography. As expected, the PCL surfaces have considerable roughness and irregularities due to its processing and are not naturally smooth. The NF surfaces are produced by electrospinning process that involves the application of a high voltage to the polymer solution, which generates a charged jet, that elongates and solidifies into fibers as it travels toward a collector [23].

SEM images of NF show a uniform fibrous structure spread in a parallel manner throughout the surface. The NW surfaces are formed by gravimetrically extruding PCL control surfaces via nanoporous anodic aluminum oxide membranes at a temperature slightly greater than the glass transition temperature of PCL [24]. The SEM images of NW surfaces show an evenly distributed uniform architecture of extrusions, perpendicular to their surface. These SEM images of NF and NW indicate that their morphologies have a unique texture topography contrasting to the non-textured PCL surface. Using ImageJ, the height and the diameter of the NWs were computed to be 1.57 ± 0.17 µm and 341.43 ± 31.96 nm respectively, while the diameter of the NFs were measured to be 569.7 ± 76.85 nm. This study conformed with the previous literature that have shown similar NW and NF surfaces produced, which enhances cellular functionality [7,25,26]. After the LbL deposition of TN and CMKC on different surfaces, the SEM images indicate no significant changes as compared to unmodified surfaces. Thereby, it is evident that the NF and NW surfaces maintain a stable nanoarchitecture throughout the LbL deposition process.

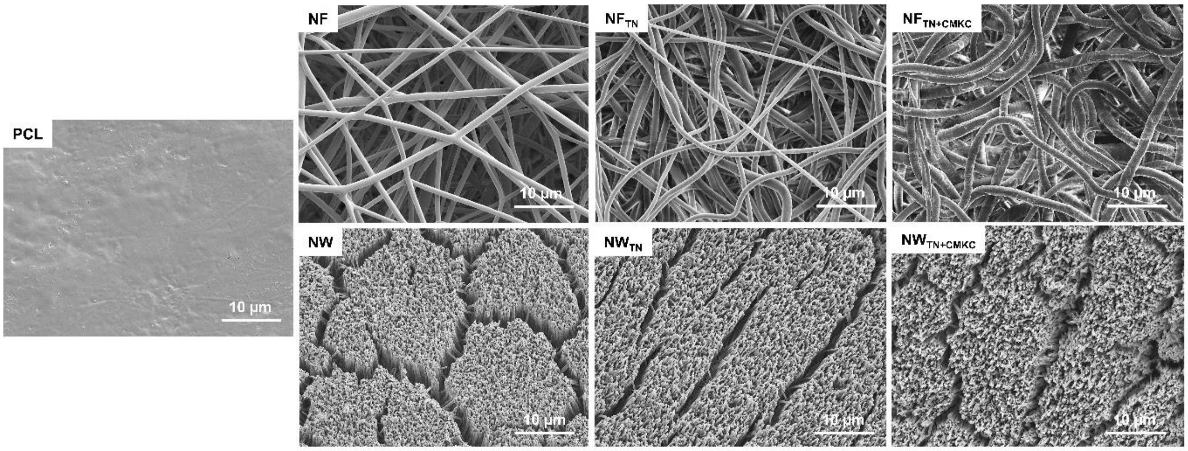

Figure 2.3.1.1: Representative SEM images of different surfaces at low (2500x) magnification.

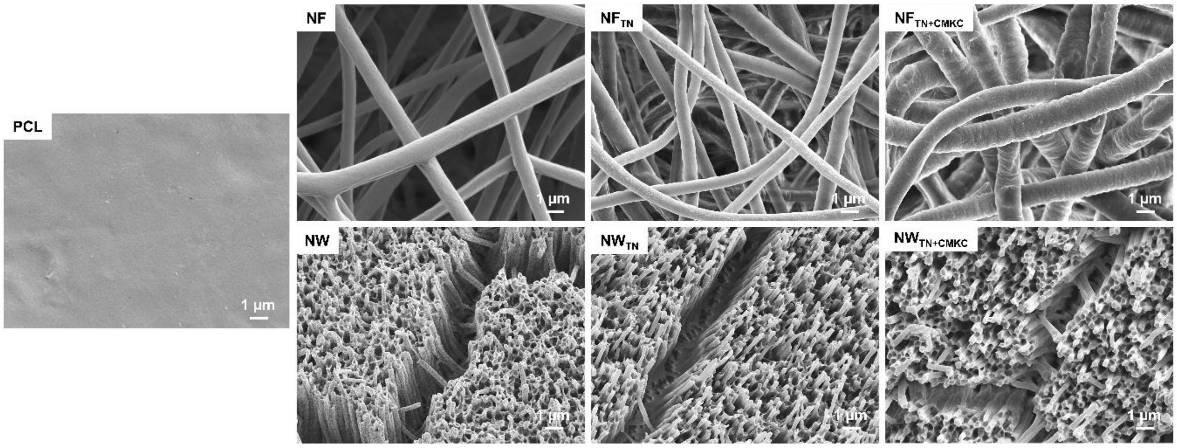

Figure 2.3.1.2: Representative SEM images of different surfaces at high (7500x) magnification.

Surface wettability is an important surface characteristic of a bio-implant that has been shown to influence interactions of blood components with surfaces [14,27]. The surface wettability of different surfaces was evaluated by contact angle measurements using a sessile drop measuring technique with the Ramè-Hart goniometer (Ramé-Hart Instrument Co., Succasunna, NJ, USA). The angle formed between a liquid droplet and a solid surface at the three-phase contact line where the liquid, solid and vapor phases meet is defined as the contact angle. The contact angle is measured between the surface and tangent line at the point of contact of the liquid droplet with the surface. Contact angle (θ) depends on various surface properties such as surface area, topography, energy, polarity due to chemistry etc. This angle provides insight about the liquid and the solid surface, which are influenced by the above-mentioned surface properties. Generally, the contact angle can be categorized into different types based on its value. Hydrophilic surfaces exhibit contact angles less than 90°, indicating that the liquid tends to spread across the surface.

Conversely, hydrophobic surfaces display angles greater than 90°, indicating that the liquid droplet maintains a more spherical shape and does not spread out much on the surface [28,29]. Furthermore, superhydrophilic surfaces can have contact angles below 5°, allowing the water droplet to spread almost completely across the surface [30].

In this study, the contact angle (θ) of 10 μL-sized droplet of DI water was used to measure the surface wettability. A camera was leveled with the surface, and the water droplet contacting the surface was captured as a photograph within five seconds of the droplet's time of contact. The associated software was then used to analyze the images and calculate the contact angles from the saved pictures. Results indicate that the PCL surface was almost hydrophobic as expected, with contact angle value 80.2° ± 10.5° **(Figure 2.3.1.3)**. This hydrophobic nature of PCL is attributed to its densely packed semi-crystalline structure, which limits water penetration and interaction with biological fluids [31,32]. All the other treated surfaces in this study exhibited a significantly reduced contact angle with respect to the PCL control. NW, NW_{TN} and $NW_{TN+CMKC}$ surfaces were hydrophilic, whereas NF, NF_{TN} and $NF_{TN+CMKC}$ surfaces were superhydrophilic. This difference in contact angles between NF and NW groups can be attributed to their structural differences. NFs typically exhibit a larger surface area to volume ratio compared to NWs, which allows greater interaction between their surfaces and the water molecules. This increase in surface area promotes more adsorption of water, thereby forming lower contact angles and thus exhibiting superhydrophilic wettability. In contrast, NWs, which have a more compact and elongated structure, tend to trap air within their nanostructures.

This entrapment of air pockets between the liquid and surface topography forms a Cassie-Baxter state, thus minimizing their interaction and thereby leading to a relatively higher contact angle [33,34].

There was no significant difference in terms of wettability between the NF, NW groups and their respective modified groups except for NW_{TN}. In comparison with NW, the NW_{TN} exhibits lower contact angle. This difference is because incorporation of hydrophilic polymers with PCL nanostructures has been shown to drastically reduce their hydrophobic characteristics [34,35] **(Figure 2.3.1.3)**. Thus, all the nanostructured PCL surfaces should potentially inhibit bacterial adhesion and improve cell proliferation on the implant surfaces due to their hydrophilic nature [36,37].

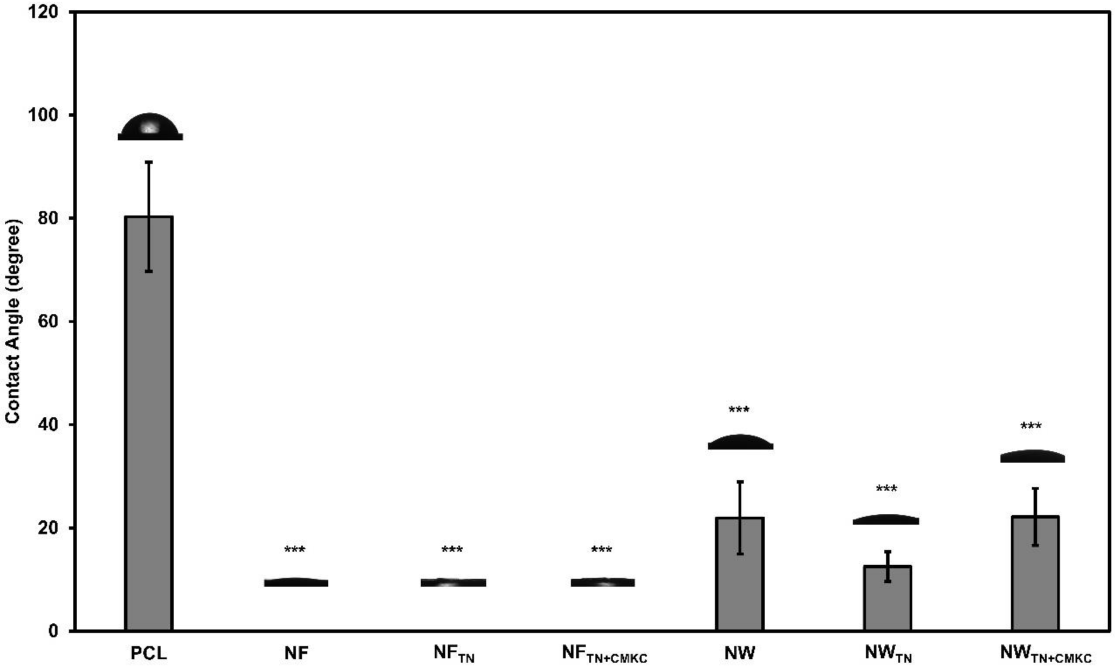

Figure 2.3.1.3: Static water contact angle of different surfaces. Images of water droplet on the surfaces are also shown in the plot. Statistical significances (*p*-value) were represented as *** $p < 0.001$.

The PCL control surface underwent several surface modifications in this study to improve its hemocompatibility and enhance its antibacterial properties. Hence, it is vital to understand the surface chemistry of different surfaces before and after modifications. Moreover, evaluating the surface chemistry is necessary to understand if LBL deposition of TN and CMKC was successful.

XPS (PHI Physical Electronics PE-5800 X-ray Photoelectron Spectrometer with an Al Kα X-ray source) was used to characterize the surface chemistry of different surfaces. Survey scans were collected for all the surfaces which help identify the elements present on the surfaces along with their relative concentration. Peak-fit analysis was conducted using CasaXPS (Version 2.3.25PR1.0). From the survey spectra, elemental analysis was also conducted for each surface using CasaXPS (Version 2.3.25PR1.0) and the composition (atomic weight percentage, % at) of each element was recorded. The XPS survey scan depicts comparison between PCL control and all other surfaces at different bonding energies ranging from 100 eV to 700 eV **(Figure 2.3.1.4)**. From the survey scan of PCL control, the presence of C1s peak (284.6 eV) and O1s peak (530 eV) was detected, which is typical of the PCL XPS spectrum reported in previous literature [38]. NF and NW were also exhibiting the same peaks of C1s and O1s, indicating that there was no change in the surface chemistry of the nanostructured PCL surfaces in comparison to the PCL control. However, after LbL deposition of TN, all the modified surfaces (NF_{TN}, $NF_{TN+CMKC}$, NW_{TN} and $NW_{TN+CMKC}$) exhibited new peak at binding energy 400 eV (N1s) that corresponds to the presence of nitrogen on the surfaces. This N1s presence was due to the successful modification of surfaces with TN.

The N1s peak can be attributed to the characteristic composition of TN because of the presence of amine groups in it [16]. However, $NF_{TN+CMKC}$ and $NW_{TN+CMKC}$ exhibited additionally a small peak at binding energy 168 eV which corresponds to the traces of sulphur (S2p) [39]. Presence of S2p peak is attributed to the sulphate group which belongs to CMKC [40]. This is due to the sulfation process that kappa carrageenan undergoes during its extraction and purification from algae [41]. The sulphur atoms in kappa carrageenan are primarily associated with sulphate ($–SO_4$) moieties, which are integral to its biological and physicochemical properties [42]. Therefore, the XPS survey scan confirms the successful LbL deposition of TN and CMKC.

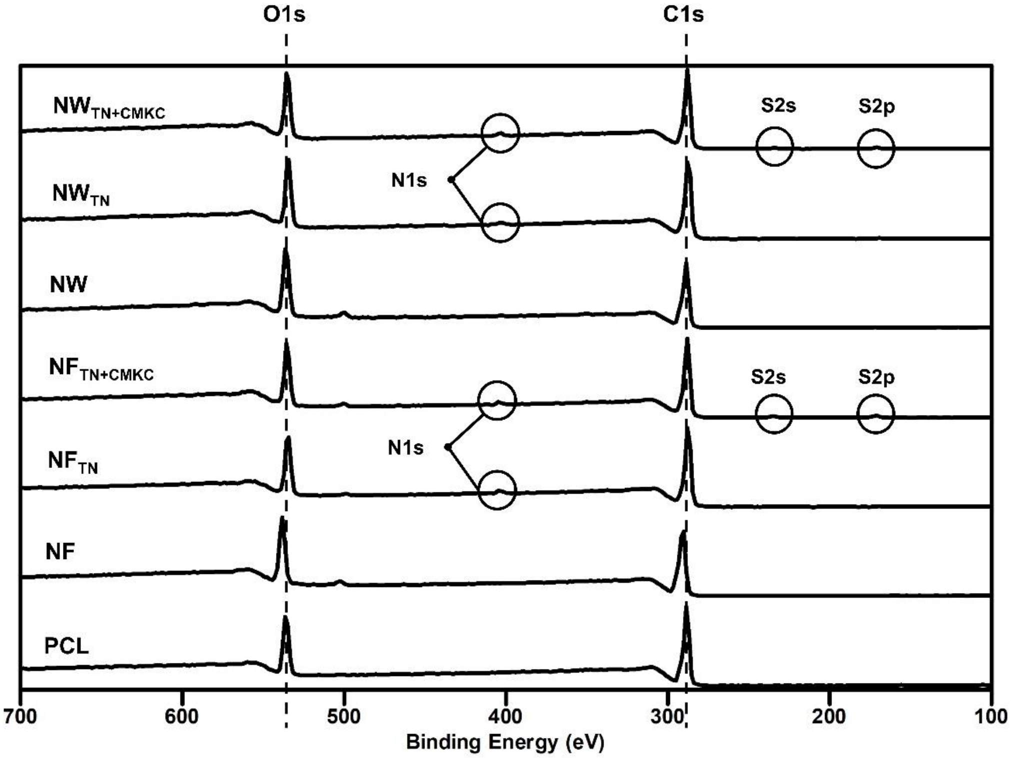

Figure 2.3.1.4: XPS survey scan of different surfaces.

From the XPS survey scans, the elemental composition (atomic weight percentage, %at) of the surfaces was calculated **(Table 1)**. PCL, NF and NW surfaces showed no traces of nitrogen or sulphur as expected. On the other hand, all the modified surfaces (NF_{TN}, $NF_{TN+CMKC}$, NW_{TN} and $NW_{TN+CMKC}$) showed presence of nitrogen. Also, $NF_{TN+CMKC}$ and $NW_{TN+CMKC}$ surfaces displayed minute traces of sulphur as expected.

Table 1: Elemental analysis (%at) of different surfaces from XPS survey spectra.

	%C1s	**%O1s**	**%N1s**	**%S2p**
PCL	76.53	23.47	0.00	0.00
NF	73.33	26.67	0.00	0.00
NF_{TN}	75.11	23.40	1.49	0.00
$NF_{TN + CMKC}$	72.89	24.80	1.36	0.95
NW	69.79	30.21	0.00	0.00
NW_{TN}	73.35	25.06	1.58	0.00
$NW_{TN + CMKC}$	71.58	26.24	1.55	0.63

To characterize surfaces for understanding its detailed information about the crystallinity and phase composition of the materials, XRD is a pivotal technique. The characterization of PCL control and nanostructures is important for understanding the physical properties which directly influence its functionality as a biomaterial. In addition to crystallinity, XRD also serves as a fundamental tool to estimate the presence of any secondary phases or impurities within PCL nanostructured surfaces.

XRD (XRD-7000 Shimadzu) was utilized to analyze the crystalline structure of the surfaces, while using CuKα radiation at 40 kV and 30 mA. When performing XRD, a thin film (TF-XRD) geometry was utilized for the surfaces with a fixed incidence angle of 5°. Diffractograms were acquired with continuous scans from 20° to 80° at scanning speed of 1°/min. Peaks were indexed using Match! software with the PDF-2 Database. The XRD patterns of different surfaces are presented in **Figure 2.3.1.5**. PCL is a semi-crystalline polymer characterized by distinct peaks in its XRD patterns. Results indicate that PCL control shows a significant crystalline peak approximately at 21.5° and a relatively low intensity peak at about 23.5° [43–45], which are attributed to the (110) and (200) lattice planes of its orthorhombic crystal form, respectively [46]. These values align with the Joint Committee on Powder Diffraction Standards (JCPDS #50-2459) reference for PCL, which confirms the orthorhombic crystalline structure of the polymer [47]. These sharp peaks indicate a high degree of crystallinity, which is an important property influencing the mechanical and thermal behavior of the polymer [48]. XRD patterns of NW and modified NW groups remain consistent with the patterns of PCL control. But for NF and modified NF groups, the intensity of the diffraction peak became lower and broader, exhibiting relatively more amorphous characteristics compared to NW groups or PCL control. This distinction is hypothesized to arise from the differences in their fabrication processes and resultant surfaces. NFs produced through electrospinning, often display a significant amount of amorphous regions due to rapid solvent evaporation and high surface area to volume ratio inherent in fibrous structures. The processing conditions of PCL fibers can lead to the confinement of amorphous content, suggesting that the semicrystalline nature of PCL fibers can create rigid amorphous regions [49,50]. On the other hand, NWs fabricated using nano-templating methods tend to have a more ordered crystalline structure. The hierarchical structures formed in PCL nanowires often promote better crystallization due to confinement effects and slower cooling rates during fabrication, which allow for more orderly molecular packing. This suggested that the crystallinity of NF and modified NF surfaces was lower than NW and modified NW surfaces.

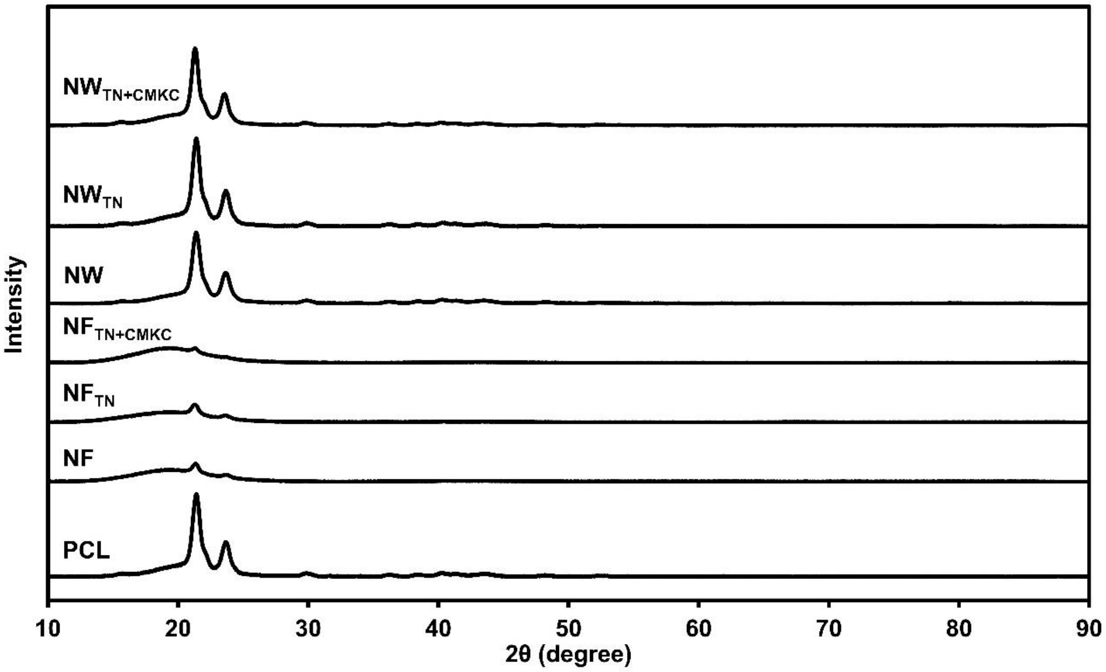

Figure 2.3.1.5: XRD spectra of different surfaces.

Understanding the mechanical properties such as material hardness, elastic modulus, stiffness and flexibility of materials is essential to determine the influence of biological interactions and material performance in biomedical applications [51]. Studies have shown that mechanical signaling from the surrounding microenvironment influences the interaction of cells with surfaces [52,53]. Hence, to understand these mechanical properties, indentation hardness and elastic modulus of all the surfaces were determined using the nanoindentation technique. **Figure 2.3.1.6** shows the hardness and elastic modulus plots of different surfaces.

Results show that NF and modified NF surfaces have high initial indentation hardness values (0.35 ± 0.02 GPa) at low displacements when compared to PCL control (0.08 ± 0.01 GPa), NW (0.03 ± 0.02 GPa) and modified NW surfaces (NW_{TN} = 0.1 ± 0.01 GPa, $NW_{TN+CMKC}$ = 0.04 ± 0.01 GPa). Polystyrene was also considered as a standard control for this study, which depicts similar behavior as that of NF groups (0.36 ± 0.02 GPa). This higher initial indentation hardness of NF surfaces can be attributed to their superior elastic properties and surface morphology. The dense fibrous network and high surface area to volume ratio contribute towards its stiffness and enhanced resistance against indentation. The interconnections between the fibers can dissipate stress in a very efficient way, allowing it to withstand high initial loads before beginning to deform plastically. On the other hand, the linear structure of NW surfaces does not effectively distribute loads, resulting in fewer points of resistance during indentation, thereby contributing to its lower initial hardness. As the displacement increases, the indentation hardness values of NF surfaces decrease till a point (5.5 - 6 µm) and then stabilizes into a plateau region (0.25 ± 0.02 GPa) before failure. Whereas the NW surfaces show longer plateau regions before failure (displacements ranging from 11 to 14 µm) at lower hardness values (0.05 ± 0.02 GPa). This indicates a deeper penetration of indenter into the material, suggesting its enhanced load-bearing capacity and durability as opposed to NF surfaces. Elastic modulus curves also showed a similar trend to the hardness curves for NF and NW surfaces, except for $NF_{TN+CMKC}$ **(Figure 2.3.1.6).** This distinctive, steep downward curve of $NF_{TN+CMKC}$ indicates a significant loss of stiffness, suggesting that the material has transitioned to plastic deformation and has become less resistant to further deformation. This behavior can possibly be due to yielding or softening mechanisms.

These results suggest that PCL NF surfaces can be utilized for high stiffness and resistance demanding applications, while PCL NW surfaces can be employed in areas requiring flexibility and durability.

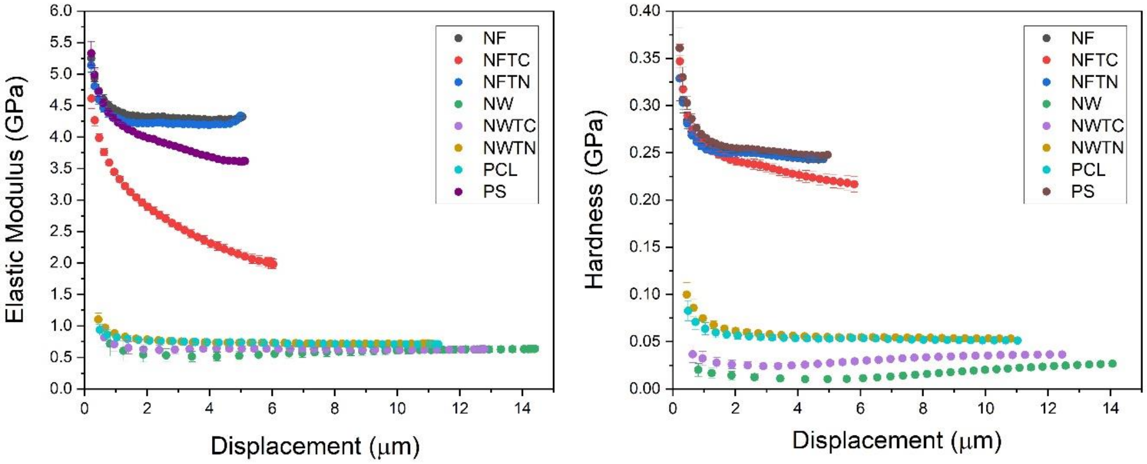

Figure 2.3.1.6: Plots of elastic modulus (GPa) vs displacement and indentation hardness (GPa) vs displacement (μm) for different surfaces.

REFERENCES

[1] M.J. Mochane, T.S. Motsoeneng, E.R. Sadiku, T.C. Mokhena, J.S. Sefadi, Morphology and Properties of Electrospun PCL and Its Composites for Medical Applications: A Mini Review, Applied Sciences 9 (2019) 2205. https://doi.org/10.3390/app9112205.

[2] C. Busuioc, A.-E. Alecu, C.-C. Costea, M. Beregoi, M. Bacalum, M. Raileanu, S.-I. Jinga, I.-M. Deleanu, Composite Fibers Based on Polycaprolactone and Calcium Magnesium Silicate Powders for Tissue Engineering Applications, Polymers (Basel) 14 (2022) 4611. https://doi.org/10.3390/polym14214611.

[3] A. Azam, K.E. Laflin, M. Jamal, R. Fernandes, D.H. Gracias, Self-folding micropatterned polymeric containers, Biomed Microdevices 13 (2011) 51–58. https://doi.org/10.1007/S10544-010-9470-X/FIGURES/6.

[4] S. Singh, A.N. Singh, A. Verma, V.K. Dubey, Biodegradable polycaprolactone (PCL) nanosphere encapsulating superoxide dismutase and catalase enzymes, Appl Biochem Biotechnol 171 (2013) 1545–1558. https://doi.org/10.1007/S12010-013-0427-4.

[5] F.S. Poletto, R.P. Silveira, L.A. Fiel, B. Donida, M. Rizzi, S.S. Guterres, A.R. Pohlmann, Size-Control of Poly(epsilon-caprolactone) Nanospheres by the Interface Effect of Ethanol on the Primary Emulsion Droplets, J Nanosci Nanotechnol 9 (2009) 4933–4941. https://doi.org/10.1166/JNN.2009.1270.

[6] V. Leszczak, B.S. Smith, K.C. Popat, Hemocompatibility of polymeric nanostructured surfaces, J Biomater Sci Polym Ed 24 (2013) 1529–1548. https://doi.org/10.1080/09205063.2013.777228.

[7] S.L. Bechara, A. Judson, K.C. Popat, Template synthesized poly(epsilon-caprolactone) nanowire surfaces for neural tissue engineering, Biomaterials 31 (2010) 3492–3501. https://doi.org/10.1016/J.BIOMATERIALS.2010.01.084.

[8] M.L. Alves Da Silva, A. Martins, A.R. Costa-Pinto, P. Costa, S. Faria, M. Gomes, R.L. Reis, N.M. Neves, Cartilage tissue engineering using electrospun PCL nanofiber meshes and MSCs, Biomacromolecules 11 (2010) 3228–3236. https://doi.org/10.1021/BM100476R.

[9] F. Chen, C.N. Lee, S.H. Teoh, Nanofibrous modification on ultra-thin poly(e-caprolactone) membrane via electrospinning, Materials Science and Engineering: C 27 (2007) 325–332. https://doi.org/10.1016/J.MSEC.2006.05.004.

[10] X. Yang, Y. Wang, Y. Zhou, J. Chen, Q. Wan, The Application of Polycaprolactone in Three-Dimensional Printing Scaffolds for Bone Tissue Engineering, Polymers 2021, Vol. 13, Page 2754 13 (2021) 2754. https://doi.org/10.3390/POLYM13162754.

[11] O. Suwantong, Biomedical applications of electrospun polycaprolactone fiber mats, Polym Adv Technol 27 (2016) 1264–1273. https://doi.org/10.1002/PAT.3876.

[12] V. Leszczak, K.C. Popat, Improved in Vitro Blood Compatibility of Polycaprolactone Nanowire Surfaces, ACS Appl Mater Interfaces 6 (2014) 15913–15924. https://doi.org/10.1021/am503508r.

[13] V. Leszczak, D.A. Baskett, K.C. Popat, Endothelial Cell Growth and Differentiation on Collagen-Immobilized Polycaprolactone Nanowire Surfaces, J Biomed Nanotechnol 11 (2015) 1080–1092. https://doi.org/10.1166/jbn.2015.2021.

[14] A.P. Khandwekar, D.P. Patil, Y. Shouche, M. Doble, Surface engineering of polycaprolactone by biomacromolecules and their blood compatibility, J Biomater Appl 26 (2011) 227–252. https://doi.org/10.1177/0885328210367442/SUPPL_FILE/SUPPLEMENTARY_MATERIAL.DOC.

[15] V. Leszczak, B.S. Smith, K.C. Popat, Hemocompatibility of Polymeric Nanostructured Surfaces, J Biomater Sci Polym Ed 24 (2013) 1529. https://doi.org/10.1080/09205063.2013.777228.

[16] S. Baghersad, L.Y.C. Madruga, A.F. Martins, K.C. Popat, M.J. Kipper, Expanding the Scope of an Amphoteric Condensed Tannin, Tanfloc, for Antibacterial Coatings, J Funct Biomater 14 (2023) 554. https://doi.org/10.3390/jfb14110554.

[17] Y.T. Hameed, A. Idris, S.A. Hussain, N. Abdullah, H. Che Man, Effect of pre-treatment with a tannin-based coagulant and flocculant on a biofilm bacterial community and the nitrification process in a municipal wastewater biofilm treatment unit, J Environ Chem Eng 8 (2020) 103679. https://doi.org/10.1016/j.jece.2020.103679.

[18] L.Y.C. Madruga, R.M. Sabino, E.C.G. Santos, K.C. Popat, R. de C. Balaban, M.J. Kipper, Carboxymethyl-kappa-carrageenan: A study of biocompatibility, antioxidant and antibacterial activities, Int J Biol Macromol 152 (2020) 483–491. https://doi.org/10.1016/J.IJBIOMAC.2020.02.274.

[19] L.Y.C. Madruga, K.C. Popat, R.C. Balaban, M.J. Kipper, Enhanced blood coagulation and antibacterial activities of carboxymethyl-kappa-carrageenan-containing nanofibers, Carbohydr Polym 273 (2021) 118541. https://doi.org/10.1016/J.CARBPOL.2021.118541.

[20] R.M. Sabino, K. Kauk, | Liszt, Y.C. Madruga, M.J. Kipper, A.F. Martins, | Ketul, C. Popat, Enhanced hemocompatibility and antibacterial activity on titania nanotubes with tanfloc/heparin polyelectrolyte multilayers, (2020). https://doi.org/10.1002/jbm.a.36876.

[21] H.Y. Lo, H.T. Kuo, Y.Y. Huang, Application of Polycaprolactone as an Anti-Adhesion Biomaterial Film, Artif Organs 34 (2010) 648–653. https://doi.org/10.1111/J.1525-1594.2009.00949.X.

[22] T. Raimondo, S. Puckett, T.J. Webster, Greater osteoblast and endothelial cell adhesion on nanostructured polyethylene and titanium, Int J Nanomedicine 5 (2010) 647–652. https://doi.org/10.2147/IJN.S13047.

[23] V. Leung, F. Ko, Biomedical applications of nanofibers, Polym Adv Technol 22 (2011) 350–365. https://doi.org/10.1002/PAT.1813.

[24] N.A. Trujillo, K.C. Popat, Increased Adipogenic and Decreased Chondrogenic Differentiation of Adipose Derived Stem Cells on Nanowire Surfaces, Materials 2014, Vol. 7, Pages 2605-2630 7 (2014) 2605–2630. https://doi.org/10.3390/MA7042605.

[25] T.T. Ruckh, K. Kumar, M.J. Kipper, K.C. Popat, Osteogenic differentiation of bone marrow stromal cells on poly(ε-caprolactone) nanofiber scaffolds, Acta Biomater 6 (2010) 2949–2959. https://doi.org/10.1016/J.ACTBIO.2010.02.006.

[26] J.R. Porter, A. Henson, K.C. Popat, Biodegradable poly(ε-caprolactone) nanowires for bone tissue engineering applications, Biomaterials 30 (2009) 780–788. https://doi.org/10.1016/J.BIOMATERIALS.2008.10.022.

[27] C. Pulletikurthi, N. Munroe, D. Stewart, W. Haider, S. Amruthaluri, R. Rokicki, M. Dugrot, S. Ramaswamy, Utility of magneto-electropolished ternary nitinol alloys for blood contacting applications, J Biomed Mater Res B Appl Biomater 103 (2015) 1366–1374. https://doi.org/10.1002/JBM.B.33317.

[28] K. Shaikh, W.A. Khan, Md.S.N. Kazi, M.N.M. Zubir, K. Shaikh, W.A. Khan, Md.S.N. Kazi, M.N.M. Zubir, Nanocellulose: Fundamentals and Applications, (2024). https://doi.org/10.5772/INTECHOPEN.114221.

[29] Y. Kelvii Kwok, Wettability on Different Surfaces, in: 21st Century Surface Science - a Handbook, IntechOpen, 2020. https://doi.org/10.5772/intechopen.92885.

[30] H. Puliyalil, G. Filipič, U. Cvelbar, H. Puliyalil, G. Filipič, U. Cvelbar, Recent Advances in the Methods for Designing Superhydrophobic Surfaces, Surface Energy (2015). https://doi.org/10.5772/60852.

[31] G. Yang, H. Lin, B.B. Rothrauff, S. Yu, R.S. Tuan, Multilayered polycaprolactone/gelatin fiber-hydrogel composite for tendon tissue engineering, Acta Biomater 35 (2016) 68–76. https://doi.org/10.1016/J.ACTBIO.2016.03.004.

[32] H.N. Patel, R. Garcia, C. Schindler, D. Dean, S.M. Pogwizd, R. Singh, Y.K. Vohra, V. Thomas, Fibro-porous poliglecaprone/polycaprolactone conduits: synergistic effect of composition and in vitro degradation on mechanical properties, Polym Int 64 (2015) 547–555. https://doi.org/10.1002/PI.4834.

[33] K. Du, Z. Gan, Cellular interactions on hierarchical poly(ε-caprolactone) nanowire micropatterns, ACS Appl Mater Interfaces 4 (2012) 4643–4650. https://doi.org/10.1021/AM301013E/ASSET/IMAGES/LARGE/AM-2012-01013E_0013.JPEG.

[34] V. Leszczak, D.A. Baskett, K.C. Popat, Smooth Muscle Cell Functionality on Collagen Immobilized Polycaprolactone Nanowire Surfaces, Journal of Functional Biomaterials 2014, Vol. 5, Pages 58-77 5 (2014) 58–77. https://doi.org/10.3390/JFB5020058.

[35] W. Wang, Y. Wang, W. Zhao, C. Zhao, A Straightforward Approach towards Antibacterial and Anti-Inflammatory Multifunctional Nanofiber Membranes with Sustained Drug Release Profiles, Macromol Biosci 22 (2022). https://doi.org/10.1002/mabi.202200150.

[36] A.G. Namboodiri, R. Parameswaran, Fibro-porous polycaprolactone membrane containing extracts of Biophytum sensitivum: A prospective antibacterial wound dressing, J Appl Polym Sci 129 (2013) 2280–2286. https://doi.org/10.1002/APP.38950.

[37] L. Ye, X. Wu, H.Y. Duan, X. Geng, B. Chen, Y.Q. Gu, A.Y. Zhang, J. Zhang, Z.G. Feng, The in vitro and in vivo biocompatibility evaluation of heparin–poly(ε-caprolactone) conjugate for vascular tissue engineering scaffolds, J Biomed Mater Res A 100A (2012) 3251–3258. https://doi.org/10.1002/JBM.A.34270.

[38] P. Louette, F. Bodino, J.-J. Pireaux, Poly(caprolactone) (PCL) XPS Reference Core Level and Energy Loss Spectra, Surface Science Spectra 12 (2005) 27–31. https://doi.org/10.1116/11.20050906.

[39] M.A. Hamdan, K.N. Mohd Amin, F. Adam, Quantitative analysis of molecular interactions in κ-carrageenan-Isovanillin biocomposite for biodegradable packaging and pharmaceutical applications using NMR, TOF-SIMS, and XPS approach, Food Chem 452 (2024) 139556. https://doi.org/10.1016/j.foodchem.2024.139556.

[40] Z. Li, Y. Guo, X. Wang, P. Li, W. Ying, D. Chen, X. Ma, Z. Deng, X. Peng, Simultaneous Recovery of Metal Ions and Electricity Harvesting via K-Carrageenan@ZIF-8 Membrane, ACS Appl Mater Interfaces 11 (2019) 34039–34045. https://doi.org/10.1021/ACSAMI.9B12501/ASSET/IMAGES/LARGE/AM9B12501_0004.JPEG.

[41] N. Shrgawi, I.J. Shamsudin, H. Hanibah, S.A.M. Noor, N. Kasim, Purification on Kappa Carrageenan by Re-Precipitation Technique, Solid State Phenomena 317 (2021) 327–332. https://doi.org/10.4028/WWW.SCIENTIFIC.NET/SSP.317.327.

[42] T.T.M. Ho, K.E. Bremmell, M. Krasowska, D.N. Stringer, B. Thierry, D.A. Beattie, Tuning polyelectrolyte multilayer structure by exploiting natural variation in fucoidan chemistry, Soft Matter 11 (2015) 2110–2124. https://doi.org/10.1039/C4SM02552K.

[43] E. Gea Rodi, C. Mangeon, E. Dessauw, V. Sansalone, T. Lemaire, E. Renard, V. Langlois, Functionalization of Miscanthus by Photoactivated Thiol-Ene Addition to Improve Interfacial Adhesion with Polycaprolactone, ACS Sustain Chem Eng 4 (2016) 5475–5482. https://doi.org/10.1021/ACSSUSCHEMENG.6B01041/ASSET/IMAGES/MEDIUM/SC-2016-01041W_0010.GIF.

[44] H.S. Barud, S.J.L. Ribeiro, C.L.P. Carone, R. Ligabue, S. Einloft, P.V.S. Queiroz, A.P.B. Borges, V.D. Jahno, Optically transparent membrane based on bacterial cellulose/polycaprolactone, Polímeros 23 (2013) 135–142. https://doi.org/10.1590/S0104-14282013005000018.

[45] R. Othman, G.T. Vladisavljević, Z.K. Nagy, R.G. Holdich, Encapsulation and Controlled Release of Rapamycin from Polycaprolactone Nanoparticles Prepared by Membrane Micromixing Combined with Antisolvent Precipitation, Langmuir 32 (2016) 10685–10693. https://doi.org/10.1021/ACS.LANGMUIR.6B03178/ASSET/IMAGES/MEDIUM/LA-2016-03178A_0008.GIF.

[46] M.P. Motloung, V. Ojijo, J. Bandyopadhyay, S.S. Ray, Morphological characteristics and thermal, rheological, and mechanical properties of cellulose nanocrystals-containing biodegradable poly(lactic acid)/poly(ε-caprolactone) blend composites, J Appl Polym Sci 137 (2020) 48665. https://doi.org/10.1002/APP.48665.

[47] A. Hasan, S. Soliman, F. El Hajj, Y.T. Tseng, H.C. Yalcin, H.E. Marei, Fabrication and In Vitro Characterization of a Tissue Engineered PCL-PLLA Heart Valve, Scientific Reports 2018 8:1 8 (2018) 1–13. https://doi.org/10.1038/s41598-018-26452-y.

[48] L.A. Can-Herrera, A.I. Oliva, M.A.A. Dzul-Cervantes, O.F. Pacheco-Salazar, J.M. Cervantes-Uc, Morphological and Mechanical Properties of Electrospun Polycaprolactone Scaffolds: Effect of Applied Voltage, Polymers 2021, Vol. 13, Page 662 13 (2021) 662. https://doi.org/10.3390/POLYM13040662.

[49] K.M. Van De Voorde, L.T.J. Korley, J.K. Pokorski, Confinement and Composition Effects on the Degradation Profile of Extruded PLA/PCL Nonwoven Fiber Blends, ACS Appl Polym Mater 3 (2021) 3878–3890. https://doi.org/10.1021/ACSAPM.1C00454/ASSET/IMAGES/LARGE/AP1C00454_0010.JPEG.

[50] P. Sajkiewicz, M.K. Heljak, A. Gradys, E. Choińska, S. Rumiński, T. Jaroszewicz, I. Bissenik, W. Święszkowski, Degradation and related changes in supermolecular structure of poly(caprolactone) in vivo conditions, Polym Degrad Stab 157 (2018) 70–79. https://doi.org/10.1016/J.POLYMDEGRADSTAB.2018.09.023.

[51] Y. Zhang, X. Wang, Y. Zhang, Y. Liu, D. Wang, X. Yu, H. Wang, Z. Bai, Y.C. Jiang, X. Li, W. Zheng, Q. Li, Endothelial Cell Migration Regulated by Surface Topography of Poly(ϵ-caprolactone) Nanofibers, ACS Biomater Sci Eng 7 (2021) 4959–4970. https://doi.org/10.1021/ACSBIOMATERIALS.1C00951/SUPPL_FILE/AB1C00951_SI_002.PDF.

[52] F. Sharifi, B.B. Patel, A.K. Dzuilko, R. Montazami, D.S. Sakaguchi, N. Hashemi, Polycaprolactone Microfibrous Scaffolds to Navigate Neural Stem Cells, Biomacromolecules 17 (2016) 3287–3297. https://doi.org/10.1021/acs.biomac.6b01028.

[53] M. Bontempi, G. Marchiori, M. Petretta, R. Capozza, B. Grigolo, G. Giavaresi, A. Gambardella, Nanomechanical Mapping of Three Dimensionally Printed Poly-ε-Caprolactone Single Microfibers at the Cell Scale for Bone Tissue Engineering Applications, Biomimetics 2023, Vol. 8, Page 617 8 (2023) 617. https://doi.org/10.3390/BIOMIMETICS8080617.

CHAPTER 3

EVALUATION OF ANTIBACTERIAL PROPERTIES OF PCL NANOSTRUCTURED SURFACES

3.1 Introduction

Bacterial infection is one of the important causes for bio-implants failure. When bacteria attach to the surface of implants, they can proliferate and form biofilms, which act as a protective environment for the bacteria. This protective environment shields them from both the host immune response and antibiotic treatments, thereby complicating infection management and leading to implant failure [1–3]. Majority of the implant-related infections is caused by the Gram-positive bacteria genus of *Staphylococcus* with *Staphylococcus aureus (S. aureus)*. This bacterium is a prominent pathogen in implant-related infections, leading to complications such as implant failure and the need for revision surgeries [3,4]. Recent studies have reported that approximately 65% of the infections associated with orthopedic implants are due to Gram-positive cocci, with *S. aureus* being one of the most common pathogens [5,6]. Studies have shown that the second most common genus was Gram-negative Pseudomonas, with *Pseudomonas aeruginosa (P. aeruginosa)* being a prominent infectious pathogen in this genus [7,8]. Studies show that they can account for 41% of positive cultures in cases of implant-related infections [9]. Even after maintaining a highly sterile environment during the implant surgeries, these bacteria can still proliferate inside the host body [10]. Therefore, mitigating this bacterial growth is crucial for implant stability and patient’s well-being.

Studies have shown that PCL’s inherent properties can facilitate bacterial adherence, which is a precursor to biofilm development [11]. For instance, fluid accumulation around PCL implants due to inflammatory responses can create a favorable environment for bacterial colonization [1]. On the other hand, studies have also shown that the adhesion of bacteria on the implant surfaces is hugely influenced by various surface characteristics of the material such as roughness, topography, wettability and chemical composition [2,3]. Thus, modifying the surface of the implants can help mitigate this bacterial adhesion and biofilm formation [12,13]. Various strategies have been explored and proven to enhance the antibacterial efficacy of PCL-based materials, including the incorporation of nanoparticles, bioactive compounds and surface modifications [14–16].

In this study, PCL nanostructured surfaces were subjected to gram-positive and gram-negative bacterial strains to understand the antibacterial properties of different surfaces. The surfaces were characterized by bacteria adhesion to evaluate the amount of live or dead bacteria and bacteria morphology to understand the morphological changes or biofilm formation of the cells. The percentage area fraction coverage of live and dead bacteria was also calculated.

3.2 Materials and Methods

3.2.1 Bacteria Culture

Gram-positive Staphylococcus aureus (S. aureus, ATCC6538) and Gram-negative Pseudomonas aeruginosa (P. aeruginosa, ATCC10145) bacterial strains were utilized to access the antibacterial properties of different surfaces. Both bacterial strains were cultured in tryptic soy broth (TSB, Sigma-Aldrich, St. Louis, MO, USA) at 37 °C for 24 hours until a concentration of 10^9 Colony Forming Units (CFU)/mL was attained. The CFU/mL was quantified by analyzing the absorbance values of the bacterial solution using a plate reader at a wavelength of 562 nm. A diluted bacterial culture of 10^6 CFU/mL was used to examine bacterial adhesion and morphology on different surfaces. The surfaces were placed in a 24-well plate and sterilized with 70% Ethanol for 30 minutes. Then, they were air dried, further sterilized under UV light for 30 minutes, and subsequently rinsed twice with PBS for 5 minutes each. After sterilization, the surfaces were incubated with the 10^6 CFU/mL bacterial solution for 6 hours and 24 hours at 37 °C in an incubator. Following incubation, the surfaces were washed twice with PBS for 5 minutes to remove any non-adhered bacteria prior to further characterization.

3.2.2 Bacteria Adhesion on Different Surfaces

A fluorescent microscope was used to determine the amount of live or dead bacteria adhering to different surfaces. Post incubation of the surfaces with the bacteria media for 6 hours and 24 hours, the media was aspirated, and surfaces were rinsed with PBS for 5 minutes each. Then, the surfaces were incubated at room temperature for 15 minutes in a staining solution comprising a 1:1 ratio of propidium iodide (dead bacteria stain) and Syto 9 (live bacteria stain) at a concentration of 3 $\mu L\ mL^{-1}$ in PBS

(ThermoFisher Scientific, Waltham, MA, USA). The stain solution was then removed, and the surfaces were rinsed again with PBS and incubated with 3.7% formaldehyde (Fisher Chemical, Fair Lawn, NJ, USA) for 15 minutes at ambient room temperature to fix the cells adhering to the surfaces. Subsequently, the formaldehyde was aspirated, and the surfaces were washed with PBS twice for 5 minutes each and stored in PBS. Ultimately, the surfaces were imaged using a fluorescence microscope (Zeiss). ImageJ was used to determine the percentage of the area fraction covered by the live or dead bacteria on the surfaces. The entire procedure, from staining to imaging, was performed in darkness.

3.2.3 Bacteria Morphology on Different Surfaces

A scanning electron microscope (SEM) was used to capture images for each surface and characterize the morphology of adherent bacteria on different surfaces. After the bacterial incubation, the media was aspirated, and the surfaces were washed once with PBS for 5 minutes. Then, the surfaces were incubated with a primary fixative solution comprising 3% glutaraldehyde (Sigma-Aldrich, St. Louis, MO, USA), 0.1 M sucrose (Sigma-Aldrich, St. Louis, MO, USA) and 0.1 M sodium cacodylate (Electron Microscopy Sciences, Hatfield, PA, USA) in DI water for 45 minutes at ambient temperature. Following this, the fixative solution was removed, and the surfaces were incubated with a buffer solution containing the fixative, except glutaraldehyde, for 10 minutes. At last, the surfaces were dehydrated with 35%, 50%, 70% and 100% ethanol solution, each for a 10-minute incubation period. Prior to SEM imaging, the surfaces were stored in a desiccator to ensure dryness. Before placing the surfaces in the SEM apparatus, a 10 nm gold coating was applied using a Denton Vacuum Desk II Gold Sputter Coater to enhance the surface conductivity of the polymer surfaces for imaging purposes.

3.2.4 Statistical Analysis

In the anti-bacterial study, a minimum of three samples ($n_{min} = 3$) of each surface were utilized for surface characterization and all experiments were repeated at least thrice ($n_{min} = 9$). Statistical one-way analysis of variance (ANOVA) and Tukey tests (t-test) were conducted for the experiment data using software OriginPro 2024 at a 5% significance level ($p \leq 0.05$).

3.3 Results and Discussion

3.3.1 Bacteria Adhesion

To evaluate the antibacterial activity of the PCL control and nanostructured surfaces, all the surfaces were incubated for 6 and 24 hours with *P. aeruginosa* and *S. aureus* bacteria. Following the incubation, the live/dead bacteria staining was conducted to assess the amount of bacteria attached to different surfaces. **Figure 3.3.1.1 and Figure 3.3.1.2** shows the fluorescence microscopic images of different surfaces after the incubation periods with *P. aeruginosa*. **Figure 3.3.1.3 and Figure 3.3.1.4** also shows plots quantifying the percentage of area fraction of the surfaces covered by live and dead *P. aeruginosa* bacteria over 6 and 24 hours of incubation periods. PS surfaces, which were used to assess the quality and viability of the bacteria culture, confirmed that the culture was successful for both the types of bacterial strains. Results indicate that there was a significant difference in % of area covered by live *P. aeruginosa*, between PCL and PS during the 6-hour incubation period. But after the 24-hour incubation period, the PCL surfaces were almost 96% covered with live *P. aeruginosa*, similar to the PS surfaces. In contrast to this, all the nanostructured surfaces reduced *P. aeruginosa* attachment in both incubation periods; however, modified NF and NW surfaces exhibited the least adhesion of live *P. aeruginosa* compared to their control surfaces. For instance, after the 24-hour incubation, the area fraction % of live *P. aeruginosa* 0.039% in NF whereas, 0.009% and 0.005% in NF_{TN} and $NF_{TN+CMKC}$ respectively. Similarly, NW had 0.42% area covered with live *P. aeruginosa*, whereas NW_{TN} and $NW_{TN+CMKC}$ had just 0.16% and 0.04% area covered respectively.

Results also indicate that, compared to PCL surfaces, NF and NW surfaces had significantly higher % area fraction of dead *P. aeruginosa* bacteria during the 6-hour incubation period **(Figure 3.3.1.4)** suggesting that these surfaces were more antibacterial than PCL. However, after the 24-hour incubation period, modified nanostructured surfaces, especially NW groups, had shown a significant reduction in % area fraction of dead *P. aeruginosa*, indicating that these surfaces are not only antibacterial but can also inhibit bacterial adhesion and growth on their surfaces. For instance, after 24-hour incubation, $NW_{TN+CMKC}$ had the least % area fraction of dead *P. aeruginosa*, approximately around 10.3%, followed by NW_{TN} with 32% area covered. Even though NF and modified NF surfaces have shown significant reduction in bacterial adhesion compared to PCL, the % area fraction covered by dead *P. aeruginosa* was higher in NF groups than NW groups. This result can be attributed to the inherent surface's topographical differences between NF and NW groups. NWs typically exhibit a unique pillar-like structure creating a complex surface environment, which hinders bacterial adhesion by providing fewer flat surfaces for their attachment. Du & Gan highlighted that the hierarchical structure of PCL NW allows for enhanced interactions with the surrounding environment, which can influence bacteria behavior [17]. Even though PCL NF surfaces possess some degree of roughness, their planar surfaces do not provide the same level of structural complexity compared to the three-dimensional architecture of PCL NW surfaces. Thus, NWs inherent topography has contributed towards creating a less conducive environment for bacterial colonization.

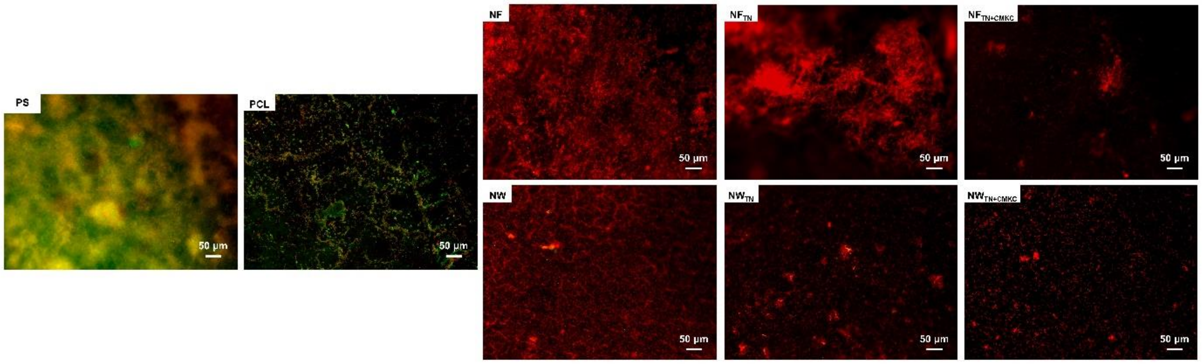

Figure 3.3.1.1: Representative fluorescence microscopic images of surfaces after 6 hours of incubation with *P. aeruginosa*.

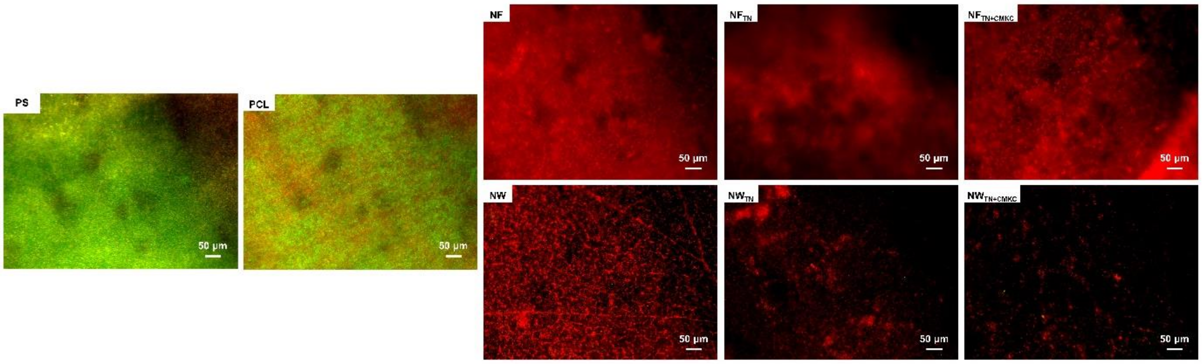

Figure 3.3.1.2: Representative fluorescence microscopic images of surfaces after 24 hours of incubation with *P. aeruginosa*.

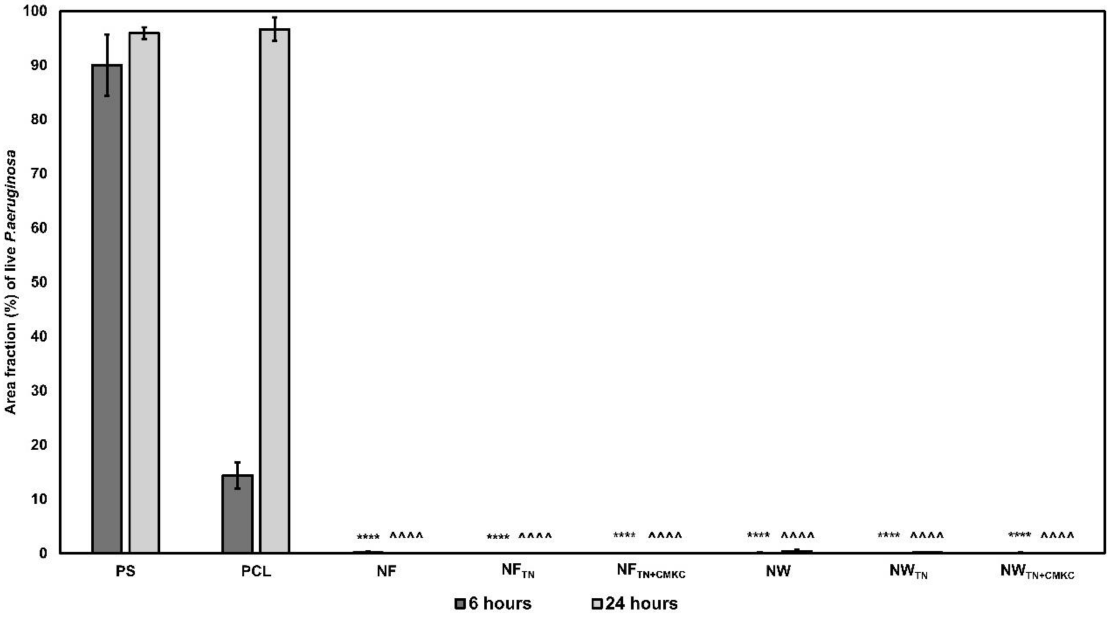

Figure 3.3.1.3: The graphs represent the percentage of the area fraction of different surfaces covered by live P. aeruginosa bacteria after 6 and 24 hours of incubation. **** and ^^^^ represent p-value <0.0001 when compared to PCL control at 6 and 24-hour timepoints respectively.

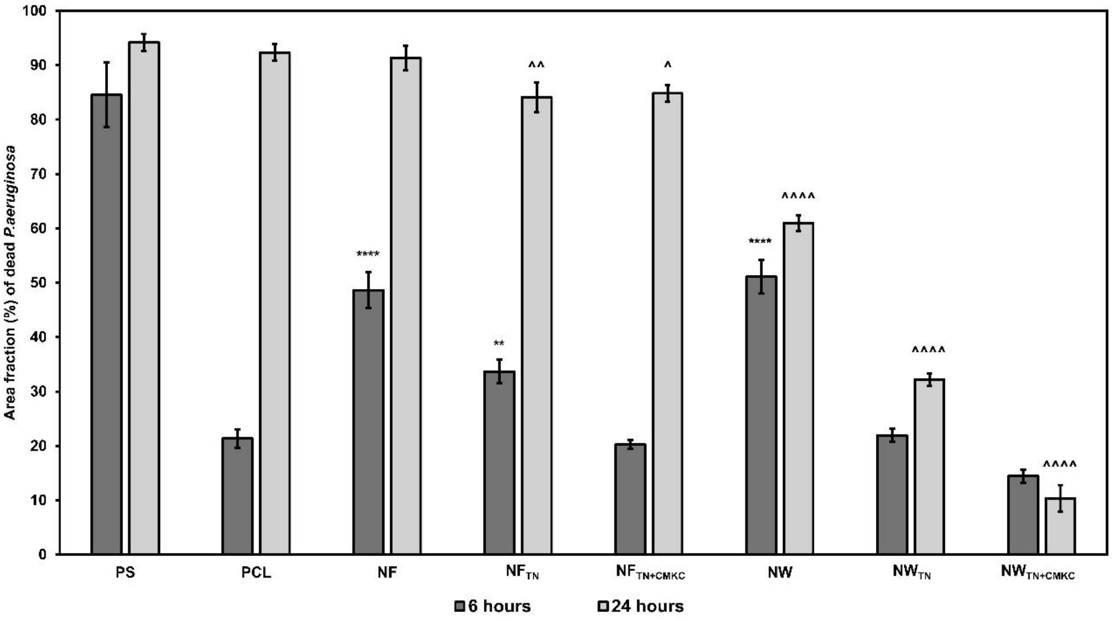

Figure 3.3.1.4: The graphs represent the percentage of the area fraction of different surfaces covered by dead *P. aeruginosa* bacteria after 6 and 24 hours of incubation. **, **** represent *p*-value <0.01 and <0.0001 when compared with PCL control at 6-hour timepoint. ^, ^^, ^^^^ represent *p*-value <0.05, <0.01 and <0.0001 when compared to PCL control at 24-hour timepoint.

Figure 3.3.1.5 and Figure 3.3.1.6 shows the fluorescence microscopic images of different surfaces after the incubation periods with *S. aureus*. **Figure 3.3.1.7 and Figure 3.3.1.8** also shows plots quantifying the % of area fraction of the surfaces covered by live and dead *S. aureus* bacteria over 6 and 24 hours of incubation periods. Similar to *P. aeruginosa*, live *S. aureus* bacteria attachment was significantly low in NF and NW surfaces compared to PCL surfaces after the 6-hour incubation period. But the % area fraction of live *S. aureus* bacteria increased even on the NF and NW surfaces after the 24-hour incubation period. However, unlike NF and NW surfaces, their modified surfaces, with TN and CMKC, exhibited increased antibacterial activity by drastically reducing live *S. aureus* attachment during both the incubation periods. For instance, after 24-hour incubation, % area fraction covered by live *S. aureus* on NF_{TN} and $NF_{TN+CMKC}$ were 1.7% and 0.51% respectively as opposed to NF with 82.5% of live S. *aureus* coverage. Similarly, NW_{TN} and $NW_{TN+CMKC}$ had just 0.72% and 0.67% when compared to NW which had 89.32% of live *S. aureus* coverage. This confirms the successful modification of NF and NW with TN and CMKC that has increased their antibacterial properties.

Results from the graphs of **Figure 3.3.1.8** represent that during 24-hour incubation period, there was a significant increase in % area fraction of dead *S. aureus* bacteria in all the nanostructured surfaces when compared to PCL surfaces. However, the modified NF and NW groups exhibited the most % area fraction of dead *S. aureus* bacteria compared to NF and NW groups. This again validates that NF and NW groups, modified with Tanfloc and CMKC, exhibited improved antibacterial properties.

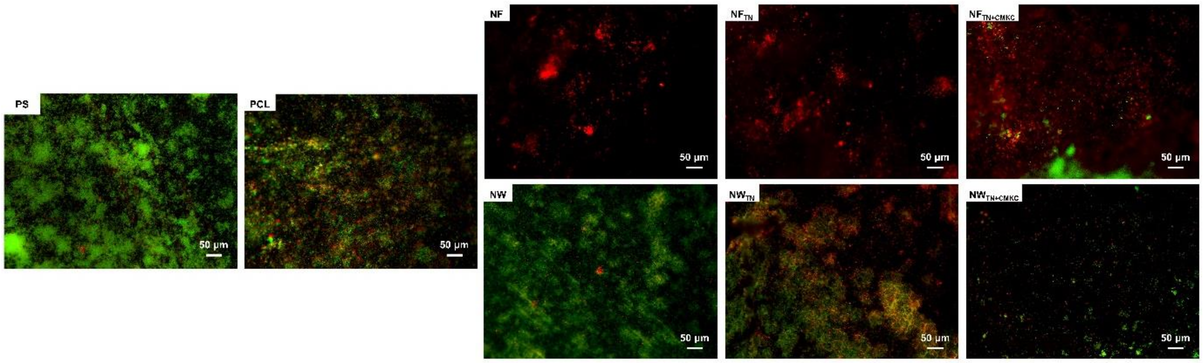

Figure 3.3.1.5: Representative fluorescence microscopic images of surfaces after 6 hours of incubation with *S. aureus*.

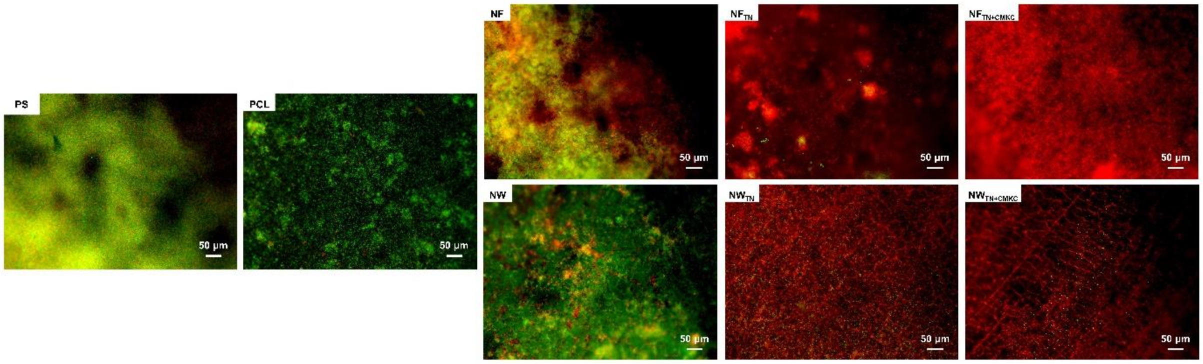

Figure 3.3.1.6: Representative fluorescence microscopic images of surfaces after 24 hours of incubation with *S. aureus*.

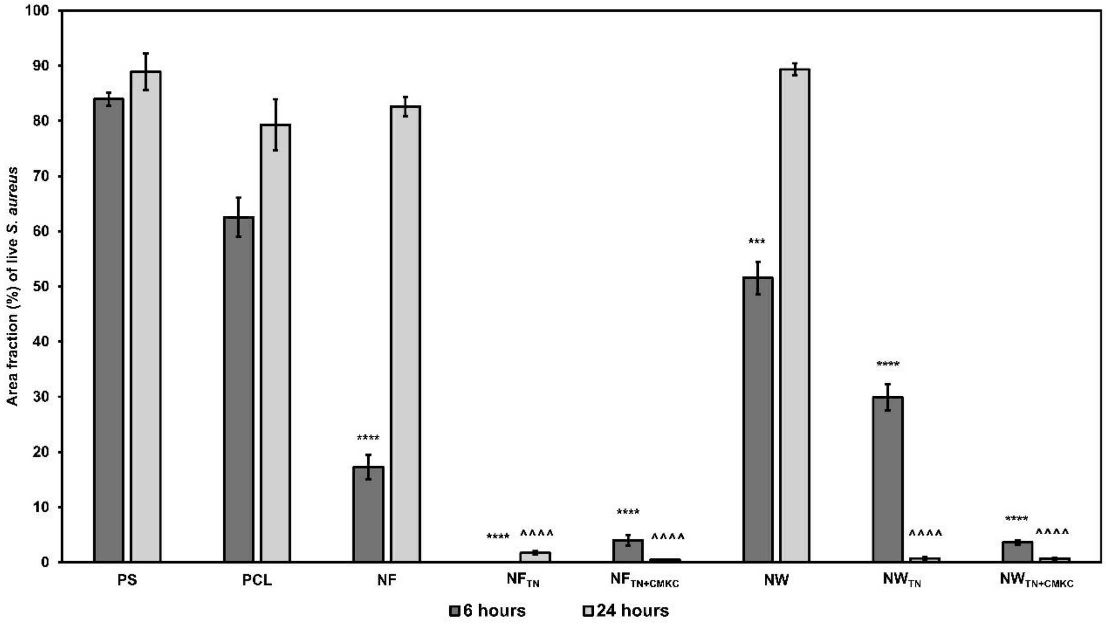

Figure 3.3.1.7: The graphs represent the percentage of the area fraction of different surfaces covered by live *S. aureus* bacteria after 6 and 24 hours of incubation. ***, **** represent *p*-value <0.001 and <0.0001 when compared to PCL control at 6-hour timepoint. ^^^^ represent *p*-value <0.0001 when compared to PCL control at 24-hour timepoint.

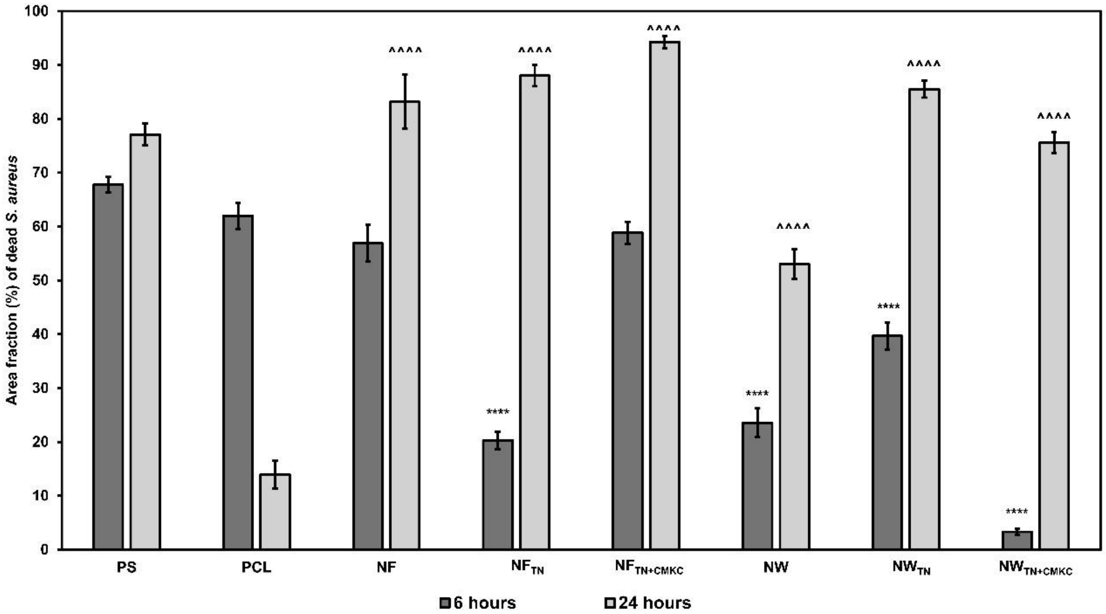

Figure 3.3.1.8: The graphs represent the percentage of the area fraction of different surfaces covered by dead *S. aureus* bacteria after 6 and 24 hours of incubation. **** and ^^^^ represent *p*-value <0.0001 when compared to PCL control at 6 and 24-hour timepoints respectively.

The amount of attachment of *S. aureus* bacteria on surfaces is high compared to *P. aeruginosa.* This difference in bacterial adhesion can be attributed to the presence of surface structures like pili and adhesins on the bacteria, which affect their binding effect. *P. aeruginosa* is characterized by its motility and the presence of pili, which are hair-like appendages that facilitate attachment to the surfaces [18]. On the other hand, *S. aureus* possesses a variety of adhesins that enhance its ability to attach to surfaces, including fibronectin-binding proteins and clumping factors [19,20]. These proteins can interact with the material surface enhancing adhesion. *P. aeruginosa*, while also possessing adhesins, tend to rely more on flagella and motility for attachment, which may not be as effective as the adhesive mechanisms employed by *S. aureus* [21]. Another important factor is the relative size of both the bacteria. *S. aureus* is a spherical-shaped bacteria with 0.5 to 1 µm diameter [20] whereas *P. aeruginosa* is a rod-shaped bacterium having length of 1-5 µm and width of 1 µm [18]. Due to this size difference, it is possible for the smaller *S. aureus* to agglomerate and cluster even in tiny spaces and further grow into colonies. Therefore, a substantial difference can be observed in the amount of bacterial adhesion between the two bacteria strains.

3.3.2 Bacteria Morphology

Understanding the morphological changes of viable bacteria on the implant surfaces is vital to determine how bacteria attach, proliferate and form biofilms. SEM images of different surfaces were captured after the bacteria were fixed by following appropriate fixing mechanisms. **Figure 3.3.2.1** and **Figure 3.3.2.2** shows the SEM images of surfaces after 6 and 24 hours of *P. aeruginosa* incubation respectively. Bacteria cells and colonies are highlighted with color in the figures for better visualization and distinction from the topography of the surfaces.

Similar to the results discussed in the previous section, initially the NF and NW groups exhibit reduced bacterial adhesion on their surfaces compared to the PCL control surfaces. However, after 24-hour incubation period, the modified NF and NW groups tend to show greater inhibition for bacterial adhesion and biofilm formation compared to their control groups. This is because incorporation of TN and CMKC onto surfaces significantly enhances their antibacterial properties, primarily due to their unique biochemical interactions with bacterial cells. TN exhibits inherent antimicrobial activity due to its amphoteric nature, allowing it to function as both polycation and polyanion in polyelectrolyte coatings. This duality of TN enables it to effectively disrupt bacterial cell walls and membranes, leading to bacterial cell lysis and death [22,23]. Moreover, the addition of CMKC, known for its biocompatibility and antibacterial properties, complements the action of TN. The negatively charged carboxymethyl groups in CMKC create an electrostatic repulsion between CMKC and the negatively charged surfaces of bacterial cells. This repulsion can disrupt the initial stages of bacterial adhesion, which is the critical step in biofilm formation [24]. The presence of carboxymethyl groups also enhances the solubility and bioactivity of KC, allowing for better interaction with bacterial cells. This interaction can lead to increased permeability of the bacterial cell membrane, resulting in cell lysis and death [25]. In addition to the direct antibacterial effects of CMKC, its antioxidant properties may also play a crucial role in mitigating bacterial activity. Antioxidants help reduce oxidative stress in the surrounding environment, which can be detrimental to bacteria survival [26]. This synergistic effect attributed to the unique properties of both TN and CMKC helps create an unfavorable environment for bacterial colonization. Therefore, these findings confirmed the improved antibacterial activity of TN and CMKC on PCL nanostructured surfaces.

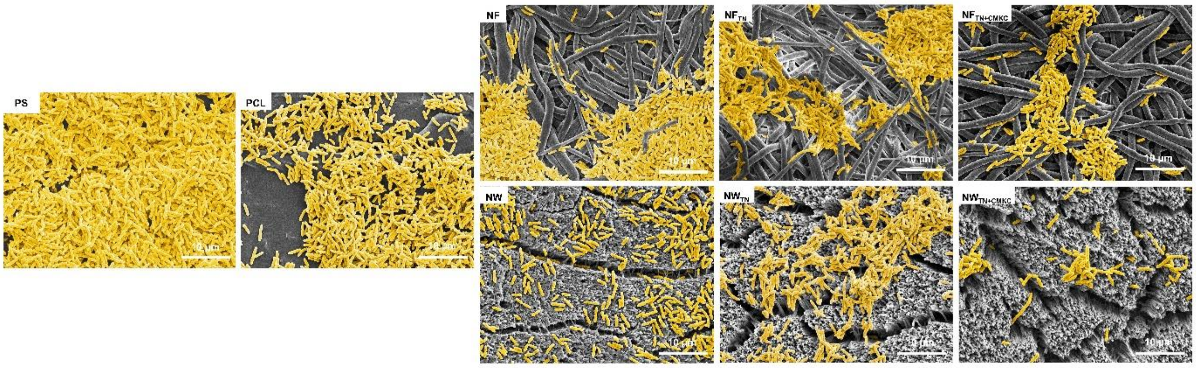

Figure 3.3.2.1: Representative SEM images of bacteria morphology after 6 hours of *P. aeruginosa* incubation captured at 2500x magnification.

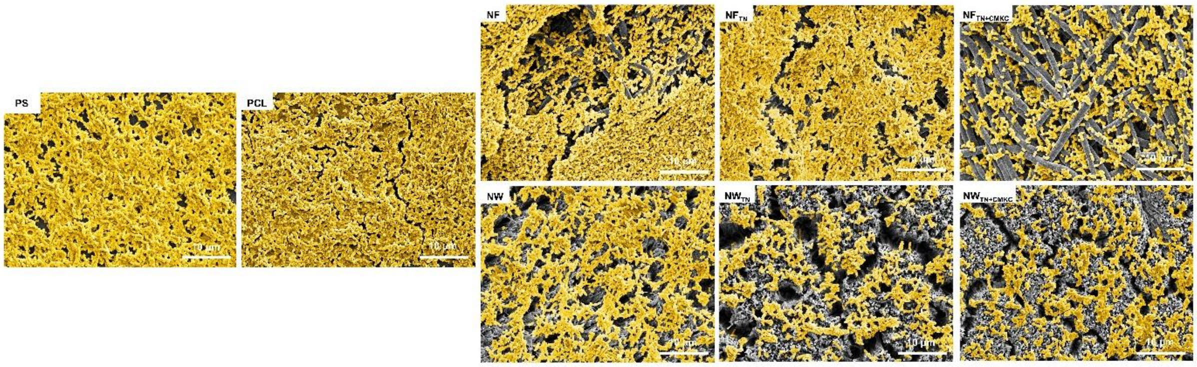

Figure 3.3.2.2: Representative SEM images of bacteria morphology after 24 hours of *P. aeruginosa* incubation captured at 2500x magnification.

Figure 3.3.2.3 and **Figure 3.3.2.4** show the SEM images of surfaces after 6 and 24 hours of *S. aureus* incubation respectively. Similar results were observed with Gram-positive *S. aureus* bacteria. Biofilm formation and bacterial colonization are observed on the control surfaces; however, the synergistic effect of nanostructured surfaces and their modification with TN and CMKC has significantly helped to reduce the biofilm formation and bacterial adhesion on the surfaces.

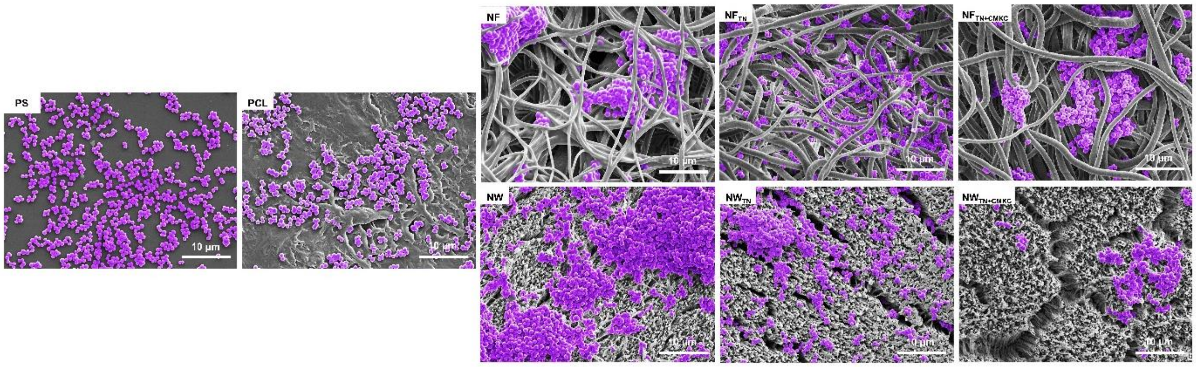

Figure 3.3.2.3: Representative SEM images of bacteria morphology after 6 hours of *S. aureus* incubation captured at 2500x magnification.

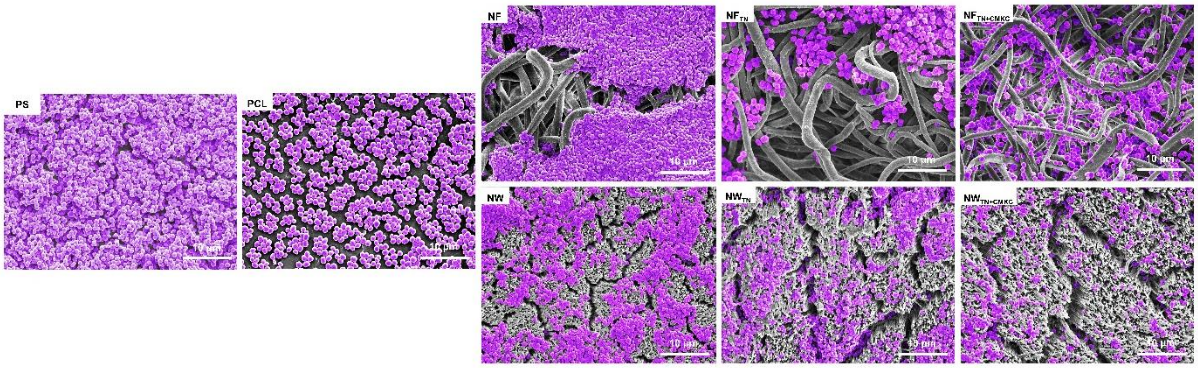

Figure 3.3.2.4: Representative SEM images of bacteria morphology after 24 hours of *S. aureus* incubation captured at 2500x magnification.

REFERENCES

[1] O.A. Sindeeva, E.S. Prikhozhdenko, I. Schurov, N. Sedykh, S. Goriainov, A. Karamyan, E.A. Mordovina, O.A. Inozemtseva, V. Kudryavtseva, L.E. Shchesnyak, R.A. Abramovich, S. Mikhajlov, G.B. Sukhorukov, Patterned drug-eluting coatings for tracheal stents based on pla, plga, and pcl for the granulation formation reduction: In vivo studies, Pharmaceutics 13 (2021) 1437. https://doi.org/10.3390/PHARMACEUTICS13091437/S1.

[2] M. Wang, T. Tang, Surface treatment strategies to combat implant-related infection from the beginning, J Orthop Translat 17 (2019) 42–54. https://doi.org/10.1016/J.JOT.2018.09.001.

[3] M. Ribeiro, F.J. Monteiro, M.P. Ferraz, Infection of orthopedic implants with emphasis on bacterial adhesion process and techniques used in studying bacterial-material interactions, Biomatter 2 (2012) 176–194. https://doi.org/10.4161/BIOM.22905.

[4] A. Singh, A.K. Dubey, Various Biomaterials and Techniques for Improving Antibacterial Response, ACS Appl Bio Mater 1 (2018) 3–20. https://doi.org/10.1021/ACSABM.8B00033/ASSET/IMAGES/MEDIUM/MT-2018-00033S_0017.GIF.

[5] A. Singh, A.K. Dubey, Improved antibacterial and cellular response of electrets and piezobioceramics, Https://Doi.Org/10.1177/0885328221991965 36 (2021) 441–459. https://doi.org/10.1177/0885328221991965.

[6] L. Townsend, R.L. Williams, O. Anuforom, M.R. Berwick, F. Halstead, E. Hughes, A. Stamboulis, B. Oppenheim, J. Gough, L. Grover, R.A.H. Scott, M. Webber, A.F.A. Peacock, A. Belli, A. Logan, F. De Cogan, Antimicrobial peptide coatings for hydroxyapatite: electrostatic and covalent attachment of antimicrobial peptides to surfaces, J R Soc Interface 14 (2017). https://doi.org/10.1098/RSIF.2016.0657.

[7] C.R. Arciola, Y.H. An, D. Campoccia, M.E. Donati, L. Montanaro, Etiology of Implant Orthopedic Infections: A Survey on 1027 Clinical Isolates, Https://Doi.Org/10.1177/039139880502801106 28 (2005) 1091–1100. https://doi.org/10.1177/039139880502801106.

[8] T.E. Rams, J.E. Degener, A.J. Van Winkelhoff, Antibiotic resistance in human peri-implantitis microbiota, Clin Oral Implants Res 25 (2014) 82–90. https://doi.org/10.1111/CLR.12160.

[9] M. Ha, L.M. Ngaage, R.D. Smith, J.R. Izac, P.C. Kim, D. Singh, S. Slezak, R.K. Ernst, J. Harro, Y.M. Rasko, An In Vitro Model of the Efficacy of Breast Implant Irrigant Solutions Against Gram-Negative Infections, Ann Plast Surg 89 (2022) 679–683. https://doi.org/10.1097/SAP.0000000000003302.

[10] J.M. Schierholz, J. Beuth, Implant infections: A haven for opportunistic bacteria, Journal of Hospital Infection 49 (2001) 87–93. https://doi.org/10.1053/jhin.2001.1052.

[11] E. Filipov, D. Delibaltov, R. Stefanov, B.S. Blagoev, G. Avdeev, P. Terziyska, R. Stoykov, A. Daskalova, Surface functionalization of 3D printed poly-ε-caprolactone by ultrashort laser mirostructuring and ZnO nanolayer deposition, J Phys Conf Ser 2710 (2024) 012018. https://doi.org/10.1088/1742-6596/2710/1/012018.

[12] C. Zhou, Y. Zhou, Y. Zheng, Y. Yu, K. Yang, Z. Chen, X. Chen, K. Wen, Y. Chen, S. Bai, J. Song, T. Wu, E. Lei, M. Wan, Q. Cai, L. Ma, W.L. Wong, Y. Bai, C. Zhang, X. Feng, Amphiphilic Nano-Swords for Direct Penetration and Eradication of Pathogenic Bacterial Biofilms, ACS Appl Mater Interfaces 15 (2023) 20458–20473. https://doi.org/10.1021/ACSAMI.3C03091/SUPPL_FILE/AM3C03091_SI_005.MP4.

[13] H. Lee, D.S. Won, S. Park, Y. Park, J.W. Kim, G. Han, Y. Na, M.H. Kang, S.B. Kim, H. Kang, J.K. Park, T.S. Jang, S.J. Lee, S.A. Park, S.S. Lee, J.H. Park, H. Do Jung, 3D-printed versatile biliary stents with nanoengineered surface for anti-hyperplasia and antibiofilm formation, Bioact Mater 37 (2024) 172–190. https://doi.org/10.1016/J.BIOACTMAT.2024.03.018.

[14] E. Sepehri, S.M. Mousavi, E. Saljoughi, M. Bahreini, M. Doaei, S. Kiani, Enhancing anti-biofouling property by incorporating graphene oxide-silver nanocomposite into polycaprolactone membrane for ultrafiltration application, Journal of Chemical Technology & Biotechnology 98 (2023) 2517–2531. https://doi.org/10.1002/JCTB.7478.

[15] H.R. Bakhsheshi-rad, E. Hamzah, W.S. Ying, M. Razzaghi, S. Sharif, A.F. Ismail, F. Berto, Improved bacteriostatic and anticorrosion effects of polycaprolactone/chitosan coated magnesium via incorporation of zinc oxide, Materials 14 (2021) 1930. https://doi.org/10.3390/MA14081930/S1.

[16] J.S. Son, E.J. Hwang, L.S. Kwon, Y.G. Ahn, B.K. Moon, J. Kim, D.H. Kim, S.G. Kim, S.Y. Lee, Antibacterial Activity of Propolis-Embedded Zeolite Nanocomposites for Implant Application, Materials 2021, Vol. 14, Page 1193 14 (2021) 1193. https://doi.org/10.3390/MA14051193.

[17] K. Du, Z. Gan, Cellular interactions on hierarchical poly(ε-caprolactone) nanowire micropatterns, ACS Appl Mater Interfaces 4 (2012) 4643–4650. https://doi.org/10.1021/AM301013E/ASSET/IMAGES/MEDIUM/AM-2012-01013E_0014.GIF.

[18] S.P. Diggle, M. Whiteley, Microbe profile: Pseudomonas aeruginosa: Opportunistic pathogen and lab rat, Microbiology (United Kingdom) 166 (2020) 30–33. https://doi.org/10.1099/MIC.0.000860/CITE/REFWORKS.

[19] C. Na, C.J. McNamara, N.R. Konkol, K.A. Bearce, R. Mitchell, S.T. Martin, The use of force-volume microscopy to examine bacterial attachment to titanium surfaces, Ann Microbiol 60 (2010) 495–502. https://doi.org/10.1007/S13213-010-0078-4/FIGURES/7.

[20] L.G. Harris, S.J. Foster, R.G. Richards, P. Lambert, D. Stickler, A. Eley, An introduction to Staphylococcus aureus, and techniques for identifying and quantifying S. aureus adhesins in relation to adhesion to biomaterials: review, Eur Cell Mater 4 (2002) 39–60. https://doi.org/10.22203/ECM.V004A04.

[21] J.A. Pointon, W.D. Smith, G. Saalbach, A. Crow, M.A. Kehoe, M.J. Banfield, A highly unusual thioester bond in a pilus adhesin is required for efficient host cell interaction, Journal of Biological Chemistry 285 (2010) 33858–33866. https://doi.org/10.1074/JBC.M110.149385/ATTACHMENT/C305CC8E-F669-4A10-B3A8-F9ED2D92E666/MMC1.PDF.

[22] R. Singh, Y.C. Madruga, A. Savargaonkar, A.F. Martins, M.J. Kipper, K.C. Popat, R. Singh, A. Savargaonkar, K.C. Popat, L.Y.C. Madruga, A.F. Martins, M.J. Kipper, Covalent Grafting of Tanfloc on Titania Nanotube Arrays: An Approach to Mitigate

Bacterial Adhesion and Improve the Antibacterial Efficacy of Titanium Implants, Adv Mater Interfaces (2024) 2400406. https://doi.org/10.1002/ADMI.202400406.

[23] S. Baghersad, L.Y.C. Madruga, A.F. Martins, K.C. Popat, M.J. Kipper, Expanding the Scope of an Amphoteric Condensed Tannin, Tanfloc, for Antibacterial Coatings, J Funct Biomater 14 (2023) 554. https://doi.org/10.3390/jfb14110554.

[24] S. Javadiyan, C.M. Cooksley, G.S. Bouras, S.S.T. Kao, C.A. Bennett, P.J. Wormald, S. Vreugde, A.J. Psaltis, Investigation of Kappa Carrageenan's muco-adhesive, antibacterial, and anti-biofilm properties, Int Forum Allergy Rhinol 12 (2022) 302–305. https://doi.org/10.1002/ALR.22899.

[25] M. Khodadadi Yazdi, F. Seidi, A. Hejna, P. Zarrintaj, N. Rabiee, J. Kucinska-Lipka, M.R. Saeb, S.A. Bencherif, Tailor-Made Polysaccharides for Biomedical Applications, ACS Appl Bio Mater 7 (2024) 4193–4230. https://doi.org/10.1021/ACSABM.3C01199/ASSET/IMAGES/LARGE/MT3C01199_0011.JPEG.

[26] L.Y.C. Madruga, R.M. Sabino, E.C.G. Santos, K.C. Popat, R. de C. Balaban, M.J. Kipper, Carboxymethyl-kappa-carrageenan: A study of biocompatibility, antioxidant and antibacterial activities, Int J Biol Macromol 152 (2020) 483–491. https://doi.org/10.1016/J.IJBIOMAC.2020.02.274.

CHAPTER 4

EFFECTS OF PCL NANOSTRUCTURED SURFACES ON ERYTHROCYTE INTEGRITY

4.1 Introduction

Assessing the biocompatibility of biomaterials is essential to understand the behavior and interaction of erythrocytes with the surfaces. Surface properties such as topography, chemistry, wettability etc., affects how erythrocyte cells attach and interact with surfaces. Erythrocytes play a critical role in the circulatory system, primarily in oxygen transportation. Their morphological changes and adhesion on surfaces can provide insights about potential hemolytic activity or adverse reactions to the material [1,2]. Additionally, studies have shown that certain surface characteristics of biomaterials can induce oxidative stress in erythrocytes, leading to lipid peroxidation and further morphological changes [3,4]. Such changes can compromise the oxygen-carrying capacity of erythrocytes, affecting overall tissue oxygenation and potentially leading to ischemic conditions [5,6]. This suggests that the assessment of erythrocyte integrity and adhesion is not only vital for understanding the immediate effects of biomaterials, but also for predicting the long-term effects of biocompatibility and functionality within the biological environment.

In this work, PCL nanostructured surfaces were characterized by erythrocyte adhesion, cell morphology and cytotoxicity assay. The percentage change in cell morphology was also calculated.

4.2 Materials and Methods

4.2.1 Cytotoxicity of Different Surfaces

To assess the cytotoxicity induced by different surfaces, a lactate dehydrogenase (LDH) based indicator assay was utilized (Cayman's LDH Cytotoxicity Assay Kit). After 1.5 hours of incubation of different surfaces with erythrocytes, 100 µL supernatants of the cell media were transferred from each surface to a new sterile 96-well plate. A 100 µL of LDH reaction solution was added to each well containing the cell supernatants that were previously added to the 96-well plate. The well plate was incubated at 37 °C with 5% CO_2 for 30 minutes. The plate reader measured the absorbance of the resultant solution at a wavelength of 490 nm. A negative control (highest LDH release) was established by lysing erythrocytes with 10% Triton-X100. The positive control (Sp, indicating spontaneous release) was prepared using erythrocyte suspension without any surface exposure. The assay protocol provided by the manufacturer was followed to determine the cytotoxicity induced by the surfaces against erythrocytes and thus the cytotoxicity was calculated.

4.2.2 Erythrocyte Adhesion on Different Surfaces

Erythrocyte adhesion on different surfaces was characterized using fluorescence microscopy. Rhodamine-Phalloidin (F-actin stain) was used to stain the adhered erythrocyte cells on the surfaces. The stock solution was prepared by resuspending the vial in 500 µL of 100% methanol (14 µM). The working solution was prepared by resuspending 11.25 µL of the stock solution in 2.25 mL PBS (final concentration 70 nM).

The erythrocyte suspension from the incubated surfaces was aspirated to remove floating cells, and the surfaces were rinsed twice with PBS to remove the rest of the non-adherent cells. Then, the fixative (3.7% formaldehyde in PBS) was added to the surfaces with adhered cells and incubated for 15 minutes at ambient room temperature. Subsequently, the fixative solution was aspirated and rinsed with PBS thrice after the incubation. Then, the permeative (1% Triton X-100 in DI water) was added to all surfaces and incubated at room temperature for three minutes. Later, the permeative solution was aspirated, and the surfaces were rinsed thrice with PBS to ensure complete removal of any residual solution. Then, the surfaces were exposed to the staining solution, prepared at a concentration of 1:200 (50 µL rhodamine + 10 mL PBS), and incubated at room temperature for 25 minutes. Finally, the staining solution was aspirated, and the surfaces were rinsed with PBS. The surfaces were then hydrated with PBS, just enough to be immersed in. The well-plates with the surfaces were immediately covered with aluminum foil to avoid any contact with ambient lights. The surfaces were imaged using a fluorescent microscope (Zeiss). Each surface was imaged at three different locations at a magnification of 20x. The images were processed with ImageJ to adjust their brightness and contrast. The entire procedure, from staining to imaging, was performed in darkness.

4.2.3 Erythrocyte Morphology on Different Surfaces

The morphology of adhered erythrocytes on different surfaces was characterized using SEM. Prior to SEM imaging, the erythrocytes adhered to the surfaces were fixed using a standard fixing procedure. The procedure for this study follows the same steps as done for bacteria morphology, as mentioned earlier in **section 3.2.3**.

4.2.5 Statistical Analysis

In the erythrocyte adhesion, a minimum of three samples (n_{min} = 3) of each surface were utilized for surface characterization and the experiments were repeated at least thrice (n_{min} = 9). In the erythrocyte morphology, a minimum of two samples (n_{min} = 2) of each surface were utilized for surface characterization and the experiments were repeated at least thrice (n_{min} = 6). For cytotoxicity, a minimum of four samples (n_{min} = 4) of each surface were utilized for surface characterization and the experiments were repeated at least twice (n_{min} = 8). Statistical one-way analysis of variance (ANOVA) and Tukey tests were conducted for the experiment data using OriginPro 2024 software at a 5% significance level ($p \leq 0.05$).

4.3 Results and Discussion

4.3.1 Cytotoxicity of Different Surfaces

In this work, PCL surface's topography and chemistry have been modified using different processes and chemicals. Hence, it is crucial to determine whether the surface modifications induce any kind of toxicity to the cells. This is vital to understand if the modified surfaces can be incorporated in the production of bio-implants which would be biocompatible to the host body. This is particularly important in clinical diagnostics, as increased LDH levels can indicate tissue damage or disease conditions, such as myocardial infarction or various cancers [7,8]. Commercially available LDH cytotoxicity assay, which follows a coupled two-step reaction, was utilized to characterize the cytotoxicity of different surfaces. The LDH assay protocol is based on an enzymatic coupling reaction, which plays an important role in cellular metabolism by catalyzing the conversion of lactate to pyruvate. Lactate dehydrogenase (LDH) is a cytosolic enzyme present in many different cell types, which is released into the cell culture medium when the plasma membrane of the cells are damaged. This LDH released from the damaged cells serves as an indicator of the cell membrane integrity and cell viability, thus a measurement of cytotoxicity [9]. The released LDH from the cells oxidizes lactate to pyruvate, concurrently reducing NAD+ to NADH. This newly formed NADH and H^+ is used by diaphorase (flavin-bound enzyme) to reduce a tetrazolium salt, iodonitrotetrazolium chloride (INT) which is used as a colorimetric indicator. The reduction of INT leads to the formation of a red colored formazan product, which is measurable at 490 nm [10]. The level of formazan produced is directly proportional to the amount of LDH released into the medium, as a result of cytotoxicity.

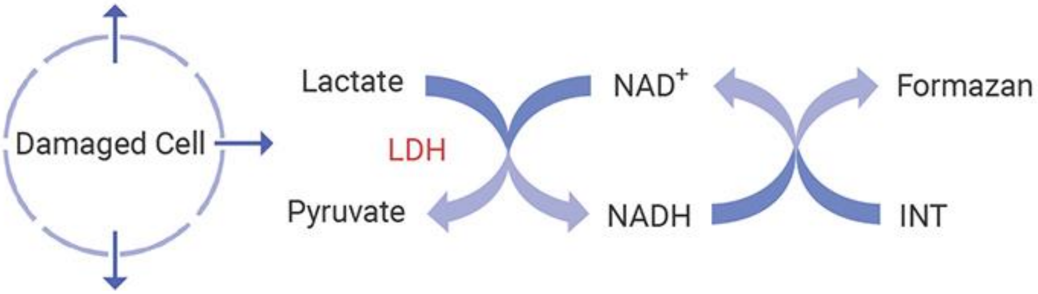

Figure 4.3.1.1: Schematic of LDH cytotoxicity assay mechanism [11]

The LDH activity of different surfaces was evaluated **(Figure 4.3.1.2)**. The maximum LDH activity was observed in the negative control (Max release) as the erythrocyte cells were lysed intentionally, to release the maximum possible amount of LDH. The positive control (Sp) was prepared by adding erythrocyte suspension to empty wells in the well-plate, which experienced natural cell death due to the interaction with the well-plate surfaces. The LDH activity on the negative control was significantly high compared to all the other surfaces exposed to the erythrocyte cell suspension, including the positive control. This significant difference in LDH activity of all surfaces with respect to the negative control indicated that the physical and chemical modifications done on the surfaces did not cause any cytotoxic effects on the cells.

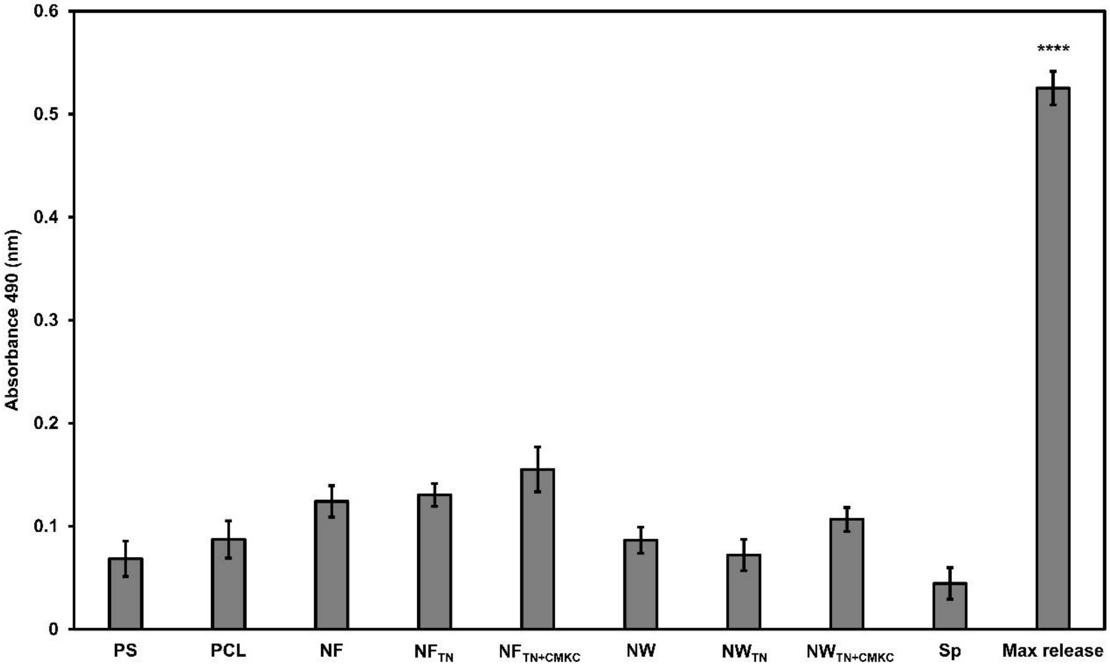

Figure 4.3.1.2: Cell cytotoxicity for erythrocytes exposed to different surfaces measured using LDH assay. Results indicate that the LDH activity on negative control (100% dead cells) was significantly high (**** represents *p*-value <0.0001) compared to the LDH activity on all the surfaces and the positive control (Sp = 100% live cells). Error bars represent the standard deviation.

4.3.2 Erythrocyte Adhesion on Different Surfaces

The erythrocyte adhesion on biomaterial surfaces is crucial for understanding the biocompatibility and cell viability of the materials. Understanding the adhesion properties of erythrocytes on surfaces is required to enhance the designs of biomaterials that can promote optimal healing and reduce complications related to blood-material interactions. When erythrocytes adhere to biomaterial surfaces, they can initiate a coagulation cascade, which is critical for wound healing and preventing excessive bleeding. For instance, hydrogels designed for hemostatic applications have shown that erythrocyte adhesion can enhance the clotting process by facilitating the aggregation of hemocytes and promoting a physiological response conducive to hemostasis [12,13]. Furthermore, the degree of erythrocyte adhesion can provide insights about the surface properties of biomaterials. Higher levels of erythrocyte adhesion may suggest that a material has favorable interactions with blood components, potentially leading to increased thrombosis, which can be beneficial in hemostatic applications [13]. In contrast, lower erythrocyte adhesion may indicate a non-thrombogenic surface, which is desirable in vascular grafts and stents to prevent thrombosis and ensure long-term patency [14,15]. The balance between promoting adhesion for hemostatic purposes and preventing excessive adhesion to avoid thrombosis is crucial for a biomaterial’s design.

To characterize the erythrocyte adhesion, the surfaces were incubated with erythrocyte suspension for 1.5 hours and 6 hours. After incubation, the erythrocytes were fixed on the surfaces using formaldehyde. Fixation process stabilizes the cellular structures, including the cytoskeleton, which is essential for maintaining the characteristic biconcave shape of erythrocytes. The cytoskeletal network of erythrocytes primarily consists of spectrin and actin, and other associated proteins that form a two-dimensional meshwork beneath the plasma membrane. This network is vital for maintaining the discocyte shape of erythrocytes, which is essential for their function in gas exchange and circulation [16,17]. Formaldehyde interacts with amino acids in proteins, forming methylene bridges that stabilize the protein structure. This cross-linking is important for maintaining the integrity of erythrocytes during subsequent analysis [18–20]. After the fixation process, the cells are lysed with triton X-100 permeative solution and then stained with rhodamine-conjugated phalloidin. The rhodamine-phalloidin, which has high affinity to F-actin, is used to stabilize the filamentous structures and preventing their depolymerization [21,22]. As rhodamine-phalloidin binds specifically to F-actin, it helps in highlighting the presence, organization and distribution of actin filaments in the cytoskeleton of the cells [23,24]. However, erythrocytes do not release actin in a free form under normal physiological conditions. Actin is primarily found in a polymerized state as a part of the cytoskeleton of the cell [25]. Hence, staining with rhodamine-phalloidin is typically performed after fixation and lysis to visualize the actin filaments within the cells. The staining is effective because the fixation process preserves the actin filaments in their polymerized form (F-actin), allowing for specific binding of rhodamine to these structures.

Erythrocyte adhesion on different surfaces was characterized using fluorescence microscopy at 1.5 hours **(Figure 4.3.2.1)** and 6 hours of incubation **(Figure 4.3.2.2)**. PS confirmed the cell viability of the erythrocytes suspension. Results from both the incubation periods indicate that NF and NW surfaces had less significant differences in erythrocyte adhesion when compared with PCL surfaces. On the other hand, the modified NF and NW surfaces (NF_{TN}, $NF_{TN+CMKC}$, NW_{TN} and $NW_{TN+CMKC}$) exhibited significantly higher erythrocyte adhesion compared to their control groups. This can be attributed to the addition of TN and CMKC to the surfaces. Incorporation of TN and CMKC increases the hydrophilicity of surfaces which can lead to improved water retention and protein adsorption on the surfaces [26]. Also, the anionic nature of both coatings can lead to enhanced electrostatic interactions with positively charged regions on the erythrocytes cell membrane, facilitating stronger adhesion [27]. The synergistic effect of these organic compounds, along with the modified nanostructured topography of the surfaces results in enhanced erythrocyte adhesion.

Comparing the results between modified NF and modified NW surfaces, the latter exhibited better erythrocyte adhesion relative to the former. This can be attributed to their topographical differences. The NF surfaces may not provide sufficient surface area for erythrocytes to form stable attachments. The high porosity and randomly interconnected structure of NF surfaces create a less favorable environment for erythrocytes adhesion. Erythrocytes require a certain level of rigidity in their substrate for stable attachment to specific adhesion sites, which is provided by the architecture of NW surfaces. The topographical features of NWs can mimic the extracellular matrix (ECM) found in natural tissues. These hierarchical and distributed features allow for a more extensive interaction between erythrocytes and the NW surfaces, leading to enhanced adhesion compared to random and flat NF surfaces.

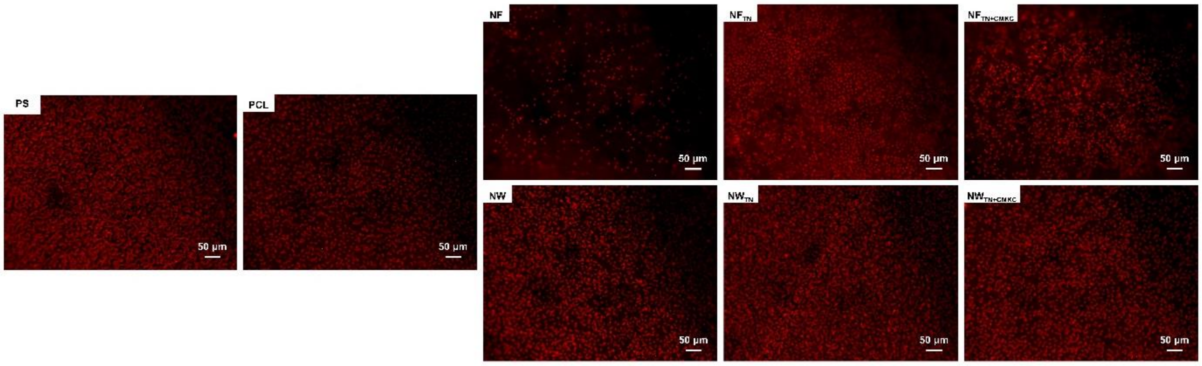

Figure 4.3.2.1: Representative fluorescence microscopic images of adhered erythrocyte cells on surfaces after 1.5 hours of incubation.

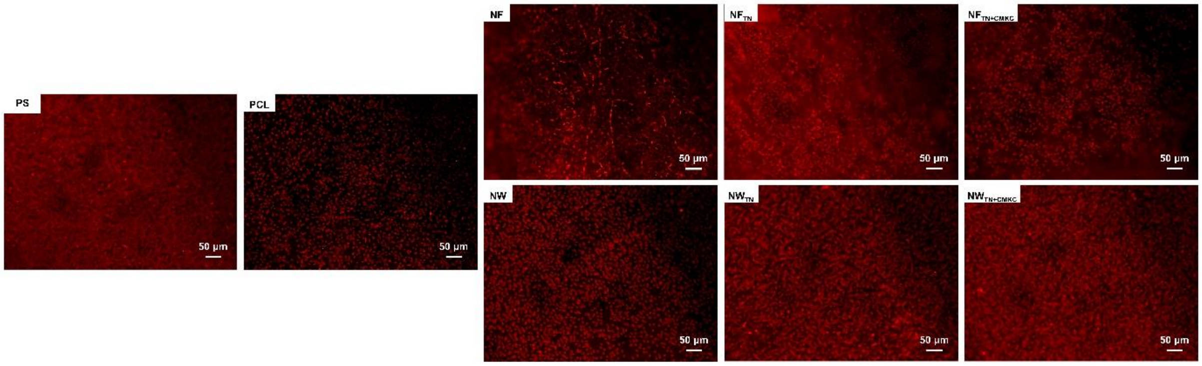

Figure 4.3.2.2: Representative fluorescence microscopic images of adhered erythrocyte cells on surfaces after 6 hours of incubation.

4.3.3 Erythrocyte Morphology on Different Surfaces

Erythrocytes, also known as red blood cells, are specialized cells, whose primary functionality is transportation of oxygen from the lungs to the body’s tissues and return carbon dioxide from the tissues back to the lungs. The unique structure of erythrocytes, characterized by their biconcave shape, maximizes surface area for gas exchange and facilitates their deformability, allowing them to navigate through the narrowest capillaries [28,29]. They are anuclear cells that contain lipids and proteins, and hemoglobin that binds to oxygen [30]. Poikilocytes are abnormally shaped erythrocytes that can indicate various pathological conditions [31–33]. Identification of erythrocytes with such disruptions and abnormalities in their cell morphology serves as a marker for hemolytic pathologies and oxidative damage to integrated membrane proteins [34,35]. Previous studies have reported that there are 18 different types of morphological changes observed in erythrocytes due to different conditions [36]. As previously mentioned in the literature review, few of such disrupted abnormal morphologies of erythrocytes include acanthocyte, echinocyte, schistocyte, spherocyte, stomatocyte, sickle cell, tear drop, elliptocyte, target cell, microlytic, macrolytic etc. Each type of these abnormalities corresponds to an associated condition, disease or deficiency. These cell morphological disruptions compromise erythrocyte's oxygen-carrying ability, which further leads to ischemic conditions [5,6]. Therefore, the capacity of erythrocytes to retain their discocyte, biconcave shape upon adhesion on surfaces is vital for effective blood flow and oxygen delivery, which indicates that the surfaces are capable of supporting normal erythrocyte functionality [12]. Hence, the erythrocyte cell morphology on different surfaces was characterized using SEM.

In this study, two types of morphological changes were observed prominently apart from a few others which weren't significant. Stomatocytes and different stages of echinocytes were the major morphological changes observed on different surfaces **(Figure 4.3.3.3)**. Stomatocytes have a mouth-like (stoma) appearance, often associated with alterations in the lipid bilayer of the cell membrane [37]. On the other hand, formation of echinocytes (erythrocytes with spicules) undergoes echinocytosis in which the surface area of the outer lipid monolayer is increased with respect to the inner monolayer. There are different stages of echinocytosis. During stage 1, the normal erythrocyte cell shape is transformed to have several irregularities on its rim. Furthermore, in stage 2, the cells transform into an elliptical body slightly distributed over its surface with different sizes of blunt spicules. Finally, it reaches a sphero-echinocyte morphology, where it is transformed into a sphere with short and sharp spicules. Even though the stomatocytes and initial stages of echinocytes are partially reversible, the sphero-echinocyte is irreversible due to extensive loss of membrane [38–40].

The SEM imaging results shows the morphological changes of erythrocytes adhered to different surfaces after 1.5 hours and 6 hours of incubation **(Figure 4.3.3.1**

and Figure 4.3.3.2). Also, the percentage of cell change on different surfaces was calculated from the SEM images and plotted as shown in **Figure 4.3.3.4**. PS was used as a standard control to monitor the morphology and cell viability of erythrocytes. After a 1.5-hour incubation period, PS had mostly stage 1 and stage 2 echinocytes on its surfaces. Compared to PS, PCL control surfaces had less echinocytes or other abnormal morphological changes after the 1.5-hour incubation period **(Figure 4.3.3.1)**. Data from **Figure 4.3.3.4** also shows that PCL surfaces had around 40% of cell change, while it was almost 97% for PS surfaces. However, after 6 hours of incubation, PCL surfaces also exhibited a drastic increase in the percentage of cell change, approximately equal to 95%, while PS surfaces had 100% cell change documented. This result can be correlated with **Figure 4.3.3.2**, where PS surfaces were completely filled with sphero-echinocytes, while PCL surfaces exhibited multiple morphological changes like echinocytes, stomatocytes and punctured cell structures with holes, which are an indication of hemolysis **(Figure 4.3.3.4)** [41]. NW surfaces has shown similar results as PCL after 1.5 and 6 hours with relatively more stomatocytes than echinocytes **(Figure 4.3.3.1, Figure 4.3.3.2 and Figure 4.3.3.4)**. No sphero-echinocytes were observed on NW surfaces unlike PS and PCL surfaces. SEM images of both the NF and modified NF surfaces (NF_{TN} and $NF_{TN+CMKC}$) didn’t show any cell attachments unexpectedly **(Figure 4.3.3.1 and Figure 4.3.3.2)**. This could possibly be due to the extensive washing of surfaces with different concentrations of ethanol, carried out during the SEM fixation process, which might have detached the weakly adhered cells from these surfaces. However, results from fluorescence study of 1.5 hours and 6 hours (**Figure 4.3.2.1 and Figure 4.3.2.2),** which has undergone fewer steps of washing during fixation and staining processes, help in visualizing the morphology of adhered erythrocytes on NF and modified NF surfaces. NF surfaces had less amount of cells compared to PCL and were randomly scattered after 1.5 hours. After 6 hours, it was evident that the cells had a significant morphological change as they can be seen tracing the fibrous structures of NF surfaces. In contrast, both the adhesion and morphology of erythrocytes were significantly improved in both NF_{TN} and $NF_{TN+CMKC}$ surfaces compared to NF. Similarly, NW_{TN} and $NW_{TN+CMKC}$ had a greater number of healthy erythrocyte cells, with the normal biconcave shape, as opposed to its control NW surfaces. For instance, results from **Figure 4.3.3.4** indicate that NW_{TN} and $NW_{TN+CMKC}$ surfaces had just 19.5% and 25.07% of cell change respectively after 1.5 hours of incubation. After 6 hours of incubation, % cell change in NW_{TN} had slightly increased to 26.2% and in $NW_{TN+CMKC}$ had increased to 31.7%, which were still significantly better and improved results compared to their control surfaces. Even this reduced % cell change contained only early stages of echinocytes and stomatocytes, and no sphero-echinocytes.

The PS surfaces exhibited expected results with respect to previous literature [42]. The morphological changes of cells on PCL surfaces can be attributed to the physiochemical interactions between the cell membrane and PCL material, which can disrupt the lipid bilayer’s integrity and alter the membrane’s mechanical properties. The primary issue with PCL surfaces is its hydrophobicity that leads to poor protein adsorption, which is essential for the initial stages of blood-material interaction. Even though PCL surfaces exhibit good biocompatibility with certain cells, their hemocompatibility is poor due to insufficient protein adsorption and subsequent platelet activation, which are highly influenced by the surface wettability [43]. Protein adsorption and platelet activation are critical for the initial erythrocyte attachment. Proteins such as fibrinogen and albumin play important roles in mediating adhesion of platelets and erythrocytes to surfaces, thereby influencing the overall hemocompatibility of the material [44–46]. However, excessive protein adsorption and platelet activation pose serious risks for hemocompatibility, particularly concerning thrombosis [45,47]. This danger of thrombosis becomes pronounced when the balance between protein adsorption and platelet activation is disrupted. Therefore, as far as protein adsorption and platelet activation are important, preventing excessive occurrences of those is crucial.

The topography and wettability of NF and NW surfaces influence the cell interactions. Leszczak's work reported that PCL NFs may exhibit reduced hemocompatibility compared to PCL NWs. This reduction is attributed to the increased promotion of platelet adhesion and clustering on the surface of NFs, which leads to thrombus formation. In contrast, PCL NWs, due to their distinct morphology and topography, may facilitate a more optimal interaction with blood components, potentially leading to lower platelet activation and aggregation [44,48,49]. These findings align with the results of this study, where NW surfaces exhibited slightly reduced morphological changes in erythrocytes, compared to NF surfaces.

Furthermore, the addition of TN and CMKC on these nanostructured surfaces exhibited a significantly drastic impact on retaining the health and morphology of adhered erythrocytes. This can be attributed to the synergistic effect provided by both physical and chemical modifications done on these surfaces, which enhanced its surface properties and erythrocyte cell compatibility. The hydrophilic nature of TN and the functional properties of CMKC, combined with nanostructured surfaces, create a more stable microenvironment for erythrocytes [26,50]. This environment helps the cells to maintain its structural integrity and functionality, and thus reducing the likelihood of hemolysis.

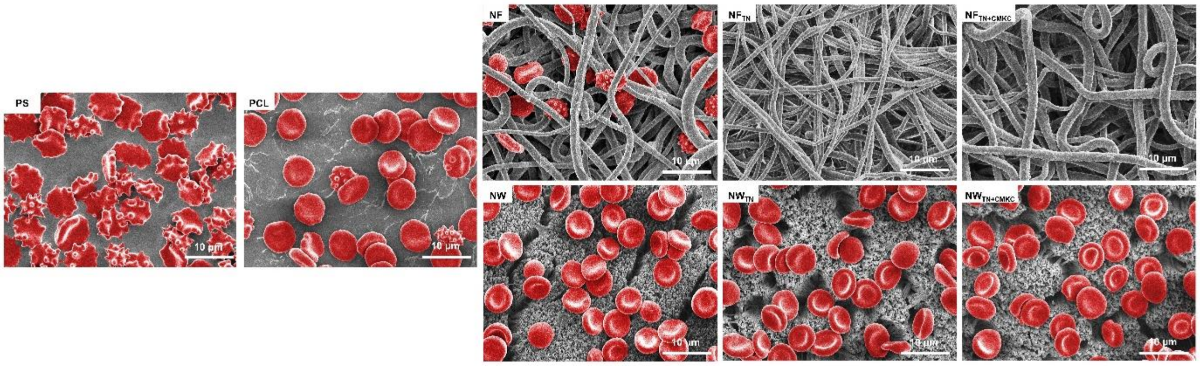

Figure 4.3.3.1: Representative SEM images depicting erythrocyte cells morphological changes on surfaces after 1.5 hours of incubation (2500x magnification).

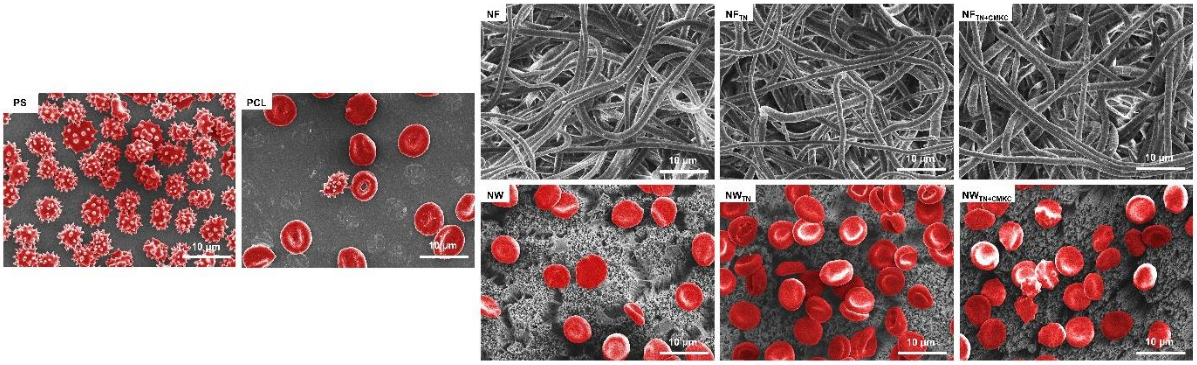

Figure 4.3.3.2: Representative SEM images depicting erythrocyte cells morphological changes on surfaces after 6 hours of incubation (2500x magnification).

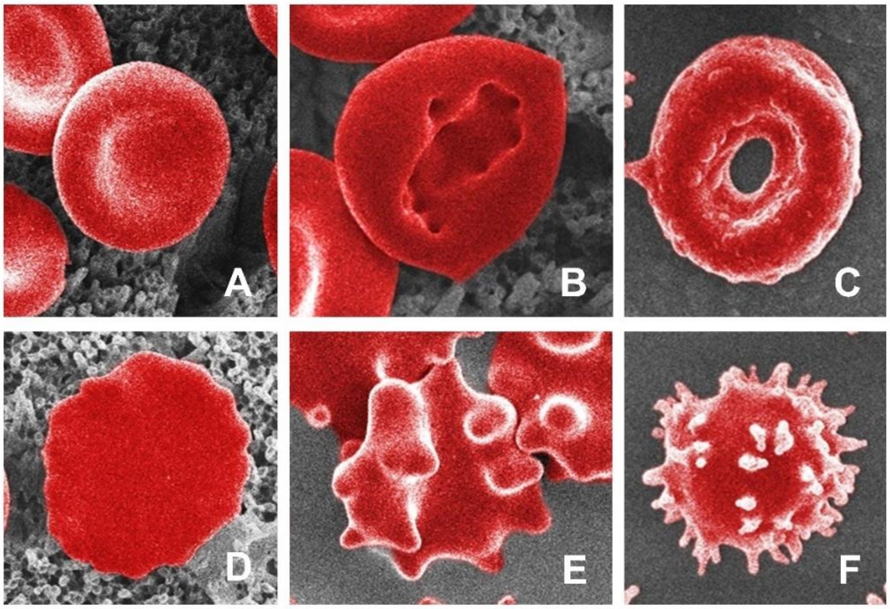

Figure 4.3.3.3: Types of morphological changes observed in erythrocytes adhered to different surfaces: (A) Normal biconcave shape (B) Stomatocyte (C) Punctured cell membrane with holes being a sign of hemolysis (D) Stage 1 Echinocyte (E) Stage 2 Echinocyte (F) Sphero-Echinocyte.

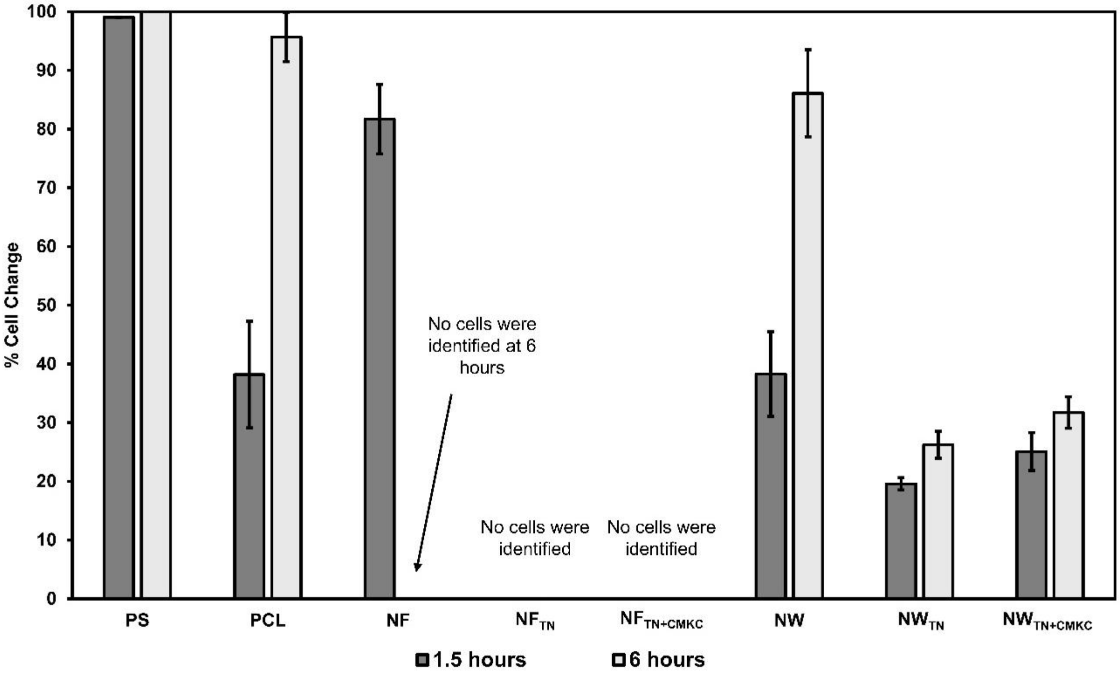

Figure 4.3.3.4: Percentage of morphological changes in erythrocytes on different surfaces after 1.5 and 6 hours of incubation, characterized from SEM images Figure 4.3.3.1 and Figure 4.3.3.2. Error bars represent standard deviation. No erythrocyte cells adhesion was identified on NF at 1.5 hours and NF$_{TN}$ & NF$_{TN+CMKC}$ during both the incubation periods.

REFERENCES

[1] C. Guo, J. Hu, L. Kao, D. Pan, K. Luo, N. Li, Z. Gu, Pepetide Dendron-Functionalized Mesoporous Silica Nanoparticle-Based Nanohybrid: Biocompatibility and Its Potential as Imaging Probe, ACS Biomater Sci Eng 2 (2016) 860–870. https://doi.org/10.1021/ACSBIOMATERIALS.6B00093/ASSET/IMAGES/MEDIUM/AB-2016-00093K_0016.GIF.

[2] H. Yuan, L. Chen, F.F. Hong, A Biodegradable Antibacterial Nanocomposite Based on Oxidized Bacterial Nanocellulose for Rapid Hemostasis and Wound Healing, ACS Appl Mater Interfaces 12 (2020) 3382–3392. https://doi.org/10.1021/ACSAMI.9B17732/ASSET/IMAGES/MEDIUM/AM9B17732_0010.GIF.

[3] Z. Wu, F. Jin, L. Wang, Y. Zhao, Y. Jiang, J. Li, P. Tu, J. Zheng, Antioxidant Effects of Baoyuan Decoction on Dysfunctional Erythrocytes in High-Fat Diet-Induced Hyperlipidemic ApoE-/- Mice, Oxid Med Cell Longev 2019 (2019) 5172480. https://doi.org/10.1155/2019/5172480.

[4] V. V. Revin, S.M. Filatova, I. V. Syusin, M.Y. Yazykova, E.S. Revina, N. V. Gromova, A.A. Devyatkin, Study of correlation between state and composition of lipid phase and change in erythrocytes structure under induction of oxidative processes, Int J Hematol 101 (2015) 487–496. https://doi.org/10.1007/S12185-015-1758-4/FIGURES/6.

[5] N. Alexandre, E. Costa, S. Coimbra, A. Silva, A. Lopes, M. Rodrigues, M. Santos, A.C. Maurício, J.D. Santos, A.L. Luís, In vitro and in vivo evaluation of blood coagulation

activation of polyvinyl alcohol hydrogel plus dextran-based vascular grafts, J Biomed Mater Res A 103 (2015) 1366–1379. https://doi.org/10.1002/JBM.A.35275.

[6] D. Kouroupis, T.G. Baboolal, E. Jones, P. V. Giannoudis, Native multipotential stromal cell colonization and graft expander potential of a bovine natural bone scaffold, Journal of Orthopaedic Research 31 (2013) 1950–1958. https://doi.org/10.1002/JOR.22438.

[7] L. Zhou, Z. Xie, Z. Shao, W. Chen, H. Xie, X. Cui, G. Qin, N. Zhao, Modeling the relationship between baseline lactate dehydrogenase and prognosis in patients with extensive-disease small cell lung cancer: a retrospective cohort study, J Thorac Dis 10 (2018) 1043–1049. https://doi.org/10.21037/JTD.2018.02.16.

[8] claresta diella, N. Mudjihartini, D. Sunardi, D.N. Chandra, Y. Yulhasri, A.M. Jayusman, Serum Lactate Dehydrogenase Activity and Its Corellation with Carbohydrate Intake in Advanced Lung Cancer Patients, World Nutrition Journal 2 (2019) 1–8. https://doi.org/10.25220/WNJ.V02.I2.0002.

[9] S. Kaja, A.J. Payne, Y. Naumchuk, P. Koulen, Quantification of Lactate Dehydrogenase for Cell Viability Testing Using Cell Lines and Primary Cultured Astrocytes, Curr Protoc Toxicol 72 (2017) 2.26.1-2.26.10. https://doi.org/10.1002/CPTX.21.

[10] S. Kaja, A.J. Payne, T. Singh, J.K. Ghuman, E.G. Sieck, P. Koulen, An optimized lactate dehydrogenase release assay for screening of drug candidates in neuroscience, J Pharmacol Toxicol Methods 73 (2015) 1–6. https://doi.org/10.1016/J.VASCN.2015.02.001.

[11] Cytotoxicity LDH Assay Kit | MedChemExpress, (n.d.). https://www.medchemexpress.com/inhibitor-kit/cytotoxicity-ldh-assay-kit.html (accessed October 13, 2024).

[12] W. Huang, S. Cheng, X. Wang, Y. Zhang, L. Chen, L. Zhang, Noncompressible Hemostasis and Bone Regeneration Induced by an Absorbable Bioadhesive Self-Healing Hydrogel, Adv Funct Mater 31 (2021) 2009189. https://doi.org/10.1002/ADFM.202009189.

[13] L. Teng, Z. Shao, Q. Bai, X. Zhang, Y.S. He, J. Lu, D. Zou, C. Feng, C.M. Dong, Biomimetic Glycopolypeptide Hydrogels with Tunable Adhesion and Microporous Structure for Fast Hemostasis and Highly Efficient Wound Healing, Adv Funct Mater 31 (2021) 2105628. https://doi.org/10.1002/ADFM.202105628.

[14] J.T. Horobin, S. Sabapathy, M.J. Simmonds, Repetitive Supra-Physiological Shear Stress Impairs Red Blood Cell Deformability and Induces Hemolysis, Artif Organs 41 (2017) 1017–1025. https://doi.org/10.1111/AOR.12890.

[15] O.K. Baskurt, H.J. Meiselman, Erythrocyte aggregation: Basic aspects and clinical importance, Clin Hemorheol Microcirc 53 (2013) 23–37. https://doi.org/10.3233/CH-2012-1573.

[16] T. Franco, P.S. Low, Erythrocyte adducin: A structural regulator of the red blood cell membrane, Transfusion Clinique et Biologique 17 (2010) 87–94. https://doi.org/10.1016/J.TRACLI.2010.05.008.

[17] Y.K. Park, C.A. Best, K. Badizadegan, R.R. Dasari, M.S. Feld, T. Kuriabova, M.L. Henle, A.J. Levine, G. Popescu, Measurement of red blood cell mechanics during

morphological changes, Proc Natl Acad Sci U S A 107 (2010) 6731–6736. https://doi.org/10.1073/PNAS.0909533107/SUPPL_FILE/SM1.MOV.

[18] P.A. Arndt, B.M. Kumpel, Blood doping in athletes—Detection of allogeneic blood transfusions by flow cytofluorometry, Am J Hematol 83 (2008) 657–667. https://doi.org/10.1002/AJH.21196.

[19] S. Chow, D. Hedley, P. Grom, R. Magari, J.W. Jacobberger, T.V. Shankey, Whole blood fixation and permeabilization protocol with red blood cell lysis for flow cytometry of intracellular phosphorylated epitopes in leukocyte subpopulations, Cytometry Part A 67A (2005) 4–17. https://doi.org/10.1002/CYTO.A.20167.

[20] B. Metz, G.F.A. Kersten, P. Hoogerhout, H.F. Brugghe, H.A.M. Timmermans, A. De Jong, H. Meiring, J. Ten Hove, W.E. Hennink, D.J.A. Crommelin, W. Jiskoot, Identification of formaldehyde-induced modifications in proteins: Reactions with model peptides, Journal of Biological Chemistry 279 (2004) 6235–6243. https://doi.org/10.1074/JBC.M310752200/ASSET/493E0C23-C00B-443C-82DC-381A0F5FE250/MAIN.ASSETS/GR9.JPG.

[21] M. Asghari-Khiavi, B.R. Wood, A. Mechler, K.R. Bambery, D.W. Buckingham, B.M. Cooke, D. McNaughton, Correlation of atomic force microscopy and Raman micro-spectroscopy to study the effects of ex vivo treatment procedures on human red blood cells, Analyst 135 (2010) 525–530. https://doi.org/10.1039/B919245J.

[22] D. Tao, J. Wu, Y. Feng, J. Qin, J. Hu, J. Gong, New method for the analysis of cell cycle–specific apoptosis, Cytometry Part A 57A (2004) 70–74. https://doi.org/10.1002/CYTO.A.10117.

[23] I. Miyakawa, K. Mitomi, Y. Ueda, N. Sando, The Close Location of Actin Patches to Mitochondria during Sporulation of the Yeast Saccharomyces cerevisiae, Cytologia (Tokyo) 71 (2006) 439–445. https://doi.org/10.1508/CYTOLOGIA.71.439.

[24] K.D. Costa, W.J. Hucker, F.C.P. Yin, Buckling of actin stress fibers: A new wrinkle in the cytoskeletal tapestry, Cell Motil Cytoskeleton 52 (2002) 266–274. https://doi.org/10.1002/CM.10056.

[25] A. Hrovat, A.B. Zavec, A. Pogačnik, R. Frangež, M. Vrecl, Establishing and functional characterization of an HEK-293 cell line expressing autofluorescently tagged β-actin (pEYFP-actin) and the neurokinin type 1 receptor (NK1-R), Cell Mol Biol Lett 15 (2010) 55–69. https://doi.org/10.2478/S11658-009-0034-0/MACHINEREADABLECITATION/RIS.

[26] S. Ilanlou, M. Khakbiz, G. Amoabediny, J. Mohammadi, H. Rabbani, Carboxymethyl kappa carrageenan-modified decellularized small-diameter vascular grafts improving thromboresistance properties, J Biomed Mater Res A 107 (2019) 1690–1701. https://doi.org/10.1002/JBM.A.36684.

[27] S. Abbasi-Ravasjani, H. Seddiqi, A. Moghaddaszadeh, M.E. Ghiasvand, J. Jin, E. Oliaei, R.G. Bacabac, J. Klein-Nulend, Sulfated carboxymethyl cellulose and carboxymethyl κ-carrageenan immobilization on 3D-printed poly-ε-caprolactone scaffolds differentially promote pre-osteoblast proliferation and osteogenic activity, Front Bioeng Biotechnol 10 (2022) 957263. https://doi.org/10.3389/FBIOE.2022.957263/BIBTEX.

[28] C.S. Olver, Erythrocyte Structure and Function, Schalm's Veterinary Hematology, Seventh Edition (2020) 158–165. https://doi.org/10.1002/9781119500537.CH20.

[29] V. V. Revin, N. V. Gromova, E.S. Revina, N.A. Mel'Nikova, L.A. Balykova, I.N. Solomadin, A.Y. Tychkov, N. V. Revina, O.Y. Gromova, I. V. Anashkina, V.A. Yakushkin, Study of the Structure, Oxygen-Transporting Functions, and Ionic Composition of Erythrocytes at Vascular Diseases, Biomed Res Int 2015 (2015) 973973. https://doi.org/10.1155/2015/973973.

[30] M. Diez-Silva, M. Dao, J. Han, C.T. Lim, S. Suresh, Shape and Biomechanical Characteristics of Human Red Blood Cells in Health and Disease, MRS Bull 35 (2010) 382–388. https://doi.org/10.1557/MRS2010.571.

[31] J. Ford, J. Ford, Red blood cell morphology, Int J Lab Hematol 35 (2013) 351–357. https://doi.org/10.1111/IJLH.12082.

[32] M.M. Christopher, M.G. Hawkins, A.G. Burton, Poikilocytosis in Rabbits: Prevalence, Type, and Association with Disease, PLoS One 9 (2014) e112455. https://doi.org/10.1371/JOURNAL.PONE.0112455.

[33] S. Man Tsui Rafay Ahmed Noreen Amjad Irfan Ahmed Jingwei Yang Francis Manno Ishan Barman Wei-Chuan Shih Condon Lau Suet Man Tsui, R. Ahmed, N. Amjad, I. Ahmed, J. Yang, F. Manno, I. Barman, W.-C. Shih, C. Lau, S. Man Tsui, Single red blood cell analysis reveals elevated hemoglobin in poikilocytes, Https://Doi.Org/10.1117/1.JBO.25.1.015004 25 (2020) 015004. https://doi.org/10.1117/1.JBO.25.1.015004.

[34] F.A. Ansari, S.N. Ali, R. Mahmood, Sodium nitrite-induced oxidative stress causes membrane damage, protein oxidation, lipid peroxidation and alters major metabolic

pathways in human erythrocytes, Toxicology in Vitro 29 (2015) 1878–1886. https://doi.org/10.1016/J.TIV.2015.07.022.

[35] J.G. Mohanty, E. Nagababu, J.M. Rifkind, Red blood cell oxidative stress impairs oxygen delivery and induces red blood cell aging, Front Physiol 5 FEB (2014) 75882. https://doi.org/10.3389/FPHYS.2014.00084/BIBTEX.

[36] H. Singh Virk, · Ketul, C. Popat, Erythrocyte interaction with titanium nanostructured surfaces, In Vitro Models 2022 1:4 1 (2022) 347–363. https://doi.org/10.1007/S44164-022-00031-Y.

[37] G. Lim H. W., M. Wortis, R. Mukhopadhyay, Red Blood Cell Shapes and Shape Transformations: Newtonian Mechanics of a Composite Membrane, Soft Matter 4 (2009) 83–139. https://doi.org/10.1002/9783527623372.ch2a.

[38] H. Xia, G. Khanal, B.C. Strachan, E. Vörös, N.Z. Piety, S.C. Gifford, S.S. Shevkoplyas, Washing in hypotonic saline reduces the fraction of irreversibly-damaged cells in stored blood: a proof-of-concept study, Blood Transfusion 15 (2017) 463. https://doi.org/10.2450/2017.0013-17.

[39] M.U. Martínez-Martínez, L.M.D.G. Llamazares-Azuara, D. Martínez-Galla, P.B. Mandeville, F. Valadez-Castillo, S. Román-Acosta, J.A. Borjas-García, C. Abud-Mendoza, Urinary sediment suggests lupus nephritis histology, Lupus 26 (2017) 580–587. https://doi.org/10.1177/0961203316669241/ASSET/IMAGES/LARGE/10.1177_0961203316669241-FIG4.JPEG.

[40] K. Sanford, B.J. Fisher, E. Fowler, A.A. Fowler, R. Natarajan, Attenuation of Red Blood Cell Storage Lesions with Vitamin C, Antioxidants 2017, Vol. 6, Page 55 6 (2017) 55. https://doi.org/10.3390/ANTIOX6030055.

[41] I. Mustafa, A. Al Marwani, K. Mamdouh Nasr, N. Abdulla Kano, T. Hadwan, Time Dependent Assessment of Morphological Changes: Leukodepleted Packed Red Blood Cells Stored in SAGM, Biomed Res Int 2016 (2016) 4529434. https://doi.org/10.1155/2016/4529434.

[42] P. Wong, A hypothesis of the disc–sphere transformation of the erythrocytes between glass surfaces and of related observations, J Theor Biol 233 (2005) 127–135. https://doi.org/10.1016/J.JTBI.2004.09.013.

[43] L. Liu, S. Guo, J. Chang, C. Ning, C. Dong, D. Yan, Surface modification of polycaprolactone membrane via layer-by-layer deposition for promoting blood compatibility, J Biomed Mater Res B Appl Biomater 87B (2008) 244–250. https://doi.org/10.1002/JBM.B.31103.

[44] V. Leszczak, B.S. Smith, K.C. Popat, Hemocompatibility of polymeric nanostructured surfaces, J Biomater Sci Polym Ed 24 (2013) 1529–1548. https://doi.org/10.1080/09205063.2013.777228.

[45] L.C. Xu, J.W. Bauer, C.A. Siedlecki, Proteins, platelets, and blood coagulation at biomaterial interfaces, Colloids Surf B Biointerfaces 124 (2014) 49–68. https://doi.org/10.1016/J.COLSURFB.2014.09.040.

[46] H.S. Lee, N. Tomczyk, J. Kandel, R.J. Composto, D.M. Eckmann, Hemocompatibility of chitosan/poly(acrylic acid) grafted polyurethane tubing, J Mater Chem B 1 (2013) 6382–6391. https://doi.org/10.1039/C3TB21218A.

[47] M. Weber, H. Steinle, S. Golombek, L. Hann, C. Schlensak, H.P. Wendel, M. Avci-Adali, Blood-Contacting Biomaterials: In Vitro Evaluation of the Hemocompatibility, Front Bioeng Biotechnol 6 (2018) 395774. https://doi.org/10.3389/FBIOE.2018.00099/BIBTEX.

[48] V. Leszczak, K.C. Popat, Improved in vitro blood compatibility of polycaprolactone nanowire surfaces, ACS Appl Mater Interfaces 6 (2014) 15913–15924. https://doi.org/10.1021/AM503508R/ASSET/IMAGES/LARGE/AM-2014-03508R_0015.JPEG.

[49] H.B. Hagh, L.D. Unsworth, F. Doustdar, A. Olad, Fibrous electrospun polycaprolactone nanomat reinforced with halloysite nanotubes: Preparation and study of its potential application as tissue engineering scaffold, Polym Adv Technol 34 (2023) 1671–1685. https://doi.org/10.1002/PAT.6001.

[50] R.M. Sabino, K. Kauk, L.Y.C. Madruga, M.J. Kipper, A.F. Martins, K.C. Popat, Enhanced hemocompatibility and antibacterial activity on titania nanotubes with tanfloc/heparin polyelectrolyte multilayers, J Biomed Mater Res A 108 (2020) 992–1005. https://doi.org/10.1002/JBM.A.36876.

CHAPTER 5

CONCLUSIONS AND FUTURE WORK

5.1 Conclusions

Cardiovascular diseases have always been a persistent burden on global health standards. However, the recent alarming trends of increase in its occurrence and being a major cause for high mortality rates of adults has posed severe risks and has emphasized on the need for better cardiovascular devices in the medical field. Blood-contacting medical devices used today are prone to several complications like thrombosis, bacterial adhesion and restenosis post implantation into the patient's body. Current techniques used to address this issue are revision surgeries for device replacement or long-term drug therapies that have not shown promising results in the long run. These conditions affect the health of the red blood cells and other blood components, eventually degrading the health of the host. Thus, researchers are searching for effective material-based solutions to these problems. The surface characteristics and material properties of the implant devices are important factors that influence the cell-material interactions. Studies related to the use of biopolymers, incorporation of bioactive molecules and organic compounds are ongoing, to investigate their effects with the biological components of the host body. Research have been done to understand the effects of nanostructured polymer surfaces on platelet adhesion and protein adsorption. Nonetheless, very few studies have investigated the influence of these biodegradable polymeric surfaces, coupled with organic coatings, on the cell integrity and viability of erythrocytes (red blood cells). In this study, PCL nanostructured surfaces (NF and NW) were fabricated and modified with organic compounds, such as TN and CMKC, for investigating their material properties, antibacterial properties and influence on erythrocyte integrity.

PCL nanostructured surfaces were fabricated using different techniques. NF surfaces were fabricated by electrospinning technique, while NW surfaces were fabricated using a nano-templating technique. The surfaces were also modified further by coating them with TN and CMKC, to assess the improvements in biocompatibility and antibacterial properties. Later, the surfaces were evaluated for their surface properties using different characterization techniques. The morphology of the surfaces was analyzed (SEM) and revealed the topographical differences between the two nanostructured surfaces and their PCL control surfaces. There was no significant difference in the morphology of the surfaces post modification with TN and CMKC. Surface wettability analysis (Contact angle) has shown that NF and modified NF surfaces were superhydrophilic, and NW and modified NW surfaces were hydrophilic, in contrast to their hydrophobic PCL control surfaces. Surface chemistry analysis (XPS) revealed peaks of nitrogen and sulphur in TN modified and CMKC modified groups respectively, compared to unmodified surfaces. These results account for the presence of amine groups in TN and presence of sulphate groups in CMKC, which indicated the successful modification of the nanostructured surfaces. Surface crystallinity analysis (XRD) was conducted, and the results exhibited no significant differences in the patterns between PCL control, NW and modified NW surfaces. Intensity of diffraction peaks for NF and modified NF surfaces became lower and broader, exhibiting relatively more amorphous characteristics compared to NW and PCL surfaces. Mechanical properties of surfaces, such as indentation hardness and elastic modulus, were analyzed using nano-indentation technique. Results indicated that NW surfaces have enhanced load bearing capacity and thus increased durability and flexibility, whereas NF surfaces exhibited high initial hardness values and superior elastic properties.

Following the fabrication and modification of surfaces, PCL nanostructured surfaces were subjected to gram-positive (*S.aureus*) and gram-negative (*P. aeruginosa*) bacterial strains, at two different incubation periods, to understand the antibacterial properties of different surfaces. The surfaces were characterized by bacteria adhesion to evaluate the amount of live or dead bacteria and bacteria morphology to understand the morphological changes or biofilm formation of the cells. The percentage area fraction coverage of live and dead bacteria was also calculated. It was observed that nanostructured surfaces modified with TN and CMKC exhibited improved antibacterial properties by reducing bacterial adhesion and inhibiting biofilm formation. This can be attributed to the synergistic effect of nanostructures combined with organic compounds. Modified NW surfaces exhibited the least % of area covered by bacteria.

Furthermore, nanostructured surfaces were evaluated to understand their effects on erythrocyte integrity and viability. Cytotoxicity assay was conducted to assess if the surface modifications done induce any toxicity towards adhered cells. Results has shown significantly low LDH activity on all the surfaces when compared to the negative control, indicating that the physical and chemical modifications done on the surfaces did not induce any cytotoxic effects on the cells. Surfaces were characterized for erythrocyte adhesion using fluorescence microscopy, to assess their viability towards erythrocytes. Modified NF and NW surfaces exhibited better erythrocyte adhesion compared to their control surfaces, which can be attributed to the synergistic effect of addition of TN and CMKC along with nanostructured surfaces. Erythrocyte morphology was examined using SEM and the results indicated that modified NF and NW surfaces significantly retained the healthy erythrocyte morphology and integrity than their control surfaces.

In conclusion, the PCL nanostructured surfaces, modified with TN and CMKC, exhibited improved antibacterial properties and enhanced positive effects on erythrocyte cell integrity, compared to unmodified surfaces. These findings indicate that PCL nanostructured surfaces coupled with organic compounds like TN and CMKC can provide a stable and biocompatible medical device surface that can prevent health complications in the host body.

5.2 Future works

In future studies, it would be crucial to evaluate the effects of variable sizes of NF and NW on erythrocytes, platelets, leukocytes, proteins and other blood components. It is also important to observe the effect of change in the concentrations of TN and CMKC. It would also be helpful to understand the effect of these surfaces on erythrocytes exposed for a prolonged duration. All the studies have been done in static conditions. It is also crucial to examine the responses in a dynamic environment to assess the biocompatibility of the surfaces. Adhesion, differentiation and proliferation of different types of cells like endothelial cells, osteoblasts and smooth muscle cells can be characterized to understand their responses upon contact with theses surfaces. Further studies must examine the ability of these surfaces to remain stable for longer periods. Also, research must be done to improve the durability and stability of these surfaces. Incorporation of these modified surfaces in real-time applications of medical devices such as vascular stents, grafts, catheters etc. might be a potential scope of future works.

LIST OF ABBREVIATIONS

Abbreviation	**Definition**
AAO	Anodic Aluminum Oxide
ANOVA	Analysis Of Variance
BHV	Bioprosthetic Heart Valve
BMS	Bare-Metal Stents
CFU	Colony Forming Units
CMKC	Carboxymethyl Kappa-Carrageenan
CO_2	Carbon dioxide
CVD	Cardiovascular Diseases
DCB	Drug-Coated Balloon
DES	Drug Eluding Stent
ECM	Extracellular Matrix
H^+	Hydrogen ion
INT	Iodonitrotetrazolium Chloride
ISR	In-Stent Restenosis
JCPDS	Joint Committee on Powder Diffraction Standards
KC	Kappa-Carrageenan
LbL	Layer-by-Layer

LDH	Lactate Dehydrogenase
MCA	Monochloroacetic Acid
MHV	Mechanical Heart Valve
MSC	Mesenchymal Stem Cell
MWCO	Molecular Weight Cut-Off
NAD+	Nicotinamide Adenine Dinucleotide, oxidized form
NADH	Nicotinamide Adenine Dinucleotide, reduced form
NaOH	Sodium Hydroxide
NF	Nanofibers
$\mathrm{NF}_{\mathrm{TN}}$,	Nanofibers modified with Tanfloc
$\mathrm{NF}_{\mathrm{TN+CMKC}}$	Nanofibers modified with Tanfloc and CMKC
NW	Nanowires
$\mathrm{NW}_{\mathrm{TN}}$	Nanowires modified with Tanfloc
$\mathrm{NW}_{\mathrm{TN+CMKC}}$	Nanowires modified with Tanfloc and CMKC
-OH	Hydroxyl group
OLA	Oleic Acid
P. aeruginosa	Pseudomonas aeruginosa
PBS	Phosphate-Buffered Saline
PCI	Percutaneous Coronary Intervention

PCL	Polycaprolactone
PEG	Polyethylene Glycol
PETG	Polyethylene Terephthalate Glycol
PHA	Polyhydroxyalkanoate
PLA	Polylactic Acid
PS	Polystyrene
PU	Polyurethane
PVA	Polyvinyl Alcohol
PVDF	Polyvinylidene Fluoride
S. aureus	Staphylococcus aureus
S2p	Sulphur 2p peak in XPS
SEM	Scanning Electron Microscopy
$–SO_4$	Sulphate group
TN	Tanfloc
TSB	Tryptic Soy Broth
VAD	Ventricular Assist Device
WHO	World Health Organization
XPS	X-Ray Photoelectron Spectroscopy
XRD	X-Ray Diffraction Analysis